Investigations into the Effects of Biofuel Contaminants on Solid Oxide Fuel Cells

PAR

Hossein MADI

EPFL

ÉCOLE POLYTECHNIQUE
FÉDÉRALE DE LAUSANNE

Suisse
2016

To my wife Morgane
and son Bardia
without whom this thesis would have
been completed a year later.

Acknowledgements

I wish to express deep gratitude to my supervisor Dr. MER Jan Van herle for his invaluable supervision, advices, encouragement, and insight throughout the research process. His consistent trust during my thesis work is greatly appreciated.

Thank you Prof. Christian Ludwig for co-supervising and scientific discussions. Prof. Ludwig made me realize and believe that most questions can be answered in a "simpler" way by a careful theoretical argument, without carrying out a long experiment.

My appreciation also goes to Dr. Stefan Diethelm, who was always there to lend a helping hand in experimental work.

My colleagues and friends from FuelMat and IPESE groups deserve great credits for numerous exchange of ideas, critical feedbacks and valuable comments: Ema, Stephane, Priscilla, Manuel, Giorgio, Fabio, Thierry, Arata, Matthias, Dylan, Stefano, Victor, Alberto, Maziar, Raman, Araz, Nils and Sophia.

I am deeply thankful to my parents for giving me life in the first, for educating me, for unconditional support and encouragement to pursue my interests, even when the interest went beyond boundaries of language and geography. My brothers, Mohammad and Reza for all their life supports, we keep and go together! Hamid, for listening, even sometimes, to his older, experienced brother! Sisters, Leila and Tayebeh for shaping my character at the base.

I also thank my family-in-law who encouraged and prayed for me all the time. They truly made Switzerland my second home. It has always been a pleasure talking to you Alois! It is never late to learn new things and not ever give up, these are what I learned from him.

Last, but not least, I would like to thank my wife, Morgane, for her invaluable support throughout my Ph.D. time – you are the invisible backbone of this work!

<div align="right">H. M.</div>

Preface

This thesis is submitted as a partial fulfillment of the requirements for the Ph.D. degree at the École Polytechnique Fédérale de Lausanne of Switzerland.

The four year study was carried out at the Institute of Mechanical Engineering, FuelMat Group from July 2012 to July 2016 under the supervision of MER Dr. Jan Van herle and co-supervision of Prof. Christian Ludwig.

An external research stay was conducted from August 2015 to November 2015 at the Department of Energy Conversion and Storage, Risø- DTU in Denmark. Supervisor at Risø was Dr. Anne Hauch.

The thesis is written as a monograph, but a number of papers have been published based on the work in this research study (see List of Publications).

Hossein Madi
Lausanne, 5 June 2016

Abstract (English/Deutsch)

Solid Oxide Fuel Cells (SOFCs) have gathered considerable attention as a clean, highly efficient conversion device for the production of both electricity and heat from fuels. Due to their high operating temperatures, SOFCs do not require pure hydrogen as fuel, but exhibit a high fuel flexibility, a major advantage concerning the high cost of hydrogen production. Nonetheless, certain requirements apply in terms of fuel purity. The presence of contaminants such as sulfur compounds, siloxanes, halogens, volatile organic compounds and tars within the fuel stream, even at trace levels can significantly reduce the lifetime of key components such as the fuel cell stack and reformer.

Cleaning technologies can remove harmful impurities from the biofuels so as to meet the cleanliness requirements of SOFC stacks, though these come at higher cost. The purpose of this study is to provide guidelines regarding the maximum impurity concentrations in the biofuels which SOFCs can tolerate. This work has two principal aims: (i) to identify any threshold tolerance limits of different contaminants, if they exist and (ii) to investigate degradation mechanisms caused by contaminants. Siloxane D4, hydrogen chloride and sulfur were selected as biogas impurities. In addition, the effect of toluene (a common impurity in wood gasifier product gas) was also investigated on the performance of Ni-YSZ SOFCs.

Short tests lasting 100-500 h were carried out to study the influence of the selected impurities on state-of-the-art Ni anode-supported SOFCs. Experiments were performed on single cells provided by Topsoe Fuel Cell (TOFC) and SOLIDpower and in some cases on 11-cell short stacks, provided by TOFC. Contamination tests were performed on simple hydrogen feed and more complex feeds such as simulated biogas or reformed biogas. Furthermore, in the cases of contamination with siloxane D4 and hydrogen chloride, single cell results were compared with those of short stacks. *In-situ* (electrochemical impedance spectroscopy- EIS) and *ex-situ* (electron microscopy and chemical analysis) characterization methods were used to identify the prevailing degradation mechanisms.

Suggestions were made, which Ni-YSZ anode processes are affected by each contaminant. Siloxane deposit as SiO_2 and block electrode pores and TPB (triple-phase-boundary) electrochemical reaction zone; HCl adsorbs on Ni particles to hinder the electrochemical reaction; sulfur, both from H_2S and thiophene, adsorbs reversibly on Ni and leads to an immediate sharp cell voltage drop, which remains small at low S-concentrations.

It was found that the complete removal of siloxanes is necessary, that S-compounds are acceptable to a level of 0.5 ppm and that there is no need to remove HCl and tar compounds from the biogas, for the concentration levels in which they are expected to be found in anaerobic digester gas.

Zusammenfassung

Festoxidbrennstoffzellen (englisch solid oxide fuel cells, SOFC) sind eine viel beachtete saubere und effiziente Technologie für die Strom- als auch die Wärmeproduktion. Auf Grund der hohen Betriebstemperaturen von SOFCs, wird als Treibstoff kein reines Wasserstoffgas vorausgesetzt, was Flexibilität in der Wahl des Treibstoffes zulässt und bei hohen Preisen für die Wasserstoffproduktion besonders Vorteilhaft ist. Jedoch gelten auch da gewisse Anforderungen an die Reinheit der Treibstoffe. Verunreinigungen wie Schwefelverbindungen, Siloxanen, Halogenen, flüchtige organischen Verbindungen und Teerstoffen in der Treibstoffzufuhr, auch nur Spuren davon, können die Lebensdauer von Schlüsselkomponenten wie dem Brennstoffzellenstapel und dem Reformer erheblich reduzieren.

Reinigungstechnologien können schädliche Verunreinigungen in Biotreibstoffen entfernen, um den Reinheitsanforderungen einer SOFC zu genügen, jedoch zu einem höheren Preis. Das Ziel dieser Forschungsarbeit ist es die maximalen Toleranzgrenzen der Schadstoffkonzentrationen im Biotreibstoffen so zu bestimmen, dass diese von SOFCs toleriert und somit in Richtlinien festgelegt werden können. Diese Arbeit hat zwei Hauptziele: (i) die Bestimmung von Grenzwerten für verschieden Verunreinigungssubstanzen, sofern diese existieren und (ii) die Untersuchung von Schädigungsmechanismen in den Komponenten der SOFC unter der Einwirkung von Verunreinigungen. Siloxan D4, Chlorwasserstoff und Schwefel wurden als Biogasverunreinigungen untersucht. Zusätzlich wurde der Effekt von Toluol (eine verbreitete Gasverunreinigung bei der Herstellung im Holzvergaser) auf die Leistungsfähigkeit einer Ni-YSZ SOFC untersucht.

Kurzversuche von 100-500 Stunden wurden durchgeführt, um den Einfluss der erwähnten Verunreinigungssubstanzen auf eine moderne Ni-Anode SOFC zu untersuchen. Die Experimente wurden an Einzelbrennstoffzellen durchgeführt, hergestellt von Topsoe Fuel Cell (TOFC) und SOLIDpower, und in einigen Fällen an Brennstoffzellenstapeln mit elf Zellen von TOFC. Die Kontaminationsversuche wurden mit einfacher Wasserstoffzufuhr und komplexeren Treibstoffzufuhren, wie simuliertes oder reformiertes Biogas durchgeführt. Für die Untersuchungen mit Siloxan D4 und Chlorwasserstoff wurden die Resultate der Einzelbrennstoffzellen zusätzlich mit den Experimenten mit den Brennstoffzellenstapeln verglichen. *In-situ* (elektrochemische Impedanzspektroskopie, EIS) und *ex-situ* (Elektronenmikroskopie und chemische Analyse) Charakterisierungsmethoden wurden genutzt, um die vorherrschenden Mechanismen in den Brennstoffzellen zu bestimmen.

Voschläge wurden gemacht, welche Ni-YSZ Anodenprozesse von welchen Verunreinigungssubstanzen beeinflusst werden. Siloxan lagern sich als SiO_2 ab und blockieren die Elektrodenporen und die electrochemische Reaktionszone an der Dreiphasengrenze (englisch triple-phase-

boundary, TPB); HCl adsorbiert auf Ni Partikeln und verhindert electrochemische Reaktionen; Schwefel, von H2S oder Thiophen, lagert sich reversibel auf dem Nickel ab und führt zu einem schlagartigen Abfall der Zellspannung, der bei tiefen Schwefelkonzentrationen klein ausfällt. Es wurde festgestellt, (i) dass es notwending ist alle Siloxan vollständig zu entfernen, (ii) dass die Schwefelverbindungen tolerierbar sind bis zu einer Konzentrationen von 0.5 ppm, und (iii) dass HCl und Teerstoffe nicht aus dem Biogas gefiltert werden müssen für die erwarteten Konzentrationen in anaeroben Faulgas.

Stichwörter: Festoxidbrennstoffzellen (SOFC), Verunreinigungtoleranzschwelle, Siloxane, Chlorwasserstoff, Thiophen, Toluol, Zersetzungsmechanismen, Ni-YSZ, Einzelzellen, Stacks

Contents

Contents

Nomenclature

Abbreviations

AD .... Anaerobic Digester

ADIS .... Analysis of Differential Impedance Spectra

ASR .... Area Specific Resistance

ATR .... Auto-Thermal Reforming

BoP .... Balance of Plant

CHP .... Combined Heat and Power

CNLS .... Complex Non-linear Least Squares

COS .... Carbonyl Sulfide

DRT .... Distribution of Relaxation Time

EDX .... Energy Dispersive X-ray Spectroscopy

EIS .... Electrochemical Impedance Spectroscopy

FU .... Fuel Utilization

HCl .... Hydrogen Chloride

ICP-MS .... Inductively Coupled Plasma Mass Spectrometry

LFG .... Landfill Gas

LOD .... Limit of Detection

LSM .... Sr-doped $LaMnO_3$

MFC .... Mass Flow Controller

OCV .... Open Circuit Voltage

POLITO .... Politecnico di Torino

POx .... Partial Oxidation

Nomenclature

ppm .... Part Per Million

sccm .... Standard Cubic Centimeter per Minute

SEM .... Scanning Electron Microscopy

SOFC .... Solid Oxide Fuel Cell

SR .... Steam Reforming

THT .... Tetrahydrothiophene

TOFC .... Topsoe Fuel Cell

TPB .... Triple Phase Boundary

VMS .... Volatile Methyl Siloxanes

VOCs .... Volatile Organic Compounds

VOSiC .... Volatile Organic Silicon Compounds

WDS .... Wavength-Dispersive X-ray Spectroscopy

WGS .... Water Gas Shift

WWTP .... Waste Water Treatment Plant

YSZ .... Yttria-Stabilized Zirconia

Chemical Compounds

CO .... Carbon monoxide

CO_2 .... Carbon dioxide

COS .... Carbonyl Sulfide

CH_2Cl_2 .... Dichloromethane

CH_3Cl .... Chloromethane

CH_3OH .... Methanol

CH_4 .... Methane

C_4H_4S .... Thiophene

C_6H_5Cl .... Chlorobenzene

C_7H_8 .... Toluene

$C_8H_{24}O_4Si_4$ .... D4- Octamethylcyclotetrasiloxane

$C_{10}H_{30}O_5Si_5$ .... D5- Decamethylcyclopentasiloxane

$C_{10}H_8$ .... Naphthalene

Cl_2 .... Chlorine

H_2 …………………… Hydrogen

H_2O …………………… Water

H_2S …………………… Hydrogen sulfide

HCl …………………… Hydrogen chloride

N_2 …………………… Nitrogen

Ni …………………… Nickel

$NiCl_2$ ………………… Nickel(II) chloride

SiO_2 …………………… Silicon dioxide

$Si(OH)_4$ ………………… Silicic acid

1 Introduction

1.1 Motivation

The global average air temperature at the surface of the earth has increased by about 0.85 °C over the period 1880 to 2012, and is expected to continue to rise [1]. Human activities such as burning coal, oil and in general fossil fuels to generate electricity, have increased the amount of greenhouse gases that contribute to global warming. In the past decades, there has been an increasing pressure in reducing the environmental impact of heat and power cogeneration technologies. The U.S. Energy Information Administration (EIA) projects 48% increase in world energy consumption by 2040. Thus, development of clean energy sources and their conversion becomes progressively important to the global environment.

Alternative generation systems that utilize renewable energy sources are of interest due to their high operation efficiencies and low CO_2 emission levels [2]. Today, in the field of electric power systems a lot of research effort is being put into the development of alternative energy conversion systems. Fuel cell technology is one such alternative [3], with the Solid Oxide Fuel Cell (SOFC) type offering the best prospects for stationary cogeneration. Advantages of fuel cells include high conversion efficiency, low to zero emissions during operation, flexibility of operation and ease of integration with other systems.

SOFCs are conversion devices that electrochemically oxidize gaseous fuels and produce electricity. SOFCs (and in general fuel cells) consist of two electrodes (the anode and the cathode) separated by an electrolyte. The electrodes are electronic conductors and the electrolyte is an ionic conductor. SOFCs have an extensive potential range of applications, including multi-fuel diversity and high system efficiencies because of direct conversion. These features allow a variety of process integrations, including the efficient utilization of heat.

The particular advantage of the SOFC concept over all other types of fuel cells is its ability to operate over an extended temperature (600-1000 °C) with a variety of fuels, both gaseous – such as methane, biogas, and liquids – such as methanol and ethanol (including bio-ethanol). This capacity of SOFCs to operate with fuels originating from renewable resources like biomass

is of special interest in this work. Biomass is a renewable, widely available and practically carbon neutral energy source. Biomass can be gasified to produce the so-called biosyngas or it can be digested to generate biogas.

Waste-derived fuels, e.g. anaerobic digester gas from manure and other agro-residues, waste water treatment plants (WWTP) and from municipal solid wastes, are gaining attention to contribute a share in the energy transition [4]. The global biogas potential is estimated to lie around 36,000 PJ [5], 6.5% of the world total primary energy supply in 2012.

The exploitation of biogas fuel in SOFC systems has been studied for several years [6–8]. Practical and operational experience has been gained through several pilot plants. Industrial installations are also gaining momentum. Several plant configurations are potentially available for the high-efficiency power generation in biogas-fed SOFC systems. Large integrated biogas SOFC plants with either atmospheric or pressurized SOFC operation, SOFC-GT hybrid power generation with a gas turbine and carbon capture via anode-exhaust oxycombustion, were analysed recently [9]. The overall electrical efficiency of the analysed plant configurations ranged from 50 to 70%. Hybridization of the SOFC with a gas turbine effectively boosts the efficiency to 70% when fuel utilization (FU) is 90%. Fuel utilization indicates the percent of fuel that reacts in the fuel cell.

Biogas may contain a wide range of impurities such as sulfur compounds, siloxanes, halogens, volatile organic compounds (VOC) and tars [10]. Fuel quality requirements generally apply to SOFC anode catalysts [4]. The maximum tolerance to contaminants is usually expressed in terms of ppmv, or even ppbv, of specific compounds that the fuel cell can withstand. The durability of SOFCs is strongly dependent on the amount of contaminants that reaches the porous electrodes, especially the three-phase boundary where gas, electrode and electrolyte particles meet. Pore blocking in the electrodes and progressive corrosion of the interconnects can also be affected by fuel impurities. Hence, ultra-clean fuel gas is beneficial to increase the lifetime. So far most of the attention was on the impact of sulfur and chlorine compounds – that decompose respectively to H_2S and HCl at the SOFC relevant operating conditions – as anode fuel contaminants. However, biogenous fuels are studied more closely and new contaminants are encountered.

The detailed fuel gas quality specifications for fuel cells are not well understood and documented. Contaminants removal can be done to a certain extent, yet it can be difficult and economically not feasible to achieve "complete" removal. The raw fuel gas should be filtered to a certain level, so that the product gas can be used as fuel for SOFCs but it is challenging to specify tolerance limits for impurities. The existence of such contaminants, both from gasified and digested biomasses, has led to investigations on anode materials with different structures and compositions that may interact with the contaminants. Better understanding of the precise effect of each contaminant on the anode electro-catalyst is required. In particular, the experimental determination of the tolerance levels for chosen contaminants would be highly valuable for SOFC applications.

1.2 Objectives and research questions

In anaerobic digestion biogas from primary and secondary[1] sludge of waste-water treatment plants, sulfur, chlorine and siloxane compounds can be found at the ppm level, along with traces of other VOCs, e.g. aromatics (mostly benzene and toluene), alkanes and alcohols. These impurities can reach downstream SOFCs and could cause degradation of the cell performance and overall system durability. In this PhD thesis, the effect of the most prominent contaminants on the Ni-YSZ anode supported SOFCs is investigated. Commercial single cells and short stacks were provided by Topsoe Fuel Cell (TOFC) and SOLIDpower.

The main scope of this thesis is to identify and study the effect of pollutants from WWTP anaerobic digester gas and also wood gasifiers on SOFC single cells and short stacks. Aging tests, with/without accelerated degradation and post-mortem analysis are performed. In summary, the research questions that this PhD thesis tackles are:

- **RQ1:** *Do we need to remove the impurities from biogas and biosyngas?*

- **RQ2:** *If an impurity causes a degradation, what is the potential single cell/stack threshold tolerance limit towards that contaminant?*

- **RQ3:** *What is the degradation mechanism of the relevant contaminants?*

- **RQ4:** *Do single cell and stack behave in the same manner towards a specific impurity?*

1.3 Thesis Structure

The thesis comprises 9 chapters. To provide an overview of the topics covered in this thesis a short description for each chapter is given as follows:

Chapter 2: Literature review. This chapter consists of three parts. The first part is an overview on fuel cell technology, specifically SOFCs and their degradation issues. The second part is an introduction to biomass, conversion routes and its potential as a neutral carbon fuel source. The last part focuses on the issues related to the existence of impurities in biogas and biosyngas on the performance of SOFCs.

Chapter 3: Experimental. In this chapter the experimental test benches, single cell setup and the analytical methods in evaluating the experimental results are explained.

Chapter 4: Siloxane poisoning- part A: degradation. This chapter focuses on siloxanes and their effects on the performance of SOFC Ni-YSZ anodes. The involved mechanism of degradation is clarified and quantified through several test runs and subsequent post-mortem analysis on tested samples. At the end of this chapter a degradation mechanism due to exposure to siloxane is given.

---

[1]Primary sludge is a result of the capture of suspended solids and organics through gravitational sedimentation. Secondary wastewater treatment removes biodegradable material via biological processes.

Chapter 5: Siloxane poisoning- part B: recovery assessment. Knowing the detrimental effect of siloxanes on the performance of anode catalysts, this chapter evaluates potential ways of recovery after exposure to siloxanes.

Chapter 6: Chlorine poisoning. This chapter evaluates the poisoning effect by hydrogen chloride (HCl) on state-of-the-art Ni anode-supported (AS) SOFCs at 750 °C in either hydrogen or reformed biogas fuel. Experiments were performed on both single cells and short stacks for a wide range of HCl concentrations in the fuel gas and different current densities.

Chapter 7: Sulfur poisoning. This chapter analyses the performance and degradation issues of Ni-YSZ SOFC exposed to thiophene (C_4H_4S) and H_2S. There are extensive investigations on the effect of hydrogen sulfide, as an inorganic sulfur compound on the performance of SOFC, but knowledge lacks on the effect of complex sulfur-containing molecules like thiophene. The impact of this organic sulfur compound on the performance is reported with some variation of the temperature and the impurity concentration.

Chapter 8: SOFC degradation by the effect of tars. This chapter presents an experimental study of the impact of toluene as tar compound representative on the performance of AS Ni-YSZ SOFC operating at 800 °C, fed with H_2 and biosyngas.

Finally, the concluding remarks are presented, as well as general recommendations for future work.

2 Literature Review

2.1 Introduction to Fuel Cells

A fuel cell converts the chemical energy of a fuel directly to electrical power and usable high quality heat. The efficiency of fuel cells is higher than that of combustion engines as it is not limited by the Carnot cycle [11]. Fuel cells have various advantages compared to conventional power generating systems in terms of their efficiency, reliability, size flexibility and environmental friendliness [12]. If hydrogen is the fuel, electricity, water and heat are the only products.
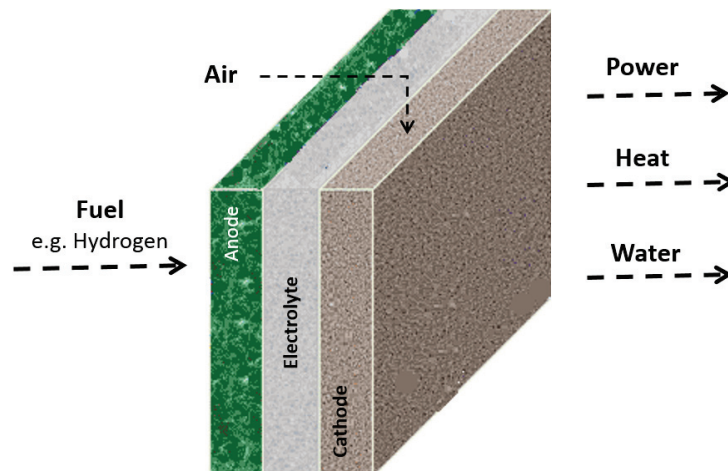
Figure 2.1 – Fuel cell inputs and outputs

Similarly to batteries, the operating principle of fuel cells relies on the electrochemical combination of reactants to generate electricity. Unlike batteries, they do not deplete themselves or need recharging and they function as long as a fuel is supplied. A fuel cell consists of two electrodes, an anode and a cathode, separated by an electrolyte membrane. Hydrogen or other fuels are oxidized at the anode, producing hydrogen ions and electrons. The hydrogen

ions migrate through the electrolyte whilst the electrons are forced through an external circuit to the cathode. The hydrogen ions and the electrons react with oxygen at the cathode side, producing water [13].

Fuel cells are sorted mainly by the kind of electrolyte they employ and the operating temperature. This classification governs the kind of electrochemical reactions that take place in the cell, the temperature, catalyst type, the fuel required and other factors. By far the greatest research interest has focused on Proton Exchange Membrane fuel cells (PEM) and Solid Oxide Fuel Cells (SOFC). The two most common differences between PEMs and SOFCs deal with the large differential in operating temperatures and required use of pure hydrogen by PEMs. PEMs operate at much lower operating temperatures (80 °C) compared to the main other fuel cell systems.

2.2   Solid Oxide Fuel Cells

SOFCs work at high temperatures, the highest of all the fuel cell types, at around 600 °C to 1000 °C. They use a hard, non-porous ceramic compound as the electrolyte. There are several advantages in SOFCs:

- They can be operated on a variety of fuels such as natural gas, biogas, biosyngas from biomass gasification or coal gas [14].

- They can achieve internal reforming, which eliminates the need for external reforming [15–18].

- They are more resistant to small quantities of sulfur in the fuel, compared to other types of fuel cell [19, 20] .

- High temperatures promote rapid electro-catalyst reactions with non-precious metals.

There are however some disadvantages related to the high temperature: long start-up time, isolation and heat loss, requirements on its ceramic materials (e.g., chemical compatibility with various ceramics employed, stability in oxidizing and reducing conditions). They are used extensively in mini (e.g., Bloom Energy's 100 kW off-grid power generators) and micro stationary power generation (e.g., SOLIDpower EnGen^{TM}-2500 2,5 kW CHP).

A SOFC consists of two porous electrodes (the anode and the cathode) sandwiched around a hard ceramic electrolyte. The role of the anode in a SOFC is to provide the sites for the fuel gas to react with the oxygen ions received from the electrolyte. Electrochemical oxidation of fuel in anodes is believed to occur only at the three phase boundary (TPB) region, where the electrode, the electrolyte and the gas phase meet, as shown in Fig.2.2. Electrochemical oxidation of H_2 can be written as follows:

$$H_2 + O^{2-} \longrightarrow H_2O + 2\,e^- \tag{2.1}$$
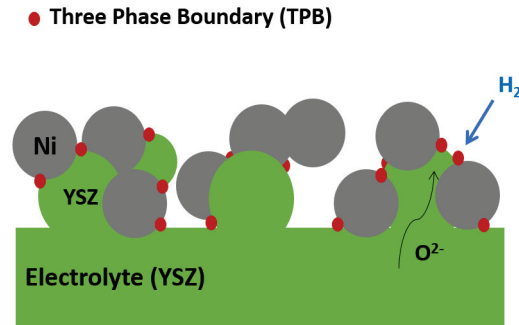
Figure 2.2 – Schematic of the three phase boundary region.

The anode has to meet a number of requirements such as high electronic conductivity, electro catalytic activity, chemical and mechanical stability, thermal compatibility with other cell components and sufficient porosity to allow gas transportation in high temperature reducing environments [21]. Therefore, anode fabrication plays an important role in determining the performance of SOFCs. Ni-YSZ is the state-of-the-art anode material for SOFCs. This structure is cheaper in manufacturing cost and provides for higher power densities compared to other materials. Through its use, as a mechanical support, it is possible to reduce the thickness of the electrolyte membrane to a few micrometers, and reduce the operating temperature to < 800 °C. However, the Ni-cermet anode suffers from several limitations, like limited tolerance to re-oxidation [22] and sensitivity to sulfur poisoning and coking [23].

In SOFCs, the cathode functions as the site for the electrochemical reaction of oxygen. The material of choice for SOFC cathode is mainly a composite of Sr-doped $LaMnO_3$ (LSM) and yttria-stabilized zirconia (YSZ) [24]. In case a ceria-based compatibility layer is used, the cathode material of choice is $LaSrFeCoO_3$. Generally, the cathode must be highly electronically conductive, be thermally and chemically compatible with the electrolyte and interconnects, and sufficiently porous [11]. Electrochemical reaction of oxygen occurs at the TPBs of the cathode side and can be described as follows:

$$\tfrac{1}{2}O_2(g) + 2e^-(cathode) \longrightarrow O^{2-}(electrolyte) \tag{2.2}$$
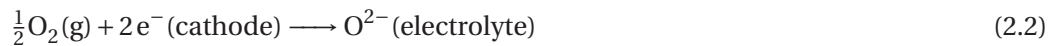
The overall cell reaction is

$$H_2 + \tfrac{1}{2}O_2 \longrightarrow H_2O \tag{2.3}$$
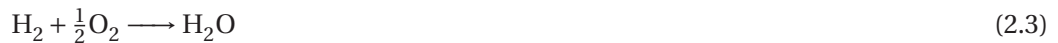
The voltage generated by the electrochemical reaction at constant temperature and pressure is a function of the Gibbs free energy change of the reaction, stated below (Eq. 2.4).This is the maximum electrical work available in a fuel cell.

$$W_{el} = \Delta G = -nFE \tag{2.4}$$

where n is the number of electrons exchanged during the reaction (n=2 in Eq.2.3), F is Faraday's constant (96,487 C/mol) and E is the reversible potential of the cell.

The reversible potential of a SOFC at temperature T, E_0 is known as Nernst potential. The Nernst equation provides a link between the ideal standard potential (E_0) for the cell reaction and the ideal equilibrium potential (E) at other partial pressure of reactants and products. The Nernst potential gives the ideal open circuit voltage, of the fuel cell. The corresponding Nernst equation for the reaction is then:

$$E = E_0 + (\frac{RT}{2F})\ln[\frac{P_{H_2}P_{O_2}^{1/2}}{P_{H_2O}}] \tag{2.5}$$

where R is the universal gas constant (8.314 J/mol K). The E_0 at 298 K for Eq. 2.3 is 1.229 V.

2.2.1 Polarization in SOFCs

The voltage of a fuel cell is always less than the thermodynamically predicted ideal voltage due to irreversible losses, which increase as current is drawn from the cell, Fig. 2.3. These loss mechanisms, known as polarization or over potential, can be ohmic, due to activation or diffusion (or concentration) polarization [11]. They have different effects on the theoretical voltage of the fuel cell.

- **Activation losses** are related to charge transfer processes and thus depend upon the nature of electrode-electrolyte interfaces. Activation overpotential loss and current density are related through an exponential relationship.

- **Ohmic losses** result from the resistance to the charge transport through the electrodes and the electrolyte. The electrolyte has the main contribution to the ohmic polarization. Thus, a high ionically conductive and a very thin electrolyte is desired to minimize the ohmic contribution.

- **Concentration polarization** is related to the transport of gaseous species through porous electrodes. A controlled microstructure i.e., high porosity and uniform large pores reduce this type of loss [25].

2.2.2 Anode Degradation Mechanism

In the framework of SOFC, degradation can be defined as the withdrawal of any functional SOFC structure from its designed state [14]. Degradation is often expressed as an increase of area specific resistances (ASRs), which are measured by IV curves and electrochemical impedance spectroscopy (EIS). The measured voltage degradation depends on the current density for a given ASR degradation. The ASR at low fuel utilisation can be calculated using
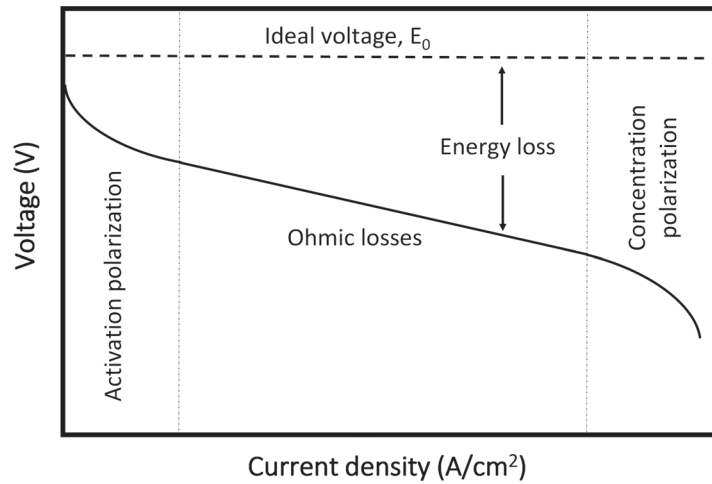
Figure 2.3 – Schematic plot of voltage versus current density of a SOFC showing different types of polarization, adapted from [11].

Eq. 2.6.

$$\text{ASR} = \frac{V_0 - V_i}{I} \tag{2.6}$$

where V_0 is the open circuit voltage (OCV), I is electrical current and V_i is the voltage at the current I.

A number of degradation pathways have been identified such as microstructural changes, crack formation, carbon deposition, and sulfur related degradation. Gerdes et al. [26] categorized the degradation mechanisms by their sources in two groups: intrinsically and extrinsically sourced degradations.

- *Intrinsically* sourced degradation occurs because of for example microstructure coarsening and impurities in raw materials.

- *Extrinsically* sourced degradation occurs when a foreign or unexpected material is introduced into the cell to induce degradation [26]. Poisoning by impurities such as sulfur, chlorine and coke are considered as extrinsic source degradation. Poisoning by impurities are also known as deactivation mechanisms for the nickel anode. The active sites and/or the pore network become blocked, which lead to an increase in the polarization resistance.

In this thesis, the focus of work is on the degradations that can be caused by impurities (extrinsic source degradations). The following part provides some examples of anode degradation mechanisms and how they contribute to the decline of the cell performance.

Delamination of anode

Delamination, in which the layers of materials separate from each other can be caused by impact or longitudinal shear stress between the layers or by carbon deposits [27]. Investigation of Alzate-Restrepo et al. [28] on feeding an electrolyte-supported Ni-YSZ with different CO/H_2 mixtures, showed that the anode exposed to 75%–25% CO/H_2 at OCV was delaminated from the electrolyte (Fig. 2.4).
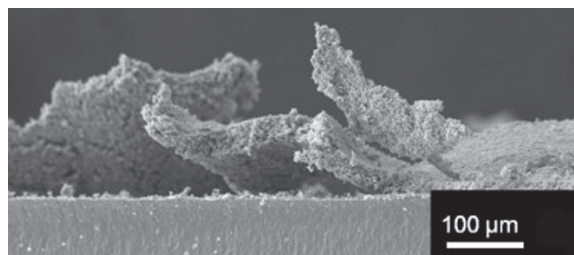
Figure 2.4 – The anode delaminated from the electrolyte after 6 h of operation with a CO-rich mixture, due to carbon formation [28].

Sulfur related degradation mechanism

In this thesis, poisoning by S-compounds is investigated in depth. In brief, experimental observations frequently report an immediate, dramatic drop (due to sulfur coverage of Ni and blockage of active sites) in cell performance followed by a slower, longer degradation. The slower degradation is due to sulfidation of Ni and formation of various bulk $Ni_X S_y$ compounds and this degradation is considered to be irreversible. Harris et al. [29] showed sulfide formation using a combination of synchrotron-based X-ray nanotomography and X-ray fluorescence techniques (Fig. 2.5). Sulfur poisoning increases as the H_2S concentration increases and the temperature decreases [30].
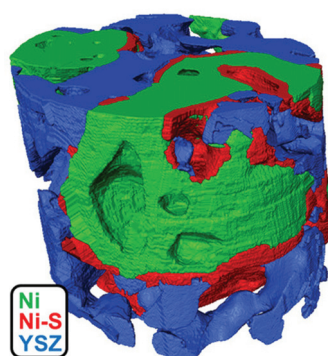
Figure 2.5 – 3-D renderings of the microstructure. The anode was exposed to 100 ppm H_2S and the sample was cooled down to room temperature while being exposed to H_2S [29].

Crack formation

The reduction and reoxidation cycles ("RedOx cycle") of nickel results in large bulk volume changes [31]. This drastic volume change may have a significant effect on the integrity of interfaces within a fuel cell and cracks may appear, which results in significant performance degradation. Thermal stress due to several reasons such as thermal gradients can lead to large deformation, and cracking might occur in the components [32]. Fig. 2.6 shows an example of crack formation in the cathode and the electrolyte. These expansions can also appear when an impurity reacts with nickel and forms NiX. This eventually leads to localized stresses and cracks may appear in the contaminated region.
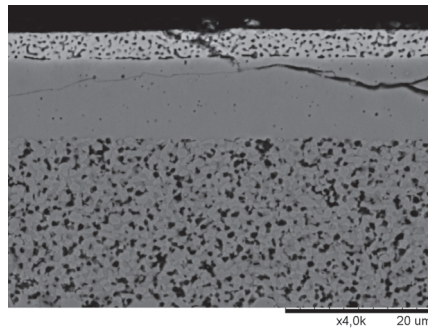
Figure 2.6 – Cracks in SOFC electrolyte due to thermal gradient.

Coarsening of Ni particles

The reorganisation of the nickel phase in the yttria-stabilised zirconia (YSZ) backbone is known as coarsening [22]. Ni coarsening in YSZ solid oxide fuel cell anodes is considered a major reason for anode degradation. High curvatures regions have higher chemical potentials compared to those with lower curvatures. Materials will therefore be transported from higher- to lower-curvature regions. It is assumed [22, 33] that the agglomeration of Ni in SOFC anodes leads to reduction in TPB length, which increases the resistance in SOFCs and results in cell degradation.
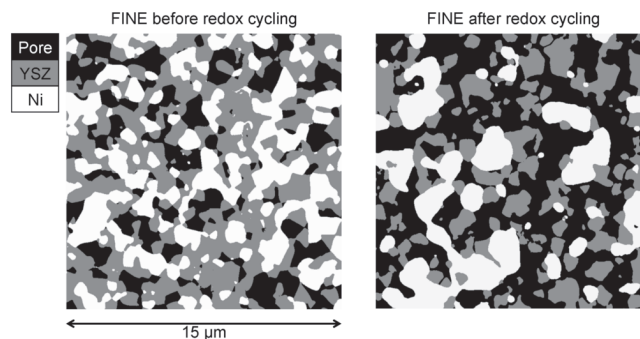
Figure 2.7 – Change in microstructures due to coarsening of Ni particles. After a RedOx cycle, Ni forms larger particles and some isolated islands, which results in a loss of TPB [34].

11

Carbon formation

As SOFCs are operated at high temperature, methane, methanol and heavier hydrocarbons can be reformed effectively by either catalytic steam reforming or partial oxidation to produce a H_2/CO rich gas. However, direct feed of carbon fuels other than hydrogen causes problems such as carbon deposition on the anode, which leads to a loss of active sites and cell performance as well as poor durability. The expansion of carbon filaments can initiate forces within the electrode structure leading to its fast breakdown.
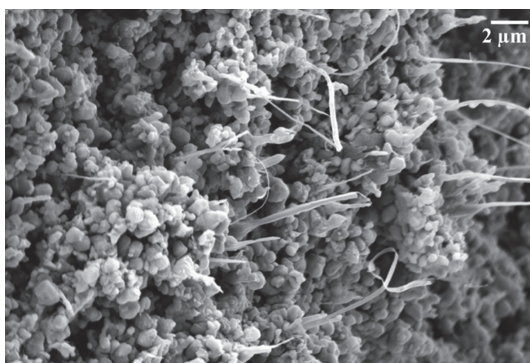
Figure 2.8 – Carbon deposited on a Ni–YSZ anode support after 2 h isothermal exposure at 800 °C to a dry pure methane feed. Whisker-type carbon filaments were present abundantly [35].

2.2.3 Fuel Options for SOFCs

Due to the high operational temperature of SOFCs, they are very fuel flexible. Hence, there is an opportunity to use methane and higher hydrocarbons in the SOFC wherein it is reformed in the porous anode material producing H_2 and CO-rich syngas. Methane and higher hydrocarbons can be reformed via several pathways, the most common one involves steam reforming (SR) (Eq. 2.7) and water-gas shift reaction (WGS) (Eq. 2.8). SR is a process in which high temperature steam (700-1000 °C) is used to produce hydrogen from a methane source such as natural gas [36]. In steam methane reforming, methane reacts with steam in the presence of a catalyst to produce hydrogen, carbon monoxide, and a relatively small amount of carbon dioxide.

$$SR: CH_4 + H_2O \longrightarrow CO + 3H_2 \qquad \Delta H^{\circ}_{298K} = 206 \; kJ/mol \tag{2.7}$$

$$WGS: CO + H_2O \longrightarrow CO_2 + H_2 \qquad \Delta H^{\circ}_{298K} = -41.09 \; kJ/mol \tag{2.8}$$
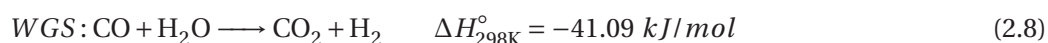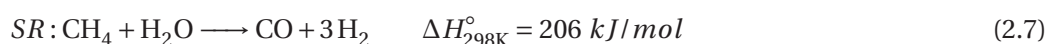
Partial oxidation of methane (Eq. 2.9) is another alternative route for the conversion of methane to syngas. Air is fed along with natural gas to the reformer. In contrast to the steam reforming reaction, partial oxidation is exothermic. During this process, methane converts to syngas with a ratio of H_2/CO equal to 2, which is a suitable feedstock for SOFC applications or the synthesis of hydrocarbons [37].

$$POx : CH_4 + 0.5O_2 \longrightarrow CO + 2H_2 \qquad \Delta H^{\circ}_{298K} = -36 \, kJ/mol \qquad (2.9)$$

An alternate reforming approach is autothermal reforming (Eq. 2.10), which is a combination of the exothermic POx and endothermic SR.

$$ATR : CH_4 + 0.5xO_2 + yCO_2 + (1-x-y)H_2O \longrightarrow (y+1)CO + (3-x-y)H_2 \qquad (2.10)$$
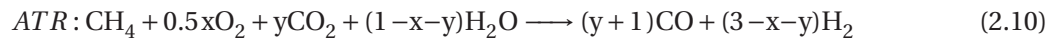
Liquid fuels such as methanol and ethanol are other attractive fuels for SOFCs. These liquid fuels have high volumetric energy densities and can be easily stored and transported. Several studies addressed the feasibility of methanol for SOFCs with direct or indirect internal reforming [38–41]. The catalytic reforming of methanol with steam can be represented by the widely accepted decomposition-shift mechanism which consists of the decomposition of methanol (Eq. 2.11) [39], methanol-steam reforming (Eq. 2.12), and WGS reaction (Eq. 2.8).

$$CH_3OH(g) \longrightarrow 2H_2 + CO \qquad \Delta H^{\circ}_{298K} = 90.5 \, kJ/mol \qquad (2.11)$$

$$CH_3OH(g) + H_2O(g) \longleftrightarrow 3H_2 + CO_2 \qquad \Delta H^{\circ}_{298K} = 49.5 \, kJ/mol \qquad (2.12)$$
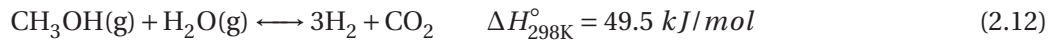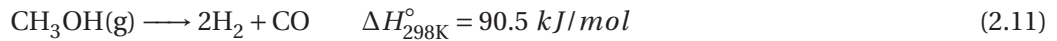
Ethanol is an interesting fuel option since it can be biochemically produced from biomass. Carbon deposition is an issue when ethanol is reformed internally. In fact, from the steam reforming of ethanol (Eq. 2.13) over Ni-YSZ, even at high steam content and high operating temperature, significant amounts of ethane and ethylene are produced due to the incomplete reforming [42]. The formation of these compounds are the major reasons for the high rate of carbon formation as they act as very strong promoters for carbon deposition.

$$C_2H_5OH + 3H_2O \longrightarrow 2CO_2 + 6H_2 \qquad \Delta H^{\circ}_{298K} = 174 \, kJ/mol \qquad (2.13)$$

Anaerobic digestion of biomass is another fuel option for SOFCs. Biogas consists principally of methane and carbon dioxide, typically 60 vol.% and 40 vol.%, respectively. In fact, the CO_2 present in the biogas stream can play an active role in reforming the methane via a reaction known as "dry reforming". An attractive feature of the dry reforming reaction is the utilization of CO_2. Dry reforming is endothermic and is favored at high temperatures. At elevated temperatures, parallel reactions such as methane cracking ($CH_4 \longrightarrow 2H_2 + C(s)$) and

Boudouard reaction ($2\,CO \longrightarrow CO_2 + C(s)$) occur, which both lead to carbon deposition.

$$CH_4 + CO_2 \longrightarrow 2\,CO + 2\,H_2 \qquad \Delta H^{\circ}_{298K} = 247\ kJ/mol \tag{2.14}$$

There are concerns about the utilization of biogas in a SOFC because of high risk of carbon deposition and the existence of contaminants [30, 43–45]. The high carbon content in biogas presents a substantial potential for carbon formation within the SOFC stack, which results in cell deactivation and stack failure. Biogas can be reformed over a catalyst (e.g. nickel) into a syngas mixture (H_2 and CO) using a reformer agent (e.g., steam). In order to mitigate the risk of carbon deposits, the CH_4-CO_2 mixture can be mixed with an appropriate oxidizer such as H_2O, or O_2.

2.3 Introduction to Biomass

Biomass is defined as biodegradable material from biological origin such as agriculture (including all vegetal matter and their derivatives), forestry, agro-industrial, animal by-products and municipal waste [46]. Biomass is the result of the photosynthesis process (Eq. 2.15), which is the reaction between CO_2 in air, water and sunlight. The process produces O_2 and the organic compounds that make up plant biomass. In other words, solar energy is stored in biomass as chemical energy. Biomass is considered a renewable energy source as long as it is based on sustainable utilization. If consumption is carried out at the same rate as new biomass is grown, there is in theory no net atmospheric CO_2 emission connected to the utilization of biomass material, therefore it is considered as a carbon neutral energy source.

$$6\,CO_2 + 6\,H_2O + Sunlight \longrightarrow C_6H_{12}O_6 + 6O_2 \tag{2.15}$$
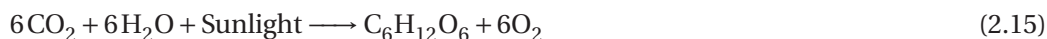
The main organic components of lignocellulosic biomass (dry) are cellulose (40 to 50 wt.% dry basis (db)), hemicellulose (20 to 40 wt.% db) and lignin (20 to 30 wt.% db) with the balance consisting of ash and extractives [47]. Ash is composed of inorganic compounds such as alkali metals, heavy metals, sulfur, chlorine and silicates. Extractives in wood include aliphatic, aromatic and alicyclic compounds. Table 2.1 gives an ultimate analyses for some biomass materials, presented as C, N, H, O and S and the ash content.

Table 2.1 – Typical lignocellulosic biomass composition (wt.%) [47].

Material	C	H	O	N	S	Ash
Wood (average)	51.6	6.3	41.5	0	0.1	1
Wheat straw	48.5	5.5	39	0.3	0.1	1
Barley straw	45.7	6.1	38.3	0.4	0.1	6
Rice straw	41.4	5	39.9	0.7	0.1	-
Lignite	56.4	4.2	18.4	1.6	-	5

2.3.1 Biomass to Biogas and Biosyngas

To utilize the chemical energy stored in biomass, a conversion technique must be applied to be able to exploit it. Direct combustion of biomass converts the stored chemical energy to heat and consequently this heat can be used for power production. There is also the possibility to convert solid biomass materials to gases, liquids or carbon rich solids which can be used later for heat and power production in gas turbines, fuel cells or combustion engines. There are two major conversion routes for biomass as shown in Fig. 2.9.
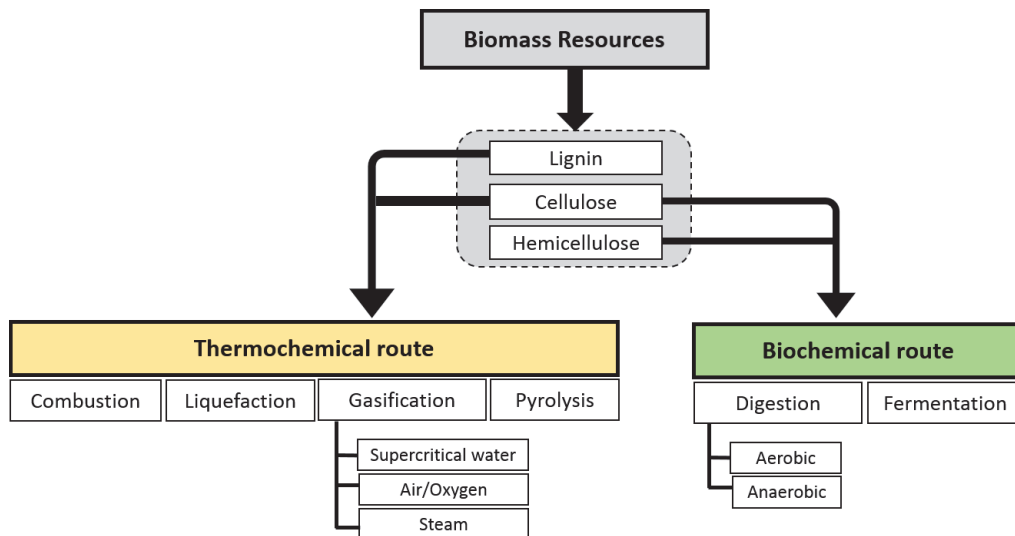
Figure 2.9 – Biomass conversion routes and processes, adapted from [48].

Thermochemical conversion techniques

In thermochemical conversion, the biomass is converted in part into gases, which are then synthesized into the desired chemicals or used directly [48]. Combustion, pyrolysis, liquefaction, and gasification are the common thermochemical conversion methods. Among these, gasification is considered as the enabling technology for modern biomass uses. In this process, biomass is converted to a combustible gas at high temperatures (800-1100 °C), when a controlled amount of oxidant such as O_2, air or steam is provided. Syngas or synthesis gas (preliminary consisting of H_2 and CO) from biomass gasifiers can be used for SOFCs.

There are several types of biomass gasifiers classified based on the movement of the fuel through the vessel, the operating pressure, temperature, the size and condition of the raw fuel [49]. Gasification is carried out generally in one of major types of gasifiers; fixed bed (up- or downdraft), fluidized bed and entrained flow. For a comprehensive list of gasification technologies refer to [50]. According to Knoef [50], 75% of existing gasifiers are downdraft, 20% are fluidized beds, 2.5% are updrafts and the rest are of various other configurations.

Fixed bed gasifiers are the most common gasifiers (Fig. 2.10). In updraft gasifiers the flows are counter-current, which means the air is passing through the biomass from the bottom and the combustible gases come out from the top of gasifier. The flows in downdraft gasifiers are co-current, both gas and feed travel downwards.

Thermochemical gasification of biomass generates a product gas, also known as biosyngas and it consists of H_2, CO, CH_4, CO_2, H_2O, N_2, higher hydrocarbons and impurities (e.g., tars, NH_3, H_2S and HCl).

Biomass $\xrightarrow{heat}$ Char + Liquids + Gases
Char + Gasification medium $\xrightarrow{heat}$ Gases + Ash
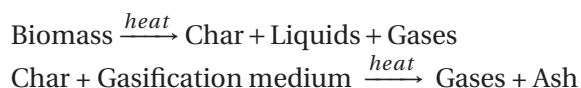
The composition of this gas varies with the characteristics of the gasification process such as operating conditions, gasification technology and feedstock. Table 2.2 lists the composition of gas produced from various sources for updraft and down draft gasifiers.
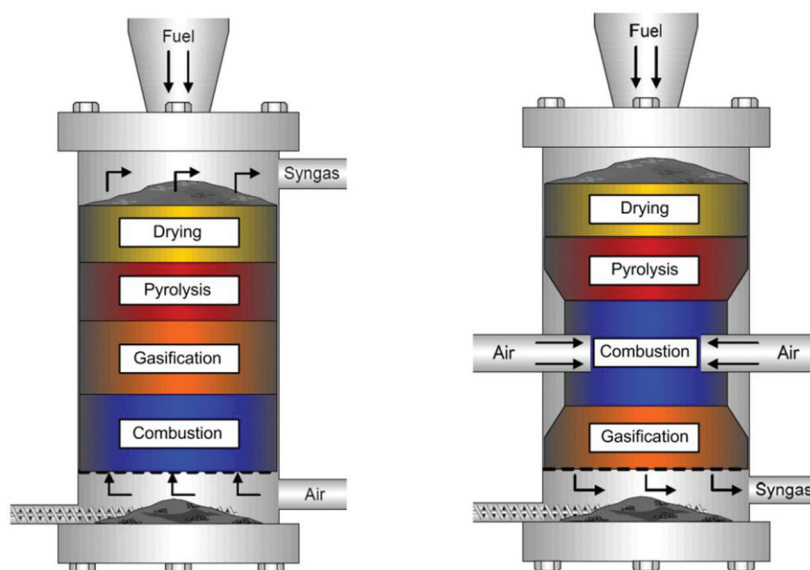
Figure 2.10 – Schematics of updraft (left) and downdraft (right) fixed bed gasifiers [51].

Biochemical conversion techniques

Biochemical conversion involves breaking down structural carbohydrates (e.g., the cellulose) using bacteria or enzymes into sugar, which can then be converted into biofuels [58]. In contrast to thermochemical processes, biochemical conversion processes are slow, but do not require much external energy. The common biochemical technologies are anaerobic digestion (or biomethanation) and fermentation.

Table 2.2 – Gas composition and tar content in the product gas from different biomass gasification under different conditions.

Biomass	Gasifier type	Gasification temperature (°C)	Gas composition (vol.%)	impurity (ppm)	Tars (g/Nm^3)	Reference
Woody chip coconut shell	up-draft	700-900	H_2 (22-27), CO (27-40), CH_4 (7-9), CO_2 (39-42)	H_2S (177), COS (49)	n.a.	[52]
Rice straw	up-draft	700-850	H_2 (6-10), CO (10-18), CH_4 (4), CO_2 (14-19), N_2 (46-63)	NH_3 (3100), Cl_2 (260)	0.47- 1.92	[53]
Cedar wood	up-draft	650-950	H_2 (30-50), CO (22-25), CH_4 (8-10), CO_2 (25-30)	H_2S (35-39), COS (< 2), HCl (80-112)	0.1	[54]
Agricultural residue	up-draft	800-820	H_2 (22-27), CO (27-40), CH_4 (7-9), CO_2 (39-42)	H_2S (2300), COS (200)	6.4- 12.4	[55]
Wood waste	down-draft	900-1050	H_2 (8-12), CO (15-22), CH_4 (1-3), CO_2 (5-8), N_2 (60-70)	n.a.	near 0	[56]
Hazelnut shells	down-draft	1000	H_2 (13), CO (23), CH_4 (4), CO_2 (11)	n.a.	near 0	[57]

Anaerobic digestion is a series of biological processes that produces a gas mainly composed of methane and carbon dioxide in addition to a solid residue [59]. Later in this chapter (section 2.4.1), biogas compositions including trace elements are provided. Biodegradable waste materials such as municipal solid waste, animal manure, food wastes, sewage and industrial wastes can be processed with an anaerobic digestion resulting in the production of biogas.

Fermentation is the other biochemical conversion method, in which a fraction of the biomass is converted into sugars using acids or enzymes. Yeasts are then used to convert the sugar into mainly ethanol. A variety of other fuels can be produced from waste resources including methanol, biodiesel, hydrogen and methane [60].

The use of biogas from anaerobic digesters for SOFCs is the interest of this thesis. In the following part more detailed information on the global production of biogas, potentials, and final uses are given.

2.3.2 Biogas Potential

The global biogas potential is estimated to lie around 10 PWh, 6.5% of the world total primary energy supply in 2012 [5]. In 2009, the European production of biogas was 93 TWh, with the following provenance: 52% from farm digesters, 36% from landfills and 12% from sewages [5]. In 2013, with an annual growth of 10%, the biogas primary energy production increased to 151 TWh [61]. This has been achieved with more than 14,500 biogas plants and around 7.9 GW of electricity generating capacity [62].

Compared to the 1990 value, there was a twenty-fold increase in biogas production. Biogas potentially accounts for nearly 7% of the overall renewable primary energy in Europe, but most of the potential remains unexploited. According to AEBIOM [63], the biogas potential in Europe for 2020 is about 40 Mtoe (equivalent to 465 TWh). However, it is worth mentioning that much of this potential comes from energy crops, which accounts for 80% of the total (the assumption is that 5% of arable land is dedicated to energy crops). Many anaerobic digesters have a mixed diet of organic waste (e.g., manure) and forage (e.g., maize or sweet sorghum silage) so that it is difficult to have detailed statistics on the current organic substrates used for biogas production.

A way to grasp the intrinsic potential of biogas resources is to look at per head (humans and other animals) biogas potential. For instance, the average citizen in developed countries uses almost 300 litres/day of water that ends up in the sewer [64]. Being the total suspended solid of sewage water 220 mg/l, roughly 60 g/person/day of putrescible organic matter (or sludge) are thus collected in the wastewater plant connected to the sewage system. A realistic methane yield from sludge is about 200 L of CH_4 per kg of dry sludge, resulting in about 20 L/person/day of biogas (assuming that 60 vol.% of biogas is CH_4). This biogas production corresponds to a LHV power of 5 W/person. A municipality of 100,000 people would thus entail a continuous biogas production rate of 500 kW. A 50% efficient SOFC plant running on sewage biogas would thus produce 250 kW of electric power in this case.

A similar calculus can be applied to animal farms. Manure from feedlot cattle has high nutrient value and is very suitable for use as an organic fertilizer. However, it can be converted into biogas, which can be burnt to generate electricity and heat, upgraded into bio-methane or feed it to a SOFC. Using feedlot manure to create bioenergy has many benefits, such as: recovering energy from waste, reducing odor problems, reducing potential for groundwater contamination, reducing the amount of waste that needs to be disposed of and many other advantages.

Quality and quantity of produced livestock manure is variable according to type of feed and livestock living conditions. Fig. 2.11 shows the daily input and output of a typical 450 kg cattle. A cow typically consumes food 2.5 to 3% of its body weight and it gains weight 1 to 1.6 kg per day, the rest leaves the animal body in the form of manure. Usually, manure is 85 to 90% water and the rest is solid material (dry matter). The technical report by Mibrandt [65] showed that 0.26-0.28 m^3 biogas can be produced from each kilogram of dry cow manure. Considering biogas contains 50-60% CH_4, 0.4-0.5 m^3 of methane can be produced by each cattle daily.

2.3.3 Biogas Final Use

Biogas is a renewable energy vector that can be used to generate electricity and heat through cogeneration. Biogas can also be burnt in boilers to recover thermal energy only. In 2013 the EU-28 biogas electricity output stood at about 4.5 Mtoe, which corresponds to almost

Manure
Faeces & urine
5 to 6% of body weight per day
Total manure: **27 kg**
Water portion: **24 kg**
Dry matter: **3 kg**

Water intake:
30 to 80 kg/day

Feed in: 2.5 to 3% of
body weight
12 kg/day
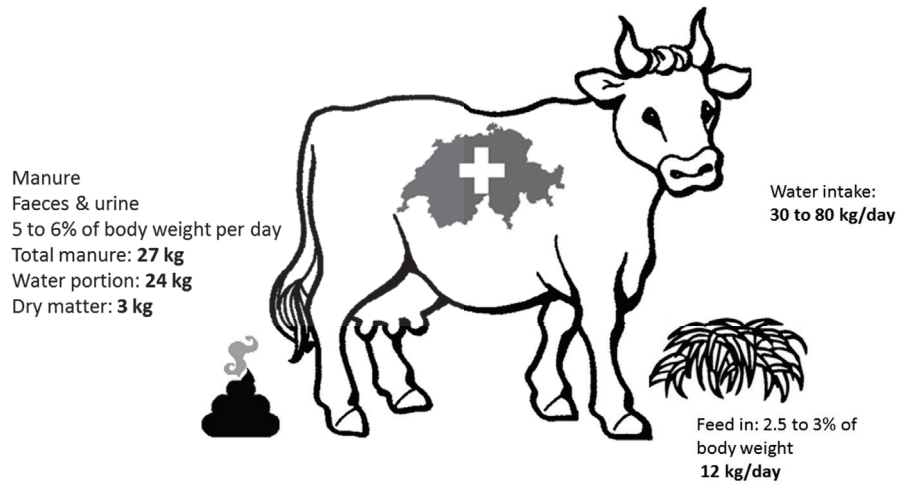
Figure 2.11 – Manure production from a 450 kg cattle (adapted from [66]).

52.3 TWh. Of this amount, about two thirds were produced in CHP mode. Heat provided to district heating networks or industrial units was less than 0.5 Mtoe (equivalent to 5.8 TWh). Self-use of thermal energy accounted for another 2 Mtoe (equivalent to 23.3 TWh) [67].

Great impetus is now being given to biogas upgrading to methane fuel (also called 'biomethane'). Different technologies can be applied to remove CO_2 and other minor impurities/gases from the biogas stream (e.g., water or water/solvent scrubbing and membrane technology) in order to obtain a purified stream containing a high concentration of CH_4 (i.e., >95 vol.) compatible with the gas grid or for gas vehicles. Hence, biomethane can be either injected into the grid or used as local transportation fuel. Biogas is exploited conventionally in Internal Combustion Engines (ICEs). The electrical efficiency of ICEs can exceed 40% for MW-size installations and is maximally 43%. However, the efficiency is lower for sub-MW plants [68]. The electrical efficiency of ICEs is surpassed by high temperature fuel cell generators like molten carbonate fuel cells (MCFC) and SOFC. Especially, the SOFC technology is the most promising one because the highest electrical efficiency can be realized [69].

In the framework of the EU-funded project SOFCOM, a 2 kWe SOFC stack was operated with sewage biogas (Fig. 2.12). The integrated biogas SOFC plant consisted of an innovative treatment of the anode exhaust gas via oxy-combustion of the same and subsequent water vapour condensation that allowed for the recovery of a high-purity CO_2 exit stream [70]. The CO_2 was recycled to a photobioreactor in which micro-algae biomass is harvested. In this way, a closed carbon-cycle was obtained in which organic carbon from sewage sludge is eventually recycled into a fuel again (algae biomass). In the photobioreactor, micro-nutrients (nitrates and phosphates) are taken from wastewater that is circulated in a semi-closed loop. Hence, a further biological water treatment process is achieved while growing biomass.
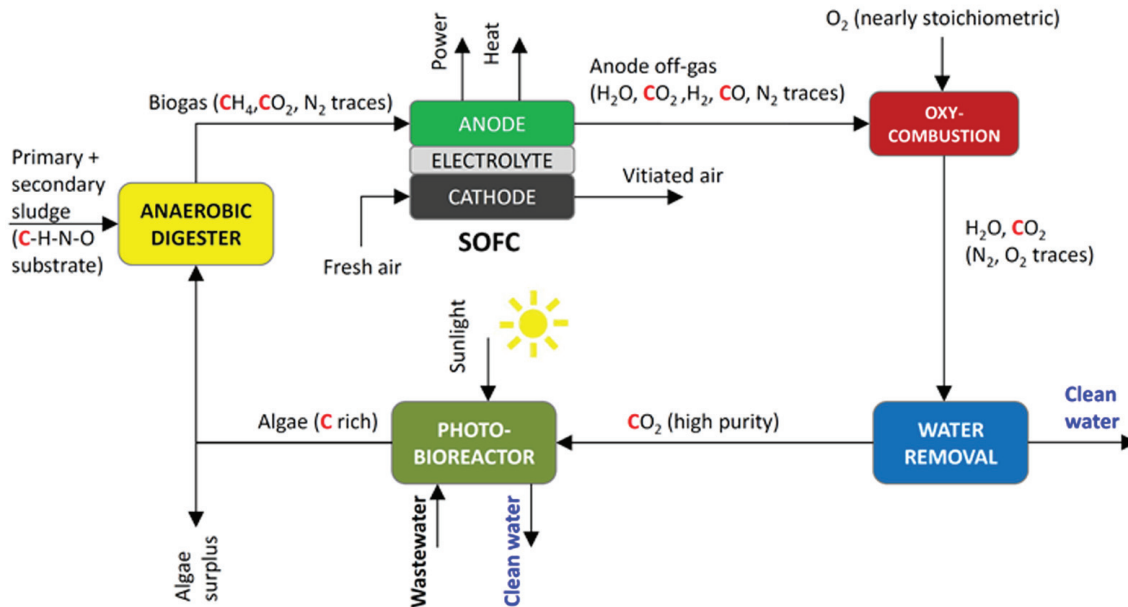
Figure 2.12 – Carbon recycle concept in the SOFCOM plant.

2.4 The Issue of Contaminants

In the following part a more specific motivation for the research conducted in this thesis is given, reasoning why the specific topics were chosen and why they are important to the scientific community. As stated in the previous section, there is a great potential in combining the plants with SOFC systems. However, there are issues related to the use of biogas due to the presence of impurities. The origin of contaminants in anaerobic digestion biogas, type, and amounts of contaminants are presented in the following section. Afterwards, the state-of-the-art effects of these impurities on the performance of SOFCs are briefly discussed.

2.4.1 The Origin and Type of Contaminants

Biogas produced in an anaerobic digester is typically composed of 50-75 vol.% CH_4, 25-45 vol.% CO_2, 1-2 vol.% H_2O and 1-5 vol.% N_2 [61]. Besides the main components, biogas contains a large variety of trace impurities such as hydrogen sulfides, siloxanes, aromatics and halogenated compounds. Although the amount of trace compounds is low compared to the main components, they can affect the performance of SOFCs and in fact, the main issue with biogas is dealing with contaminants. Several factors affect the concentration of these impurities e.g. temperature, pressure, type/origin of waste, age of waste. Table 2.3 shows typical untreated biogas impurities concentrations for landfill gas (LFG) and anaerobic digestion gas (ADG).

An option in using biogas is gas clean-up. There are technologies which can remove harmful impurities from biogas that will meet the cleanliness requirements of SOFC stacks, but the costs are high. The clean-up capital cost is currently estimated as 500–1,000 \$/kW (installed cost, ref. year 2015). A capital cost <500 US\$/kW is considered a near term target, while the long term target sets the clean-up cost below 200 US\$/kW [71].

Table 2.3 – Typical untreated biogas contaminants concentrations (ppmv) for ADG and LFG

Biogas	Sulfur compounds		Siloxanes	Halogenes substances		Halocarbons	VOCs	Ref.
	H_2S	Other S-compounds		HCl	HF, HBr and etc.			
ADG	121	0.5	0.24- 2.3	0.2-1.4	1	0.16	1.6	SMAT
ADG	24- 63	n.a.	0.1- 0.7	0.2- 0.8	n.a.	n.a.	0.7- 3	[61]
ADG	1.8 - 104	0.15- 0.66	0.6- 1	n.a.	n.a.	<0.1	0.4- 1.7	[72]
ADG	80- 130	n.a.	Up to 2.9	n.a.	n.a.	1	n.a.	[73]
LFG	77- 3400	n.a.	2	n.a.	n.a.	6- 14	100- 300	[74]
LFG	63- 5400	7.5- 19	Up to 0.7	n.a.	n.a.	7	n.a.	[75]
LFG	150- 280	n.a.	0.5- 0.7	11 - 20		10	86- 150	[43]

Sulfur

The main sulfur compound in biogas is hydrogen sulfide (H_2S). Other S-containing compounds (e.g., mercaptans such as CH_3SH) that come from S-bearing organic matter can also be found in biogas. Depending on the composition of the organic matter, the H_2S concentration in biogas can vary by 3 orders of magnitude (100 to 10,000 ppm) [76]. This contaminant is highly undesirable in fuel cell systems due to deactivation of the anode catalyst.

Siloxanes

Volatile organic silicon compounds (VOSiC), also known as volatile methyl siloxanes (VMS) or simply siloxanes, are recognized as the most undesirable compounds in the AD biogas and LFG. Siloxanes originate from silicone based compounds which are more often found in consumer products which end up in sewers (e.g., cosmetics, personal care products, adhesives and coatings, sealants). Siloxanes are indeed the building blocks of silicones. Cyclic siloxanes are given the letter D, whereas the linear compounds are designated with the letter L. The number following the letter refers to the quantity of Si atoms in the molecules [77].

Their concentration in biogas has been reported to be in the range of 2-30 mg/Nm^3 [77] and 4-80 mg/Nm^3 [78] according to site and season variability. According to literature, the most found compounds in sewage biogas are cyclic volatile polydimethylsiloxanes (D4, D5), with the D5 concentration being higher than D4 (Fig. 2.13).
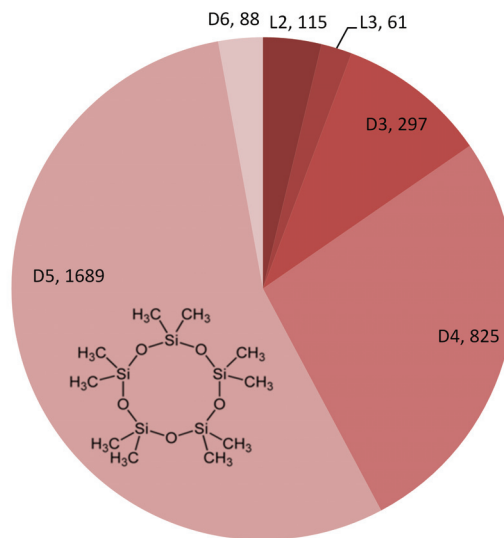
Figure 2.13 – Average concentration (ppbv) of siloxanes measured in ADG from WWTP [78].

Halogenated compounds

Halogenated compounds contain one or more halogen atoms (fluorine, chlorine, bromine or iodine) such as dichloromethane (CH_2Cl_2), chlorobenzene (C_6H_5Cl) and chloroethane (C_2H_5Cl). They are often found in landfill gas, but rarely in biogas from digesters of waste water treatment plants. During the combustion process halogens are oxidized and the combustion products are corrosive, especially in the presence of water. Aromatic and chlorinated compounds are widely used in industry. For instance, vinyl chloride is used often in polymer polyvinyl chloride (PVC), chloromethane is a common solvent and fluorinated compounds have been used as refrigerating aggregates, foaming agents and solvents.

Volatile organic compounds (VOCs)

VOCs are compounds defined to contain at least one carbon and one hydrogen atom in their molecular structure such as aromatics, hydrocarbons, aldehydes, alcohols, carboxylic acids and amines. Concentration of VOCs is higher in landfill gases compared to anaerobic digester biogas. In fact, VOCs are an intermediate product, generated by methanogenic bacteria during the transformation of organic materials into biogas. The more effective the methanogenic decomposition, the lower the VOCs in the final biogas composition. The type of VOCs depends on the source of biogas. For instance, p-cymene is the most common VOC in biogas generated from household waste as this compound can be found in food products such as butter, carrots, orange juice, oregano and nearly all spices [79].

2.4.2 Siloxane Poisoning

K. Haga et al. [80] investigated the effect of D5 at different temperatures (800 °C to 1000 °C) on the cell performance and observed a marked degradation. Their post-mortem analysis revealed the plugging of the anode structure with $SiO_2(s)$ deposits. They concluded that the presence of siloxane can cause deposition-type degradation, associated with the formation of $SiO_2(s)$. However, there was a lack of information on the effect of this impurity at lower temperatures, the trend towards different concentrations and more importantly the SOFC stack behavior.

Chapters 4 and 5 investigate in depth the effect of D4 on the performance of anode supported Ni-YSZ, single cells and short stacks.

2.4.3 Chlorine Poisoning

The effect of HCl and other chloride compounds like CH_3Cl and Cl_2 on SOFC performance has been addressed in several studies [81–84]. Table 2.4 summarizes studies on the characterization of different anode materials upon exposure to Cl-containing fuels. Li et al. [81] compared the performance degradation due to exposure to chlorine compounds HCl, Cl_2 and CH_3Cl. No performance degradation was observed up to 8 ppm of these compounds and at higher concentrations, the degradation was more severe in the case of Cl_2 and CH_3Cl compared to HCl.

Sasaki et al. [83] evaluated the poisoning effect of Cl_2 from 5 to 1000 ppm at 800 °C for the duration of 150 h. They observed continuous degradation and almost constant degradation rate of cell voltage at concentrations above 100 ppm of Cl_2. Trembly et al. [84] tested a Ni–YSZ anode on electrolyte supported cells using syngas with 20 and 160 ppmv HCl. Their results showed an excessive degradation rate in cell performance of around 17% and 26% over 100 h, respectively, and was believed to be due to the formation of nickel chloride. The results also implied that this chloride phase is not stable, because of the observed reversibility of the poisoning caused by HCl. Adsorption of chlorine onto Ni, reducing the TPB, was postulated as another explanation. Xu et al. [85] also proposed the chemisorption of HCl on Ni and the chlorination of the Ni surface as possible mechanisms. They mentioned however that the formation of solid nickel chloride is energetically unfavourable.

According to the elementary reactions in the Ni-YSZ anode, $H_2(g)$ adsorbs dissociatively on Ni surfaces and then H_{ad} reacts with oxygen ions at the TPB to form $H_2O(g)$ (Eq. 2.16).

$$2H_{ad} + O^{2-} \longrightarrow H_2O(g) + 2e^- \tag{2.16}$$

If chlorine compounds are contained in the fuel feed, the adsorption of HCl on Ni surfaces occurs (Eq. 2.17)

$$HCl(g) \rightleftharpoons Cl(ad) + 0.5H_2(g) \tag{2.17}$$

It has been reported that the presence of electronegative species such as Cl_{ad} may hinder the adsorption of H_2 on Ni surfaces, i.e. reduce the electrochemical reaction rate. According to Trembly et al. [84], the adsorption of chlorine onto Ni surfaces blocks possible reaction sites at the TPB, which may prevent the electrochemical reaction (Eq. 2.16) and lead to an increase in anode overpotential. This blockage is a continuous process and the cell performance degrades with time.

Haga et al. [82] investigated the microstructural changes of Ni-YSZ anode following exposure to chlorine compounds. They observed significant effects both near the anode surface and in the middle of the anode layer. They concluded the change to be due to the formation of $NiCl_2(g)$ (Eq. 2.19) under the prevailing experimental conditions. They mentioned this adsorption-desorption mechanism is a partially reversible poisoning process. The partial recovery was explained to be due to gaseous $NiCl_2(g)$ transported out of the fuel cell, which decreases the amount of Ni electrode catalyst and active sites.

$$Ni(s) + 2HCl(g) \rightleftharpoons NiCl_2(g) + H_2(g) \tag{2.18}$$

Chapter 6 evaluates the poisoning effect of hydrogen chloride (HCl) on state-of-the-art Ni anode-supported SOFCs at 750 °C using either hydrogen or syngas fuel. Experiments were performed on single cells and short stacks and HCl concentration in the fuel gas was increased from 1 ppmv up to 1,000 ppmv at different current densities. At the end of chapter 6 the degradation mechanism is illustrated.

2.4.4 Sulfur Poisoning

The interaction between sulfur-containing molecules and Ni-based anode materials is an important research topic in SOFCs. There are several studies concerning the loss in SOFC performance upon sulfur poisoning as a function of temperature, H_2S concentration, time, current load and anode material [20, 30, 86–88]. H_2S, even in small amounts (ppb-level), deactivates steam-reforming and water gas shift reactions. Ni-YSZ anode supported SOFCs have limited tolerance towards sulfur compounds [43, 83]. Table 2.5 summarizes studies on the characterization of different anode materials upon exposure to H_2S-containing fuels. The performance degradation is a result of an increase of the internal resistance of the SOFC.

The poisoning is sometimes reported as a two step process; an initial rapid drop in the performance followed by a slower prolonged degradation, as shown in Fig.2.14. However performance stabilization after the fast initial drop is also observed. The initial performance drop is due to dissociative chemisorption of hydrogen sulfide on nickel active sites and blocking of three phase boundary for hydrogen oxidation. The reaction is the following:
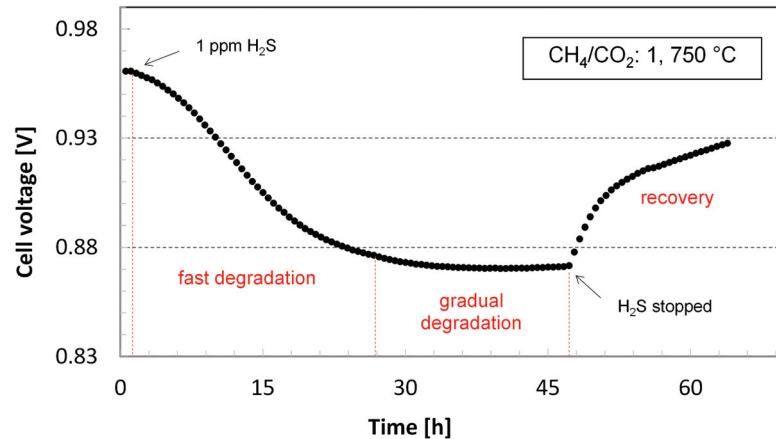
$$H_2S + Ni \rightleftharpoons NiS + H_2(g) \tag{2.19}$$

Figure 2.14 – Sulfur poisoning and regeneration processes of Ni-YSZ anode exposed to 1 ppm H_2S.

H_2S has unshared e^- pairs, which can lead to very strong chemisorption on the metal surface. The cell performance can be reversible, depending on exposure concentration and duration. Reversibility has been observed in the case of exposure to concentrations below 50 ppmv and for short duration [88]. Zha et al. [89] evaluated the cell performance recovery after exposure to 2 and 50 ppmv H_2S at 800 °C and observed recovery of 99% and 96% respectively, 50 h after stopping the H_2S exposure.

Y. Shiratori et al. [44] showed that 1 ppm H_2S contamination of biogas caused about 9% voltage drop and about 40% decrease in the reaction rate of internal dry reforming (at 1000 °C, under 200 mA/cm^2, CH_4/CO_2 = 1.5): in fact, H_2S, even in small amounts (ppb-level), deactivates steam-reforming and water gas shift reactions. This degradation was reversible and the performance was stable after stopping the sulfur supply. Hagen et al. [30] observed a significant irreversible degradation in the performance when the cell was poisoned with 2 ppmv H_2S over 500 h under 1 A/cm^2 current load. At higher H_2S concentrations (>100 ppmv), sulfur will react with nickel and bulk sulfidation (NiS, Ni$_3$S$_x$) occurs, causing irreversible damage to the anode catalyst.

The initial drop in power upon exposure to H_2S has been the focus of most studies in the literature [90, 91]. Papurello et al. [87] quantified and correlated the surface coverage of sulfur on nickel-based anodes to sulfur concentration in the fuel with experiments performed both on single cell and stack. Using the experimental data, a Temkin-like adsorption isotherm was used which describes well time-to-coverage, and which is essential in order to determine the first degradation time. Results showed that, in anode-supported cells, sulfur contamination affects the entire available Ni surface and not just the TPB. Therefore a wide deactivation of the Ni anode is expected also involving sites for heterogeneous catalysis (i.e., those sites involved for chemical reactions of internal reforming and water gas shift).

In most of the investigations, H_2S is chosen as the sulfur model compound as it is by far the most frequent sulfur molecule in gasified biomass, coal gasification and biogas. However, a variety of sulfur containing hydrocarbons are found in biogas and bio-syngas [92], such as thiophenes and benzothiophenes. They may be critical since they are not filtered to 100% [93]. Therefore, there was a need to investigate the effect of such compounds on the performance of SOFCs. **Chapter 7** investigates the poisoning effect of thiophene on the performance of AS Ni-YSZ SOFCs, short and long term exposures.

Table 2.4 – Summary of studies involving exposure to chlorine compounds.

References	Anode	Fuel gas	T (°C)	Conc. ppm	Duration	Observations
J.P. Trembly et al. [84]	Ni-YSZ	Coal syngas	800, 900	20, 160 HCl	100 h	Degradation is associated with increase charge transfer resistance. Adsorption of chlorine on Ni surface is the possible degradation mechanism.
K. Haga et al. [82]	Ni-ScSz	3% humidified H_2	800	5, 50, 1000 Cl_2	150 h	Microstructure change due to formation of Ni nanoparticle, probably via $NiCl_2$(g) sublimation.
C. Xu et al. [85]	Ni-YSZ	Coal syngas	800, 850	100 HCl	500 h	Chemisorption of HCl on Ni and the chlorination of the Ni surface as possible mechanisms.
Li et al. [81]	Ni-YSZ	H_2	750, 850	1- 8 HCl, Cl_2, CH_3Cl	10 h	No performance degradation up to 8 ppmv. Degradation is more severe in the case of Cl_2 and CH_3Cl.
Bao et al. [94]	Ni-YSZ	Coal syngas	750, 800	40	120 h	No significant degradation was observed during 100 h testing
Marina et al. [95]	Ni-YSZ	Coal syngas	650- 850	100- 800	150 h	Degradation is attributed to adsorption of Cl species onto nickel surfaces. No evidence of microstructural changes or formation of new solid phases.

Table 2.5 – Summary of studies involving short and long-term sulfur poisoning tests.

References	Anode	Fuel gas	T (°C)	H_2S conc. (ppm)	Duration	Observations
Ishikura et al. [96]	Ni-YSZ	54% H_2, 23% H_2O, 23% N_2	900	0.1 - 20	800 h	The first-step degradation was recovered completely, but the second-step recovered partially due to nickel sulfide formation.
Grgicak et al. [97]	Ni-YSZ, Co-YSZ	H_2 and CH_4	850	100	140 h	Ni- and Co- based anode were compared. Dense metal sulfide surrounded by YSZ formed, stable performance achieved.
Zhang et al. [98]	Ni-YSZ, Ni-GDC	H_2	800	5 - 700	2 h	Ni- GDC is more tolerable towards sulfur. Significant morphology change on Ni as well as GDC but not on YSZ.
Brightman et al. [99]	Ni-CGO	49% H_2, 49 % N_2, 2% H_2O	700, 750	0.5 - 3	5 - 8 h	Full recovery of sample observed for 0.5 ppmv but at higher concentration, a secondary phase formed and a change in microstructure.
Zha et al. [89]	Ni-YSZ	50 H_2, 1.5% H_2O, 48.5% N_2	900	2, 50	220 h	Higher degradation at lower temperatures. Higher cell operating temperature and larger cell current density accelerated the recovery process.
Sasaki et al. [83]	Ni-YSZ	50% pre-reformed CH_4	800	5	3000 h	Cell degradation rate with 5 ppmv H_2S was 0.68%, slightly higher than the value without H_2S of 0.3% per 1000 h
Trembly et al. [100]	Ni-GDC	Coal syngas	750	200 - 240	580 h	No major degradation for long term test. Change in morphology was observed.

2.5   Summary

This chapter consisted of three main sections. Section 2.2 introduced SOFCs with an overview on the anode degradation mechanisms. Fuel flexibility was explained as a particular advantage of this type of fuel cells, which made a bridge to the section 2.3. This section presented biomass and in particular biogas and its potential as fuel for SOFCs. The last part of this chapter (section 2.4) focused on degradation issues related to the existence of impurities in biogas. At the end of this chapter, a literature review was given on the state-of-the-art knowledge of the effect of more pronounced biogas impurities on the performance of SOFCs.

A brief summary of the main points reviewed in this chapter are as follows:

- SOFCs are high temperature fuel cells and they can be operated on conventional fuels (e.g., natural gas, gasoline and diesel) and biofuels (biogas, gasified biomass and biodiesel). With such flexibility, SOFCs offer great promise as a clean and efficient device for directly converting chemical energy to electricity while providing significant environmental benefits.

- Anode degradation mechanisms were classified as intrinsic and extrinsic sourced degradations. Several examples were provided to explain these terms.

- Biomass and its conventional routes (e.g., thermochemical and biochemical) to biosyngas were described and compared. The main gas compositions and trace elements of biosyngas from the different routes were presented.

- Among the various biofuels, biogas is considered a promising raw fuel to be used as fuel for SOFC applications. A brief literature review on the biogas potential and its final use was given.

- In addition to the main components, methane and carbon dioxide, biogas contains various harmful trace compounds. Typical untreated biogas contaminants concentrations for ADG and LFG were shown and their origins were explained.

- The effect of siloxanes on the performance of SOFC single cells, stacks and stack components is not clear.

- The literature review on the effect of chlorine compounds presented the proposed degradation mechanisms but none of them were confirmed. There is lack of information on the effect of this impurity on the stack performance.

- Sulfur is known as the most common poisoning compound for the anode catalyst materials. Many studies also show the degradation of the cell power when the cell is exposed to H_2S. However, there is lack of information on the effect of organic sulfur compounds on SOFCs.

3 | Experimental

This chapter presents the technical aspects of the experiments performed in this work. In section 3.1 the test bench, single cell setup and control system are described in detail. Section 3.2 presents the methods used to analyse the generated data.

3.1 Test Bench

The experimental test bench built up for this thesis consists of a section to prepare the feed gas with contaminants, the transfer lines to and from the fuel cell and the fuel cell set-up itself, as can be seen in Fig. 3.1.
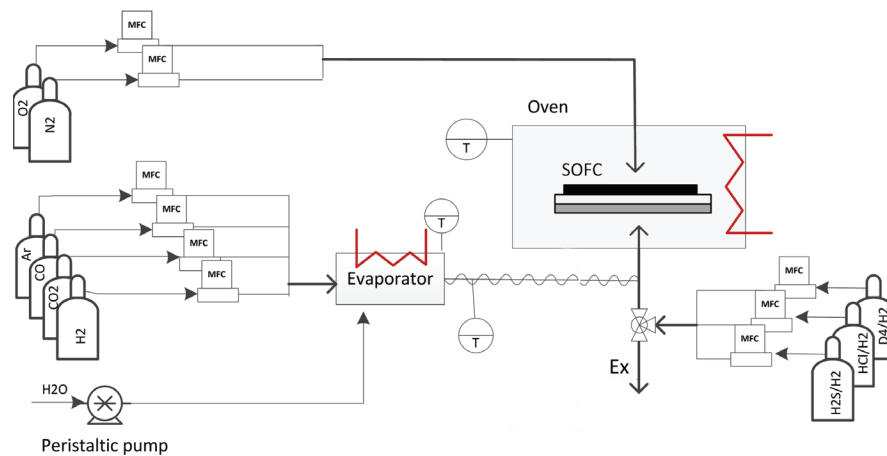
Figure 3.1 – Sketch of the single cell test bench allowing the feed of tuned gas mixtures (with ppm-level of relevant biofuel contaminants) to the fuel anode catalyst.

The feed gas section consists of a set of Mass Flow Controllers (MFC, Vögtlin Instruments AG) used on bottled gases, mixed together. The gas supply consisted of gas bottles containing pure gas (the quality is shown in brackets in molar fractions): H_2 (pure, via water electrolysis), CO (99.997%), CO_2 (99.998%), CH_4 (99.95%), Ar (99.998%), N_2 (99.998%), O_2 (99.998%).

The contaminant gas section contains 4 MFCs (Bronkhorst) and the gas bottles are pre-mixed (calibrated): 20 ppm H_2S in H_2 (Messer), 20 or 500 ppm HCl in H_2 (Carbagas, saphir class[1]), 20 ppm D4 siloxane in H_2 (Carbagas, saphir class) and 50 ppm C_4H_4S in H_2 (Carbagas, saphir class). Deionized water is fed either by the evaporation method detailed in section 3.1.3 or using a peristaltic pump. All the lines and fittings exposed to sulfur and hydrogen chloride have been treated with a quartz glass coating (SilcoNert^{TM} 2000) to ensure inertness. This surface treatment eliminates surface adsorption of active compounds on steel and glass surfaces.

The test bench control has been programmed using Labview^{TM} software. Efforts have been made to simplify the controlling system. The interface has the ability to control MFCs, the data acquisition system and electronic load. The interface can acquire the IV curve and save the recorded data (Fig. 3.2).
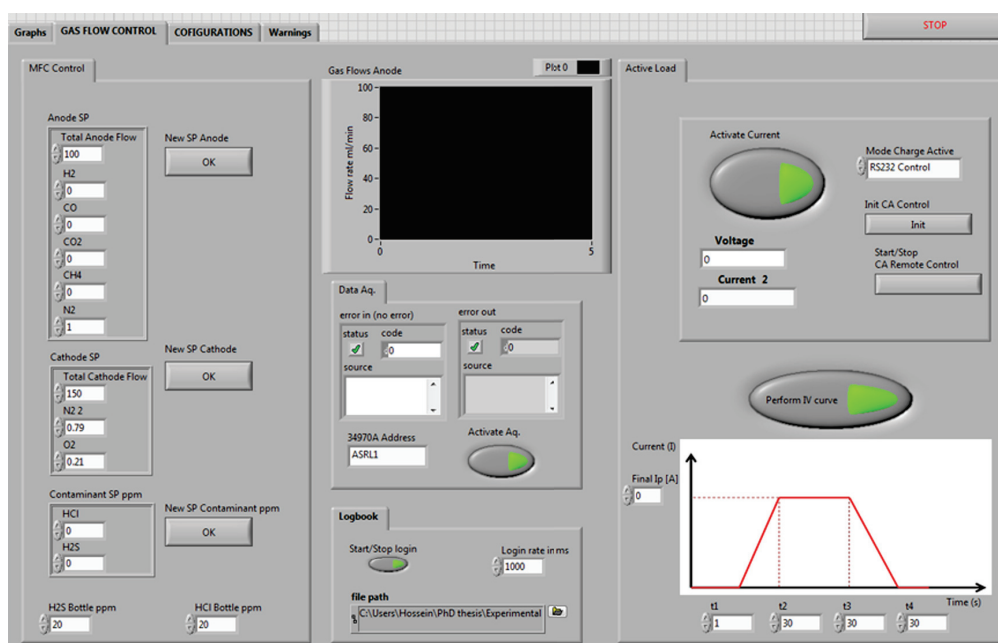
Figure 3.2 – The Labview interface that was used to control the test bench.

3.1.1 Single Cell Setup

A metallic housing setup was developed and used to mount the cell in a furnace, as shown in Fig. 3.3. The fuel was fed to the cell through a ceramic tube (Al_2O_3) to prevent possible reactions between the fuel and metallic compounds at elevated temperatures. The air was injected through a tube (high temperature austenitic SS 1.4841) from the top flange (inconel 601). The air feed tube and top flange were slurry-coated with $MnCo_2O_4$ spinel to reduce Cr

---

[1] Saphir class is a calibrated gas mixture with certificate, deviation ± 5% rel. with uncertainty of ± 2% rel..

evaporation. An alumina felt was used to distribute the air flow and a gold mesh as current collector at the cathode side. Nickel foam of thickness 0.5 mm and diameter of 5 cm was used as current collector at the anode side. The anode exhaust gases were sent out through a vent.
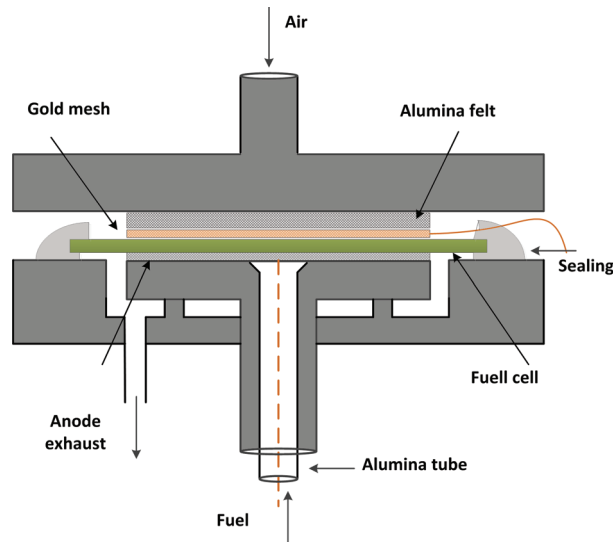
Figure 3.3 – Schematic diagram of experimental setup.

3.1.2 Short Stack

SOFC stacks consisting of a series of 11-cells each were used for the experiments. All the stacks were provided by Topsoe Fuel Cell (Denmark). Anode-supported type cells with a Ni anode are used in these stacks. The stack was operated at a fixed nominal operating point corresponding to a current of 20 A and a fuel utilization (FU) of 60%. A schematic of the experimental set-up is provided in Fig. 3.4. A mild insulation surrounds the bare stack thus allowing it to be operated in an atmosphere heated to about 450 °C.

3.1.3 Adding Impurities to the Fuel Stream

There are a variety of methods to prepare a gas mixture with trace concentration of a compound in the main fuel stream such as pre-mixed gas cylinders, permeation, injection and evaporation methods, described below.

Gas cylinders

A common way to create a gas mixture is to attach a mass flow meter to a gas cylinder and control the gas flow rate. With this method a wide range of concentrations, from high to low concentrations, using multiple-step dilution, can be prepared. Disadvantages of such a method are the high cost of gas bottles and the safety issues related to the high pressure storage. However, in this thesis, D4, H_2S, C_4H_4S and HCl were prepared in gas cylinders.

Figure 3.4 – Schematic diagram of the Topsoe short stack

Evaporation method

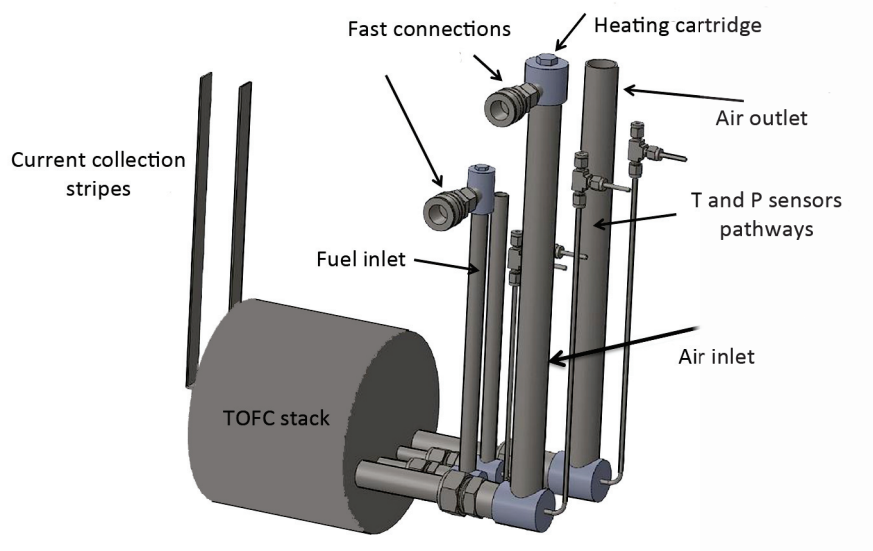In this method a carrier gas is passed through the liquid form of the impurity of interest, evaporating some of the liquid and joining the stream of gas being passed through it. This method is useful for adding single volatile liquids to the fuel gas stream. The vapor pressure of the compound is the determining factor and variation of temperature can be used to adjust the target concentration. The accuracy of this method is low compared to other techniques (± 5-15%) [101], but the error can be minimized for compounds with low vapor pressure. In this thesis, the addition of 3-4% water to the fuel stream was carried out using this method.

Injection method

A liquid or gas can be injected into a flow using a syringe pump. This device is a motor-driven system and the injection rate can be controlled changing its motor speed rate. The accuracy of this method depends on the accuracy of the injection device. In the case of liquid, normally an evaporator is used to vaporize the injected liquid before mixing it with the main gas flow. The concentration can be controlled from a few percent down to ppm, depending on the injection and the main gas flow rate. This method is used here in order to evaluate the effect of toluene on the performance of Ni-YSZ at the level of 50-5000 ppm.

Permeation tubes

The liquefied form of the gas of interest placed inside the permeation tube permeates through the walls of the tube. With this method very low concentration mixtures (even ppb) can be achieved at high accuracy compared to the other techniques (± 2-5%) [101]. Temperature,

pressure and gas flow influence the uncertainty of this method. A wide range of concentrations can easily be generated by varying either the dilution flow rate, temperature set point, length and thickness of the tube. The method was not used here.

3.2 Analytical Tools

In the following section the analytical tools that have been used to measure the degradation of SOFC performance are presented. The increase in Area Specific Resistance (ASR) is often used to express the degradation for single cell tests. There are several analytical tools to measure the ASR such as electrochemical spectroscopy and current-voltage characterization.

3.2.1 Current-Voltage (IV)

The IV curve is a common characterization technique used to calculate the ASR. There are two ways to read the ASR from a IV curve: the total ASR and the local (or differential) ASR as shown in Fig. 3.5. Careful attention must be paid when comparing IV curves as the measured voltage degradation depends on the current density (e.g., $\Delta V_2 > \Delta V_1$ in Fig. 3.5).

3.2.2 Voltage over Time

Cell polarisation over time is a common way to evaluate the performance of SOFCs single cells and stacks. In this method, the voltage is monitored over a period of time, which can span from several hours to more than a year. As illustrated in Fig. 3.6, the slope corresponds to the cell performance degradation rate. A linear degradation can be seen in this figure and if we consider that this trend stays linear during the first 100 h, the degradation rate is 70 mV/100 h.

3.2.3 Electrochemical Impedance Spectroscopy (EIS)

Electrochemical Impedance Spectroscopy (EIS) is a prevailing technique for the characterization of electrochemical systems. In contrast to IV curves, where only the overall loss of a cell can be identified, the EIS can analyse complex electrochemical systems such as SOFCs [102].

In this method, a small amplitude sinusoidal excitation signal applies to the system under investigation and measure the response. In measurements, in response to a sinusoidal voltage signal, V=V_0sin(ωt), an AC current is generated, I=I_0sin(ωt + $\phi(\omega)$), with the same frequency as V. In these equations, ω=2πf [s^{-1}] represents the angular frequency, $\phi(\omega)$ the frequency
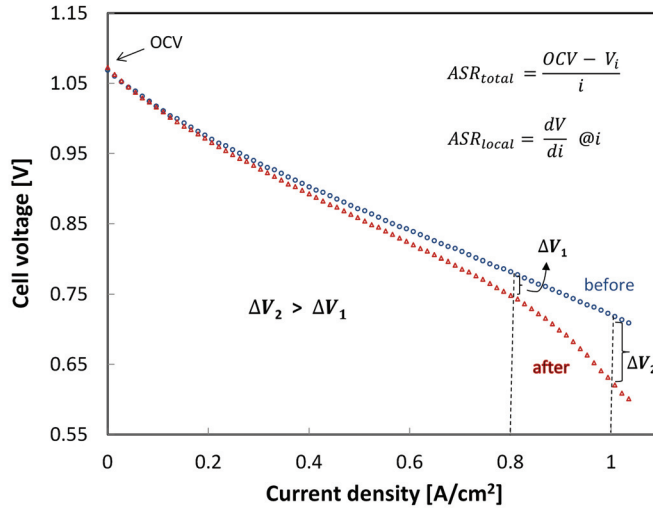
Figure 3.5 – IV curves of an SOFC before and after exposure to an impurity emphasizing the mathematic-physical dependency of the voltage degradation on the current density for a given ASR degradation.
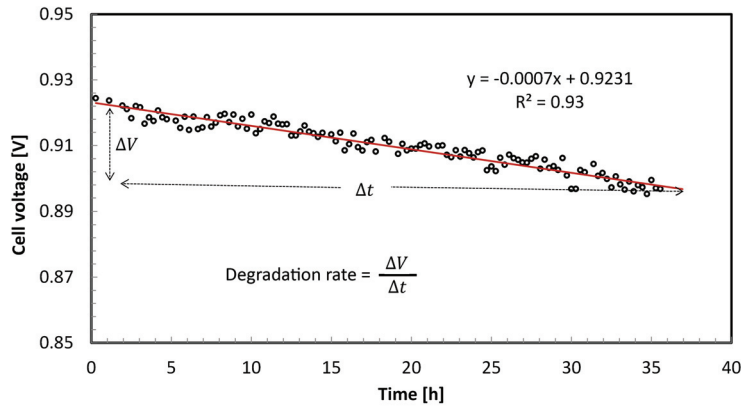
Figure 3.6 – Polarisation over time. The slope shows the degradation rate.

dependent phase shift between voltage and current. The impedance can be calculated from the ratio between the voltage and current as seen in Equation 3.1, where $\phi = \tan^{-1}\frac{Z_{img}}{Z_{real}}$ and $j = \sqrt{-1}$.

$$Z(\omega) = \frac{V}{I} = Z_0(\omega)\frac{sin(\omega t)}{sin(\omega t + \phi(\omega))} = Z_0 e^{j\phi} = Z_{real} + jZ_{img} \tag{3.1}$$

EIS measurements can be presented as Z_{img} versus Z_{real} by varying the frequency. The resulting curve is known as Nyquist plot as shown in Fig. 3.7. One advantage of the Nyquist plot is that the ohmic and polarisation resistance can be read directly. The high frequency intercept with the real axis corresponds to the ohmic resistance (R_s), whereas the intercept at

the lower frequency is the polarisation (R_p) plus ohmic resistance. Useful information can be extracted from the shape of the impedance plot such as the operating conditions, the material and the microstructure of the subject under study.
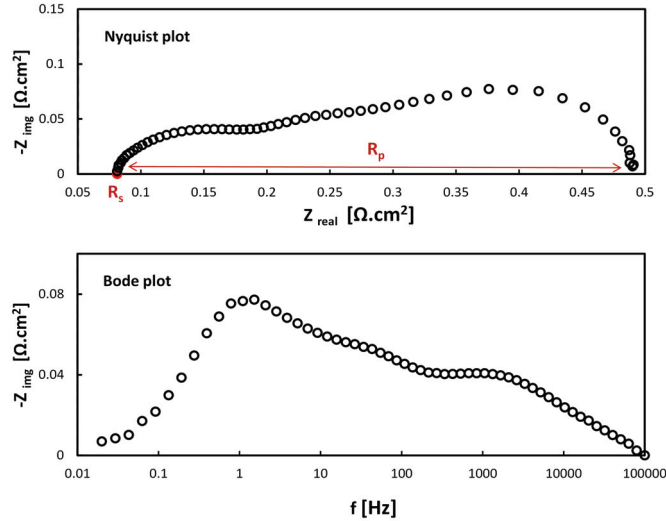
Figure 3.7 – Typical Nyquist and Bode plot recorded on an anode supported SOFC single cell.

The Nyquist plot does not show the corresponding frequency for any data point on the plot. Another way to present EIS measurements is by plotting Z_{img} versus $\log f$, known as Bode plot. The Bode plot explicitly shows frequency information. Normally Nyquist and Bode plots are presented together to give a clear picture of the AC impedance. In theory, each electrochemical process should have its own signature or arc in the EIS spectra. A major factor limiting the usefulness of EIS data is overlap or dispersion in the frequency domain among physical processes governing electrode reactions.

Analysis of Differences in Impedance Spectra (ADIS)

To determine the frequencies at which the impedance is affected the most by changing a condition or a parameter, an Analysis of Differences in Impedance Spectra (ADIS) can be used. The ADIS method identifies electrode processes by analyzing the difference between the impedance spectra obtained under operating conditions A and B (Eq. 3.2) [103]. A high-quality ADIS spectrum can be obtained only when the impedance data comply with the Kramers-Kronig transformation, which practically requires a very smooth response. This method excludes all processes that remains unchanged by variation of a particular operating parameter.

$$\Delta Z_r = [\frac{\delta Z_r(f)}{\delta ln(f)}]_B - [\frac{\delta Z_r(f)}{\delta ln(f)}]_A \qquad (3.2)$$

where Z_r is the real part of the impedance spectrum and f is the frequency.
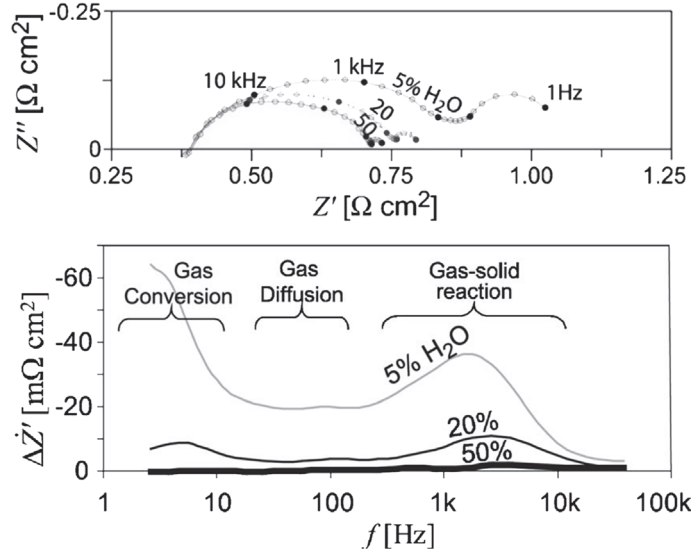
Figure 3.8 – Nyquist plot recorded on a Ni/YSZ and the corresponding ADIS spectra. Variation of steam content in the fuel is investigated, the bold line (50%) representing the background noise [103].

Equivalent circuit modeling

A common method used to analyse EIS spectra is to fit the data into an equivalent electrical circuit model. The circuit elements are the common electrical elements with known impedance behavior such as resistors, capacitors, and inductors. The impedance of the element depends on the element type and the values of the parameters that characterize that element. For instance, the impedance of a capacitor excited by a sine wave at frequency f is as follows:

$$Z_c = \frac{1}{j2\pi f C} \tag{3.3}$$

Each EIS model consists of a number of elements, in both series and parallel configurations. The common equivalent circuit models used to describe SOFCs are the combination of the following elements [102]:

- R_s: Ohmic resistance. Z=R

- L: Inductance. Z=jωL

- *RQ*: Parallel combination of R (resistance) and Q (constant phase element). Represents a process whose kinetics determine R and whose reactant species concentration affects Q. Three parameters are involved: R, Q, n. When n=1, Q is a pure capacitance. $Z = \frac{R}{1+(j\omega RC)^n}$

- *W*: Warburg-element (finite length). Represents diffusion over a fixed length and is derived from Fick's Law. At high frequencies, the behavior represents semi-infinite diffusion. $Z_W = R\frac{tanh([j\omega\tau]^\alpha)}{[j\omega\tau]^\alpha}$

- *G*: Gerischer element. Corresponds to combined reaction and diffusion processes [104]. Especially useful for mixed ionic–electronic conducting (MIEC) cathodes. $Z_G = \frac{Z_0}{\sqrt{k+j\omega}}$, where k is the chemical surface exchange coefficient.

When an equivalent circuit has been developed, the magnitudes of each of the elements can be calculated by Complex Non-Linear Least Squares (CNLS) fitting. By plotting the calculated values from the CNLS fitting, the goodness of the fit[2] of the equivalent circuit can be evaluated. The impedance simulated by an equivalent circuit reflects the physiochemical processes of the assumed electrochemical reaction model. The model parameters can be estimated if experimental data are available using CNLS fitting. RAVDAV software [105], developed by Risø-DTU, has been used in this thesis to perform the CNLS fitting.

An example of such a calculation is shown in Fig. 3.9 and Table. 3.1 presents the estimated parameters values. The equivalent circuit consists of 6 serial impedance elements, each characteristics of one loss mechanism. RQ_{ionic} and RQ_{TPB} represent high-frequency processes, the Gerischer element represents the activation polarization of the cathode. 2 RQ circuits (RQ_{diff} and RQ_{conv}) are also representing the the low frequency processes (i.e. gas conversion and diffusion losses).

Table 3.1 – Results from CNLS fitting of the EIS shown in Fig.3.9. Boukamp goodness [106] of fit is $5.8113e^{-4}$, which indicates a good fit.

Element		R (Ω)	n	f (Hz)
L_0	1.23E-07 H			
R_0		0.026		
RQ_{ionic}		0.0024	0.98	14175
RQ_{TPB}		0.032	0.73	1707
RQ_G		0.016	1	70
$RQ_{diffusion}$		0.042	0.7	9.8
$RQ_{conversion}$		0.047	0.89	0.86

---

[2]Goodness of the fit is the chi-squared parameter, which evaluates the relative errors (residuals) between the fit result and the measured curve at each single point.
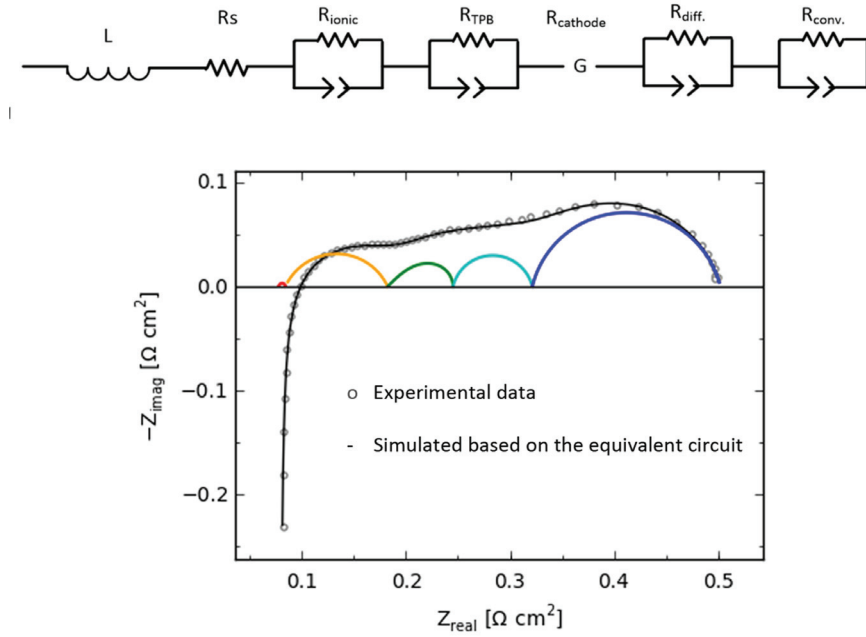
Figure 3.9 – Equivalent circuit model used to fit the impedance data of Fig. 3.7.

Distribution of Relaxation Times (DRT)

One powerful representation for impedance data with high resolution is using the Distribution of Relaxation Time (DRT). This approach is a purely mathematical method allowing the identification of anodic and cathodic polarisation processes with their individual characteristic frequencies. The method separates polarisation processes with different time constants directly from impedance data [107].

The DRT method is based on the fact that every impedance spectrum following the Kramers-Kronig relations [108] and can be represented by a sufficiently large number of RC-elements in series. The impedance of a RC-element is given by $Z_{RC}(\omega) = \frac{R}{(1+j\omega\tau)}$, with the characteristic relaxation time $\tau = RC$. For an infinite number of RC elements with continuously increasing relaxation times τ from 0 to ∞, the impedance $Z(\omega)$ can be expressed by the following equation:

$$Z(\omega) = R_0 + R_{pol} \int_0^\infty \frac{\gamma(\tau)}{1+j\omega\tau} d\tau, \qquad \int_0^\infty \gamma(\tau) d\tau = 1 \tag{3.4}$$

where R_0 represents the ohmic resistance and R_{pol} the overall polarisation. The angular frequency is defined as $\omega = 2\pi f$ and j is the imaginary unit. The term $\frac{\gamma(\tau)}{1+j\omega\tau} d\tau$ specifies the fraction of the overall polarisation with relaxation times between τ and $\tau + d\tau$.

A numerical DRT is approximated practically by considering a finite number of N RC-elements given by the discrete distribution function g_n. The corresponding equation is expressed by:

$$\underline{Z}(\omega) = R_0 + R_{pol} \sum_{n=1}^{N} \frac{g_n}{1 + j\omega\tau_n} = R_0 + \sum_{n=1}^{N} \frac{R_n}{1 + j\omega\tau_n} \tag{3.5}$$

where g_n is the contribution of the n_{th} RC-element with the relaxation time constant τ_n to the overall polarisation. More detailed information about the DRT method can be found in References [107, 109].

To calculate a DRT spectrum, the impedance spectrum has to obey the Kramers-Kroning transformation [109]. A good DRT spectrum can be achieved only when smooth data are available. DRT calculations in this work were performed using RAVDAV software [105]. Fig. 3.10 provides an example of DRT calculation compared with Nyquist and Bode plots. In this example, a cell was damaged after 200 h of operation. Impedance spectra was recorded at the beginning and end of the test. According to this figure, there is a change in the peak at 100-1000 Hz, where the damage could be located. Sensitivity analysis is required, in which one cell parameter varies at a time (e.g., temperature, cathodic oxygen partial pressure, and the anode fuel) to identify which process (or processes) is affected.
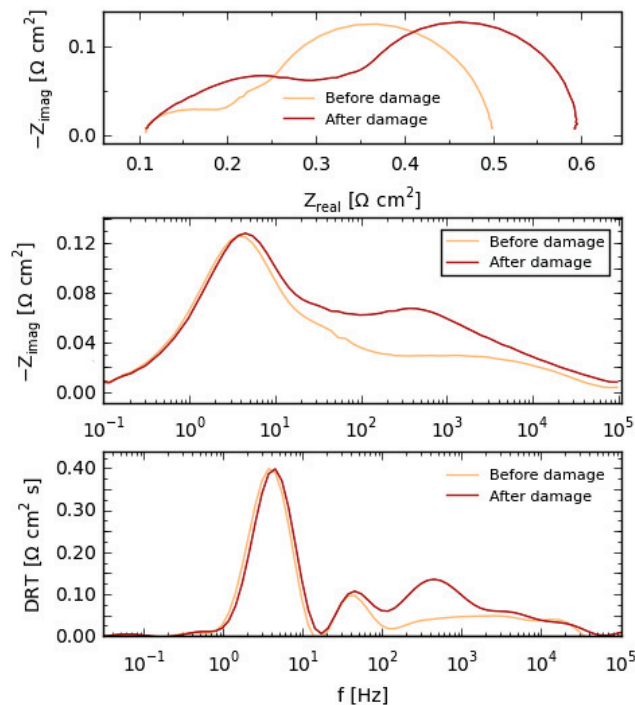

Figure 3.10 – Top to down: the Nyquist, the Bode, and the DRT spectra. Unlike the Nyquist and Bode plots, five peaks corresponding to five processes are visible in the distribution curve.

4 Siloxane Poisoning- Part A: Degradation

(partly taken from:

H. Madi, A. Lanzini, S. Diethelm, D. Papurello, J. Van herle et al., Solid oxide fuel cell anode degradation by the effect of siloxanes. Journal of Power Sources 297, 460-471, 2015
and:

H. Madi, S. Diethelm, S. Poitel, Ch. Ludwig and J. Van herle. Damage of Siloxanes on Ni-YSZ anode supported SOFC operated on hydrogen and bio-syngas. Journal of Fuel Cells, volume 15, issue 5, 718- 727, 2015)

Contribution of H. Madi: literature review, single cell testing and characterizations, data evaluation and conclusion.

This chapter focuses on organic silicon compounds (siloxanes) and their detrimental effects on the performance of SOFC Ni-YSZ anodes. The involved mechanism of degradation is clarified and quantified through several test runs and subsequent post-mortem analysis on tested samples. In particular, experiments on both Ni anode-supported single cells and 11-cell-stacks are performed, co-feeding D4-siloxane (octamethylcyclotetrasiloxane, $C_8H_{24}O_4Si_4$) as model compound for the organic silicon species.

4.1 Introduction

As a general trend, the durability of SOFCs is strongly connected to the amount of contaminants that reaches the electrodes, especially the three-phase boundary. Pore blocking in the electrodes and progressive corrosion of the interconnects can also be affected by fuel impurities. Hence, ultra-clean fuel gas is always beneficial to increase the lifetime [110, 111].
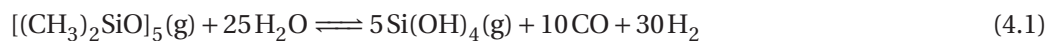
Organic silicon compounds are often found in WWTP and landfill biogas. The clean-up of biogas has been reported to be difficult due to competitive adsorption of different biogas contaminants. For instance, the adsorption of different compounds follows the ranking: water > aromatics > siloxanes > halocarbons, halocarbons and siloxanes being thus the most difficult compounds to remove [78, 112]. Several studies have been carried out on the poisoning by siloxanes in the fields of gas turbines and gas engines [113]. Combustion of siloxanes leads to the formation of microcrystalline silica, a very firm substance which has similar properties to that of glass. This material coats and glazes metal surfaces, e.g., the spark plugs, cylinders, valves and emission catalyst with white deposits and acts as a thermal insulator.

In general, silica contamination in the SOFC does not only originate from a contamination of the fuel stream. Silicon compounds can be also found in the deionised water used for the steam-reformer upstream of the SOFC or can derive from stack sealants. Therefore results in this work can be useful to more broadly assess and understand the impact of silica contamination on the performance of SOFC Ni anodes.

Haga et al. [80] observed the effect of feeding 10 ppm of D5 on a Ni anode showing how the SOFC performance is rapidly falling (within hours). Post-mortem analysis revealed the plugging of the anode structure with $SiO_2(s)$ deposits [114]. They concluded that the presence of siloxane can cause deposition-type degradation, associated with the formation of $SiO_2(s)$ according to the following reactions:

$$[(CH_3)_2SiO]_5(g) + 25\,H_2O \rightleftharpoons 5\,Si(OH)_4(g) + 10\,CO + 30\,H_2 \qquad (4.1)$$

$$Si(OH)_4(g) \rightleftharpoons SiO_2(s) + 2\,H_2O \qquad (4.2)$$

The software Factsage® was employed in this work to calculate the thermochemical equilibrium decomposition of siloxanes at the SOFC operating temperature of 700 °C. In particular, the equilibrium phase diagram for the quaternary system Ni-Si-O-H was calculated showing how – from a thermodynamic point of view – the formation of solid Ni-Si solution would also be possible as shown in the phase diagram below (Fig. 4.1).

However, the presence of solid Ni-Si phases have not been reported in the literature to our knowledge. Instead, silica deposition was widely observed on the blades of micro-turbines that were fed with biogas rich in organic silicon compounds [77]. Note that the inlet temperature of a micro-turbine is quite similar to the operating temperature of a SOFC stack.

The study of Hauch et al. [115] summarizes well the efforts in the group of Risø-DTU to understand degradation phenomena involving the segregation of silicates at the anode three-phase boundary during electrolysis operation. They identified as Si contamination sources both from the raw materials used in the anode manufacturing processes as well as the albite $(NaAlSi_3O_8)$ glass sealant. Especially, the sealant was responsible for the initial passivation
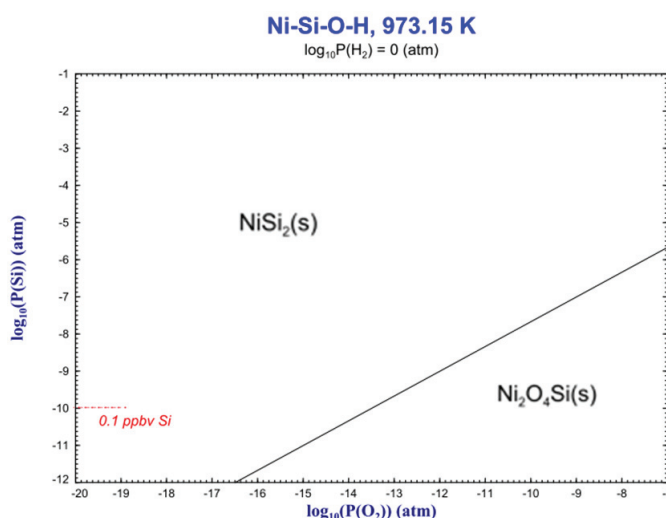
Figure 4.1 – Equilibrium phase diagram at 700 °C for the Ni-Si-O-H system ($P(H_2) = 1$ atm) using Factsage®.

of the tested cell, caused by a shift in the equilibrium from gaseous $Si(OH)_4$ – evaporated from the sealant – towards formation of glassy phase silicates transported and eventually precipitated at the triple-phase-boundaries in the Ni-YSZ electrode.

In this work we investigate the effect of organic silicon compounds (siloxanes) on the performance of the SOFC Ni anode, single cell and short stack. The main objective of this study is to evaluate the impact of D4 (octamethylcyclotetrasiloxane) – even when present at ppbv level in the fuel stream – on the anode performance and its durability. The mechanism of degradation of Si compounds on the Ni anode is elucidated. Advanced post-test characterizations were used to clarify and correlate the observed degradation in the fuel cell electrochemical performance.

4.2 Materials and Methods

4.2.1 D4 contaminant

In the present study D4-siloxane was chosen as model compound. According to the literature, D4 and D5 are the most abundant among the different detected siloxanes in biogases. We preferred using D4 for experimental reasons: this compound has a lower boiling point compared to D5 (175 °C vs 211 °C for D5) which lowers the risk of condensing the contaminant along the feeding line.

In terms of validity of the results obtained using D4 rather than D5, both compounds are expected to behave similarly in the anode environment, with fast decomposition to SiO_2(s). It is therefore believed that the choice of D4, as model compound for siloxanes, is acceptable.

In order to yield accurately the desired concentrations of D4 in the anode feed gas, certified cylinders were ordered in which a precise amount (20 ppmv) of D4 was contained in pure H_2 carrier gas. By injecting different amounts of H_2-D4 in clean reformate gas, various D4 concentrations in the anode feed were obtained.

4.2.2 Single Cell

Commercial Ni-YSZ anode-supported SOFC discs of 60 mm diameter with cathode active areas of 3 cm^2 (from SOLIDpower) and 12.5 cm^2 (from Topsoe Fuel Cell) were used. It has been specified which cell was used for each experiment.

Operation under H_2

Experiments were designed to investigate the impact of D4 on the SOFC performance operated on H_2. The cell was fed with H_2 at 800 °C under 0.25 A/cm^2 current density. After 25 h of stabilization, D4 was added to the main fuel stream for the duration of 20 h.

Operation under Reformed Biogas

For these experiments, simulated reformed biogas with the gas composition of H_2/CO/CO_2/H_2O: 50/20/10/20 vol.% was used. Once the cell was stabilized under H_2, the fuel feed was switched to this synthetic mixture. The anode fuel transfer lines were heated to prevent water condensation between the evaporator and the furnace.

4.2.3 Short Stack

SOFC stacks consisting of a series of 11-cells each were used for the experiments. All the stacks were provided by Topsoe Fuel Cell. The stack is operated at a fixed nominal operating point corresponding to a current of 20 A and a FU of %60. The feeding gas is a H_2-CO rich syngas that simulates a steam-reformed biogas. The biogas composition was taken as CH_4-CO_2 60-40 vol.% . The reformate composition was calculated assuming biogas steam-reforming with a steam-to-carbon (S/C) ratio of 2 in an equilibrium reactor operating at 750 °C. The resulting gas molar composition is CH_4 0.3%, CO_2 10.0%, CO 19.3%, H_2 50.6% and H_2O 19.9%. The contaminant is directly fed at the SOFC inlet manifold avoiding its contact with the rest of the BoP (e.g., the fuel pre-heater). Experiments on short-stacks were carried out at Politecnico di Torino (POLITO).

4.2.4 Characterization Methods

Single Cell Setup

EIS was performed with an IM6 electrochemical workstation and all EIS measurements were taken with a 50 mA perturbation amplitude in the frequency range from 100 kHz to 50 (or 20) mHz. Electrochemical measurements were done every 25 h, before and after every change in D4 concentration level.

Short Stack

An electronic load (Kikusui, Japan) operated in constant current mode was used to set the current on the stack. Copper rods were connected to the stack current terminals to flow current through the load. Voltage probes were available for measuring the potential across each of the eleven cells constituting the stack. National instruments equipment was used for data logging. Thermocouples of type K were inserted in each of the stack inlet/outlet manifolds in order to monitor the gas temperature. The inlet air and fuel temperature were measuring both around 750 °C during the experiment with D4.

Post-mortem Analysis

A scanning electron microscope (SEM) QUANTA 600 FEI equipped with Energy dispersive X-ray spectrometer (EDX) was used to take surface images of both interconnect and cells for a qualitative and semi-quantitative elemental analysis. A Hyperprobe JEOL JXA 8530F, equipped with a wavelength dispersive X-ray spectrometer (WDS) was used in addition for qualitative elemental analysis in order to locate Si deposits, with a much finer spectral resolution than EDX. The samples were cut, polished and subsequently embedded in resins. A Perkin-Elmer 3000 Varian VISTA Inductively Coupled Plasma instrument with Optical Emission Spectroscopy (ICP-OES) was used to quantitatively determine the amount of Si on the half-cell (electrolyte + anode support) after operation.

4.3 Results and Discussion

4.3.1 Single Cell

Operation under H_2

Fig. 4.2 shows the cell voltage as a function of time for siloxane D4 (5 ppmv) poisoning at 800 °C. Exposure to siloxane D4 reveals a prompt degradation over a short period of time at this concentration. The cell was exposed to siloxane D4 for 20 h; afterwards the cell regeneration behavior was examined by stopping the impurity feed. Interestingly, after initial degradation the performance of the cell could be partially restored.
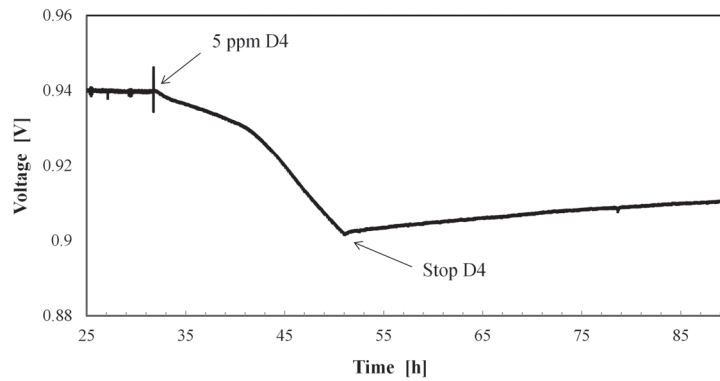
Figure 4.2 – Effect of 5 ppm siloxane D4 at 0.25 A/cm^2, 800 °C and regeneration.

EIS measurements are performed before the injection of siloxane, at the end of injection and 48 h later (Fig. 4.3). To diminish the effect of the high frequency inductance, we employed a correction method as proposed in [116]. The Nyquist plots (-Z_{img} vs. Z_{real}) show that the degradation corresponds to an increase in the polarization resistance. A slight decrease in the ohmic resistance is observed after injecting the impurity, which could be due to carbon deposits from D4 decomposition. According to the EIS measurements (Fig. 4.3), there is an increase of 16.5% in the total cell resistance (ohmic + polarization). Recovery of the cell leads to a restoring of the original ohmic resistance but the total resistance remained constant due to a small reduction in the polarization resistance (5%). Looking at the Bode plot, -Z_{img} vs. Log f, (inset graph of Fig. 4.3), exposure to D4 mainly affects high frequencies rather than lower frequencies.

Figure 4.3 – EIS measurements, at 800 °C, 0.15 A/cm^2, inlet anode gas H$_2$ and air to the cathode. SOLIDPower cell

Operation under Reformed Biogas

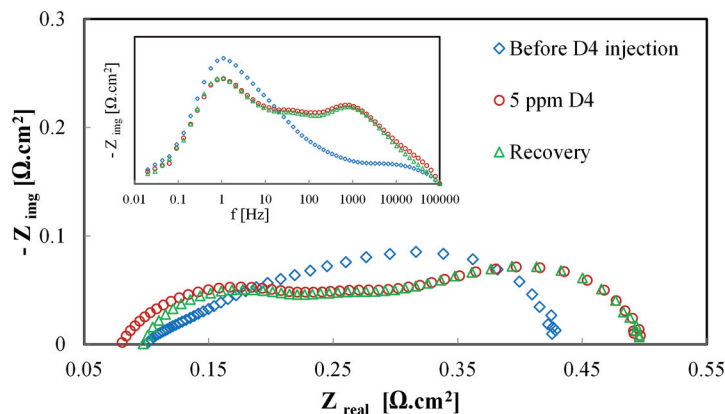Fig. 4.4 shows the time-dependent history of cell voltage at constant current density (0.25 A/cm^2) at 750 °C, FU 31% (cell from SOLIDpower). During this continuous cell voltage measurement, various tests were done with changing concentration of siloxane D4 from 0.6 to 5 ppmv. A degradation was already observed with the clean synthetic mixture without contaminant. We assume that the initial degradation is intrinsic due to the grain growth of Ni particles; according to Faes et. al. [22] this anode degradation can last for the first 500 h.

The poisoning test was carried out by changing the anode gas from clean reformed biogas to impurity-containing fuel. Injection of D4 was started after 110 h of stabilization under clean reformed biogas. D4 was injected in three steps, 0.6, 3 and 5 ppmv, with regeneration steps in between. The degradation rate changed slightly after 0.6 ppmv injection of D4, Fig. 4.4. Shifting to clean reformed biogas after this step restored the degradation rate to its original value (8 mV/20h). Increase in the degradation is clearer after increasing the D4 concentration to 3 ppmv. Shifting to clean reformed biogas was not able to remove the formed phase but the degradation rate was nevertheless lowered; still intrinsic degradation continues. Fig. 4.4 clearly reveals that cell voltage decreases gradually over time. Poisoning at 5 ppmv siloxane resulted in a fatal degradation of cell performance.
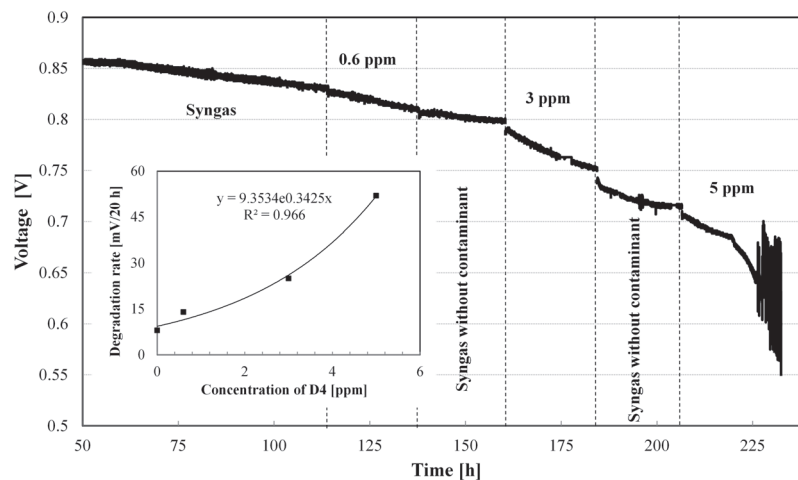
Figure 4.4 – Time-dependent decay of cell voltage at constant current density (0.25 A/cm^2) at 750 °C, with reformed biogas fuel and various D4 impurity levels. SOLIDpower cell.

A second test was performed at the same experimental conditions without the regeneration step as shown in Fig. 4.5 (cell from Topsoe Fuel Cell). During this continuous cell voltage measurement, various tests were done with changing concentration of siloxane D4 from 1 to 3 ppmv. After feeding 100 sccm synthetic reformed biogas for a duration of 400 h, the cell voltage was stable at 0.785 V under a constant current load of 0.25 A/cm^2. Upon the introduction of 1 ppmv D4 at 495 h, the cell voltage started to decrease gradually with an

49

average degradation rate of 0.25 mV/h at constant current density. At 2 and 3 ppmv D4, the cell showed a stronger decrease in performance (Fig. 4.5) with an average degradation rate of 0.34 mV/h and 0.39 mV/h, respectively.
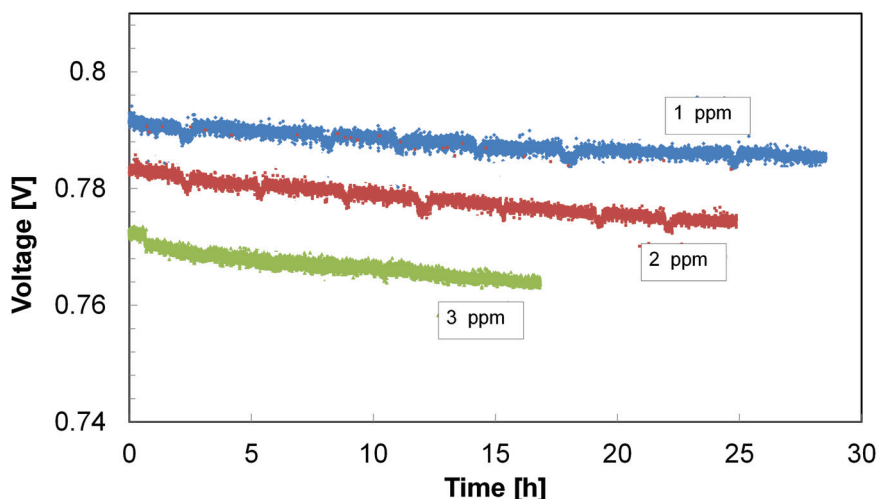

Figure 4.5 – Time-dependent history of cell voltage at constant current density (0.25 A/cm^2) at 750 °C. Degradation trend with D4-siloxane in a single-cell experiment is also presented, Topsoe Fuel Cell.

EIS measurements were used to characterize the cell of Fig. 4.5 before and after injection of D4. Fig. 4.6 shows the evolution of impedance spectra measured during the experiment. These measurements were performed regularly at intervals of 25 h. The Nyquist plot shows two main depressed arcs, which are overlapping. Three main potential losses are generally believed to co-exist, namely; ohmic resistance, activation polarization at high to medium frequencies (first arc), related to the electrochemical reactions at electrolyte/electrode interfaces, concentration polarization at low frequencies (second arc) due to mass transport of the fuel and oxidant through the electrodes. As shown in Fig. 4.6, exposure to siloxane affects both arcs but larger increase in the first arc related to high frequency processes is visible.

In order to emphasize the frequency ranges where the main changes in the impedance spectrum take place as the result of increase in D4 concentration, a Bode (-Z$_{img}$ vs. log f) representation of the imaginary part of complex impedance data is also presented in Fig. 4.6. The spectrum shows two peaks. The first peak appears in the medium to high frequency range (50-1000 Hz) and this can be attributed to activation losses. Increasing D4 concentration to the fuel stream resulted in a shift and increase of this peak. The shift is towards low frequencies from 120 Hz to 20 Hz. The second peak at low frequencies (0.1-5 Hz) increased slightly by increasing the concentration of D4, which indicates plugging of the electrode and diffusion issue by exposure to siloxane.
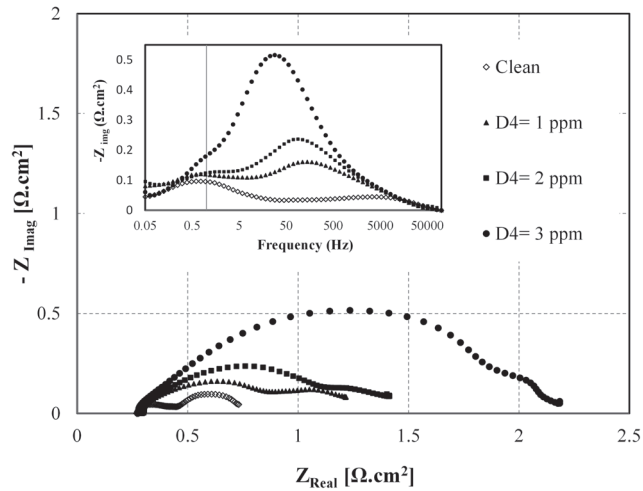
Figure 4.6 – The effect of D4-siloxane on the single-cell performance: EIS data for clean syngas and D4 concentration of 1, 2 and 3 ppmv, respectively.

4.3.2 Short Stack

The effect of D4-siloxane on the stack performance is shown in Fig. 4.7. The D4 concentration was varied from 69 ppbv up to 1 ppmv within the anode reformate feed, resulting in a strong voltage degradation even at the lowest concentrations tested. Degradation increases with the load of contaminant in the anode stream as shown in the inner plot, with a trend that is not linear. The overall contamination with D4 lasted for around 400 h. After the contamination test, the stack was cooled down in stagnant H_2/N_2 condition in order to avoid possible silica removal. The idea was to "freeze" the anode chemical composition for detailed post-test analysis and quantification of the amount of silica deposited in both anode electrode and interconnect. Results are described in the next section. The effect of the contaminant seems to start immediately upon injection (or its increase), which is in line with a poisoning of the electrochemically active sites rather than an effect of pore blocking which would require a certain time to be visible on the cell voltages.

As shown in Fig. 4.7, a strong voltage degradation (5% per 1,000 h) is already established with 69 ppbv of D4 contaminant feed. At 1 ppmv the observed degradation rate is as high as 32% per 1,000 h. The previous results confirm the strongly harmful effect of D4 already at sub-ppm levels. The degradation rate without D4 was basically zero as a rather stable voltage was observed. By comparing the degradation rate observed on the stack (Fig. 4.7) with that on the single cell (Fig. 4.5), for the same concentration of D4 equal to 1 ppm, a consistent degradation rate results, equal to 32% in both cases. Hence, the D4 interaction with stack components (especially the interconnect) seems to have a negligible effect. A better understanding on the fate of D4 in stack environment and on the anode are provided through post-mortem analysis following in the next section.
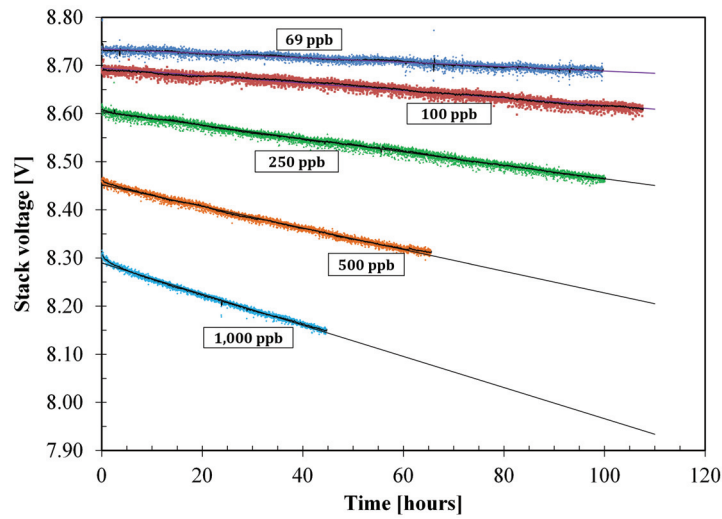
Figure 4.7 – Durability test for the stack up to 1 ppmv of D4 with reformed biogas fuel. The FU is 60% with a current of 20 A (corresponding to a current density of 0.22 A/cm^2). The stack temperature is around 700 °C. Test performed at POLITO. (Courtesy of POLITO)

4.4 Post-test Analysis

4.4.1 Single Cell

Careful SEM-EDX analyses were performed on both current collectors and cells. Fig. 4.8 shows SiO$_2$(s) material covering most of the nickel foam (Si appears white on this backscattered electron image), which was used as current collector. This nickel foam was analyzed by EDX and a large amount of Si was detected. A gradient in deposition amount can be seen from the fuel inlet (pos. 1) to the fuel outlet (pos. 7). For comparison, a Ni foam tested without D4 can be seen in the right part of the figure.
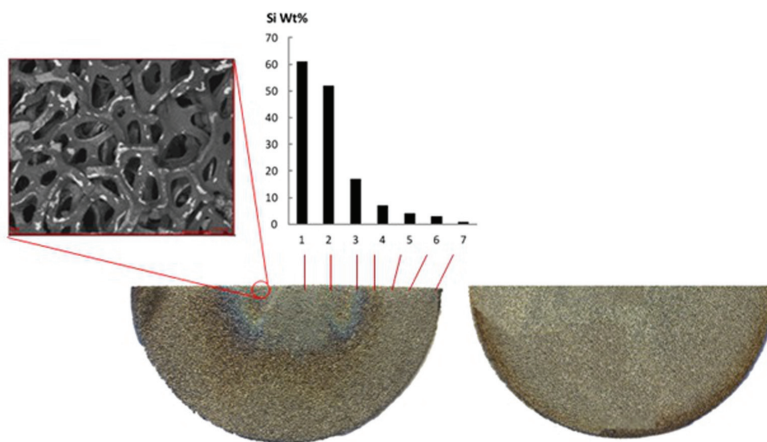
Figure 4.8 – Ni mesh tested with siloxane.
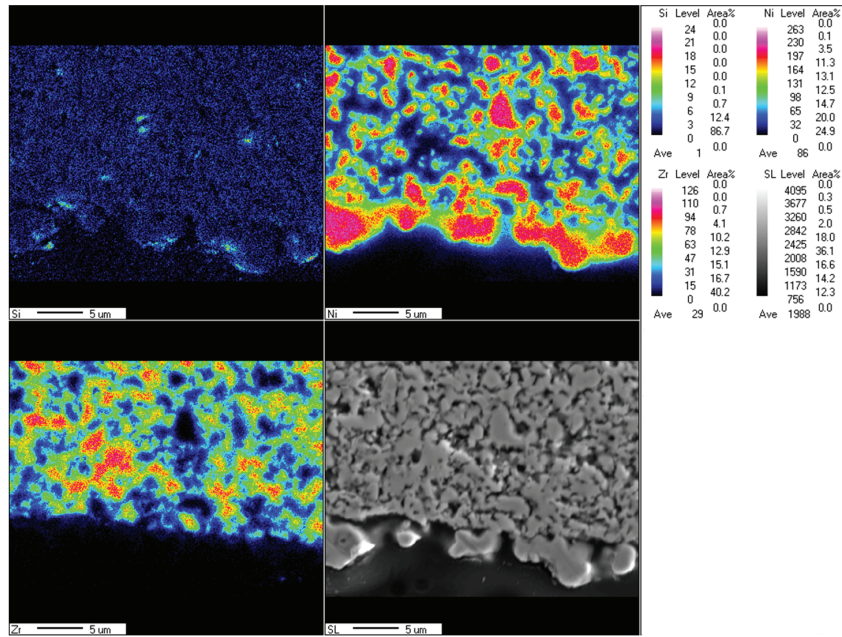
Figure 4.9 – WDS elemental mapping of the interface between anode contact layer and anode support at the fuel inlet for a freshly reduced sample not exposed to D4. (Courtesy of Topsoe Fuel Cell)

It has to be mentioned that, when using EDX for the anode support, there is signal overlap between the Zr-L X-ray and the Si-K X-ray which could cause an overestimate of the Si amount. For this reason, WDS was used as additional technique to map the location of the Si in the anode. A reference sample not tested with D4 is shown in Fig. 4.9. It can be noticed that few spots of silicon are nonetheless present. These may be ascribed to contamination of the sample during specimen preparation.

Instead, in Figs. 4.10 (A) and (B) the elemental mapping of a cell tested for longer time than that shown in Fig. 4.5 (150 h and high concentrations of D4 up to 5 ppm, test not shown here), clearly indicates that Si is deposited in significant amounts everywhere and with a gradient going from the anode contact layer towards the interface with the electrolyte. It can be concluded that Si condenses and deposits everywhere on the anode support down to the electrolyte interface at the three-phase boundary, which could be responsible for the observed loss in electrochemical performance. In fact, the TPB reacts immediately to the SiO_2 poisoning, in contrast to filling up of the pore structure.
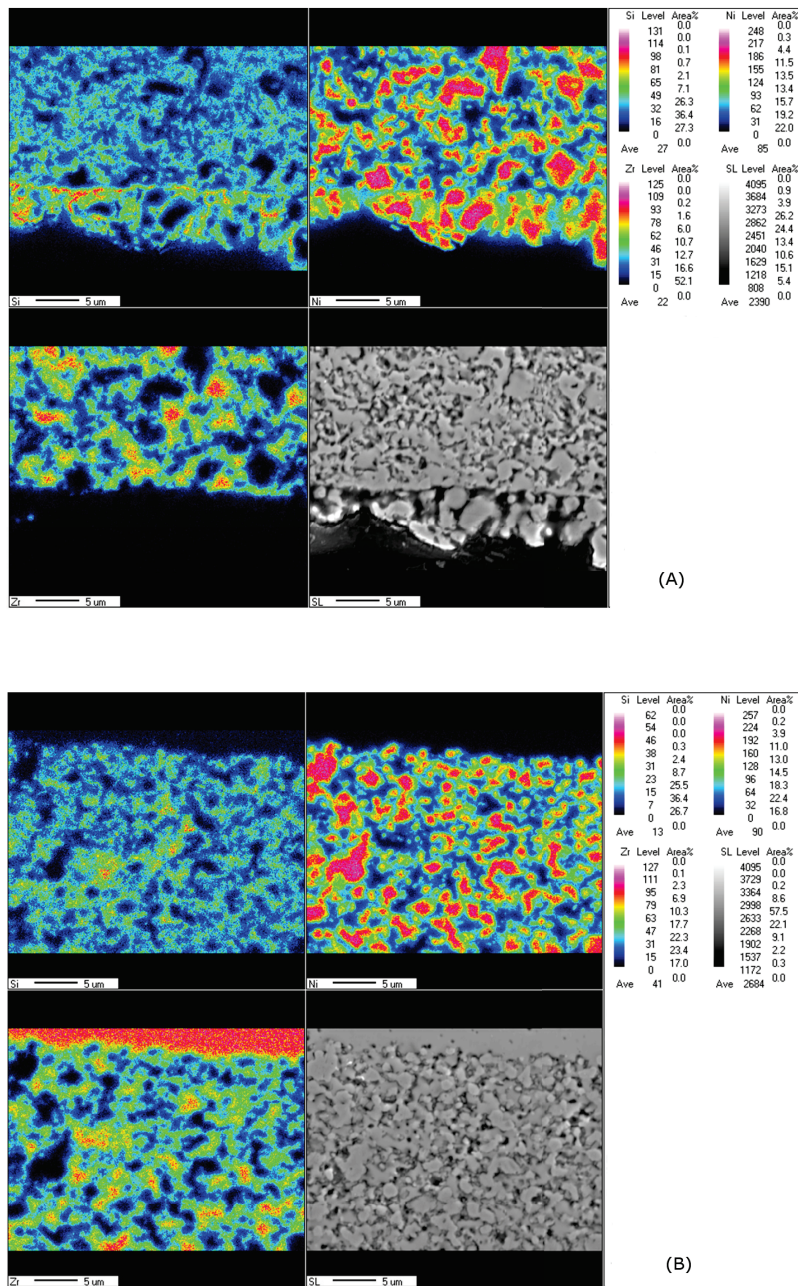
Figure 4.10 – WDS elemental mapping of a sample exposed to D4. A) Interface between anode contact layer and anode support at the fuel inlet. B) Interface between anode and electrolyte at fuel inlet. (Courtesy of Topsoe Fuel Cell)

A quantitative chemical analysis (ICP-OES) has also been performed on the sample; results are shown in Table 4.1), where the amount of Si expressed in ppm (weight basis, wt.) is measured on a half cell (without cathode). One can see, that there is only few ppmv of Si in a fresh sample not tested with D4, which could be due to the glass sealing used in the cell testing or from cell manufacturing raw materials. Considering the EPFL test, shown in Fig. 4.5, during which the

sample was exposed up to 3 ppmv D4 for about 60 h, one can see that the ICP-OES analysis shows a high amount of Si deposited on the cell, 7700 ppm wt. and even higher (1.13%) for the sample exposed up to 5 ppmv D4 for 150 h (test not shown here, elemental mapping shown in Fig. 4.10).

Table 4.1 – Elemental analysis for Si in different tested half cells using ICP-OES. (Courtesy of Topsoe Fuel Cell)

sample	Measured silicon (ppm wt.)
Freshly reduced	150+/-20
Test Fig. 4.5	7700
Test Fig. 4.10	11300

4.4.2 Short Stack

The same type of post-test characterization has been performed on cells and interconnects from the stack testing with and without D4 co-feeding. By EDX analyses it was possible to conclude that there is a significant deposition of the siloxane on both interconnects and anode support, as seen in Fig. 4.11 and Table 4.2. Furthermore, in line with the cell characterizations shown higher, it was possible to notice a clear gradient in deposition going from fuel inlet to fuel outlet, as shown in Fig. 4.12. The EDX Si-K signal goes from 26 wt.% at the fuel inlet to 4 wt.% at the fuel outlet on the interconnect.

Table 4.2 – EDX analysis of a central part of an interconnect (IC) and anode. (Courtesy of Topsoe Fuel Cell)

	Element	Wt.%
IC	Si-K	5.91
Anode contact layer	Si-K	0.35

Silicon deposition in bulk cells (with the cathode removed) from stacks tested with siloxane added to the fuel was analysed by ICP-OES, giving values of 1.3 - 2.0 wt.% Si at the fuel inlet and 0.04 wt.% at the fuel outlet. In contrast, two reference cells tested without D4 gave much lower values of 80-150 ppmv Si, in agreement with Table 4.2. In fact, Si can originate from raw materials used in the manufacturing process of the cell active layers or from the glass-ceramic sealant used in the stack. The same quantitative technique was then employed to measure the amount of Si deposited on cells exposed to D4-siloxane for hundreds of hours (samples analyzed were taken from the stack whose performance results are summarized in Fig. 4.7. Quantitative data from the chemical analysis are summarized in Table 4.3. Results in Table 4.3 clearly show that Si mostly deposits at the fuel inlet areas when siloxane is present in the fuel feed. Si starts to condense on the anode surface as soon as it reaches it, which is consistent with the higher amounts found at fuel inlet regions.
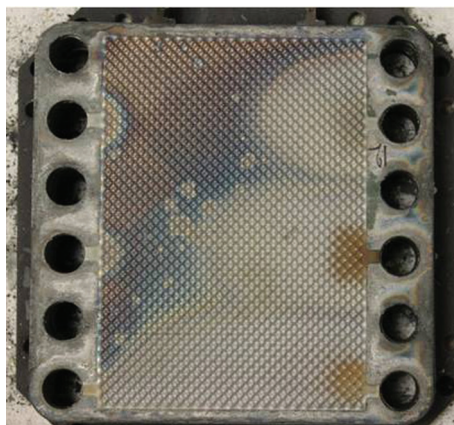
Figure 4.11 – The interconnect after exposure to Siloxanes. (Courtesy of Topsoe Fuel Cell)
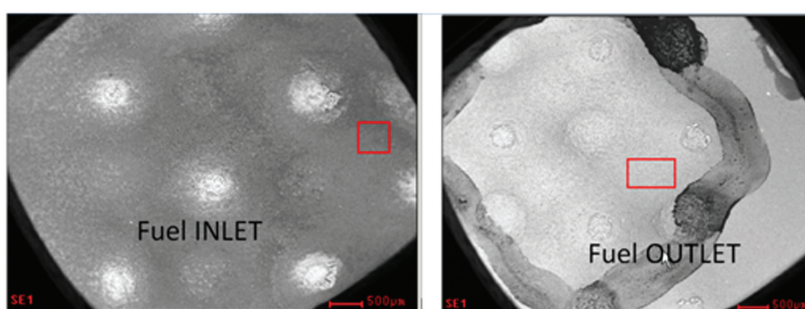
Figure 4.12 – EDX analyses of interconnect close to fuel inlet (left) and fuel outlet (right). The amount of Si from the surface of fuel inlet sample was 26.44 wt.% compare with the fuel outlet which was 5.16 wt.%. (Courtesy of Topsoe Fuel Cell)

In section 4.3.2, where single cell and short stack performance are compared, we concluded that the D4 interaction with short stack components (interconnects and sealing) does not lead to enhanced degradation rates. In this section, it is clarified that Si is depositing largely on the interconnect, but not exclusively. The relevant degradation mechanism foresees siloxane decomposition to SiO_2(s) that precipitates preferentially in the gas channel region – where the interconnect and anode current collector layer are located. Nonetheless, part of the SiO_2 is revolatized and diffuses towards the TPB region where it reprecipitates causing the blocking of active sites for electrochemical reactions. The $Si(OH)_4$ vapour is effectively transported within the H_2-rich gas mixture diffusing from the anode channel towards the electrode/electrolyte interface.

4.5 Conclusion

The degradation of anode supported Ni-YSZ by siloxane D4 as a common biogas impurity was evaluated by electrochemical characterization and electrode post-test chemical analysis.

Table 4.3 – Quantitative silicon measurements on tested cell samples from stack experiments with/without D4-siloxane contamination. 'A' and 'B' refer to stack cells tested in reformed biogas without D4 contamination. 'C' refers to the stack tested with D4-siloxane in the anode feed. Measurements were repeated on 4 different samples for stack 'C'. The cathode was removed from the cells. (Courtesy of Topsoe Fuel Cell)

	Measured silicon (wt. ppm)	+/-
Stack 'A' –no D4	150	40
Stack 'B' –no D4	80	20
Stack 'C' - fuel inlet-D4	1990	100
Stack 'C' - fuel outlet-D4	370	30
Stack 'C' - fuel inlet-D4	1330	100
Stack 'C' - fuel outlet-D4	390	30

According to post-test analysis, a gradient in deposition of Si between inlet and outlet fuel sections was evidenced, with more Si deposited at the fuel inlet regions both within and on the cell, on the current collector (of single cell) and on the interconnect plate (of short stack). This shows that the deposition took place due to the decomposition of the siloxane as given by Eqs. 4.1 and 4.2, where it is converted into $Si(OH)_4(g) + CO + H_2$ and then deposited as $SiO_2(s)$ everywhere from the interconnect deep into the anode support structure until the electrolyte interface. According to the proposed degradation mechanism, the siloxane is fast decomposed to $SiO_2(s)$ as it reaches the fuel cell anode chamber, thus depositing silica both on the interconnect and anode current collector. Some Si remains instead in the vapour phase as $Si(OH)_4(g)$ that further diffuses to the TPB region where it eventually precipitates too (see Fig. 4.13).
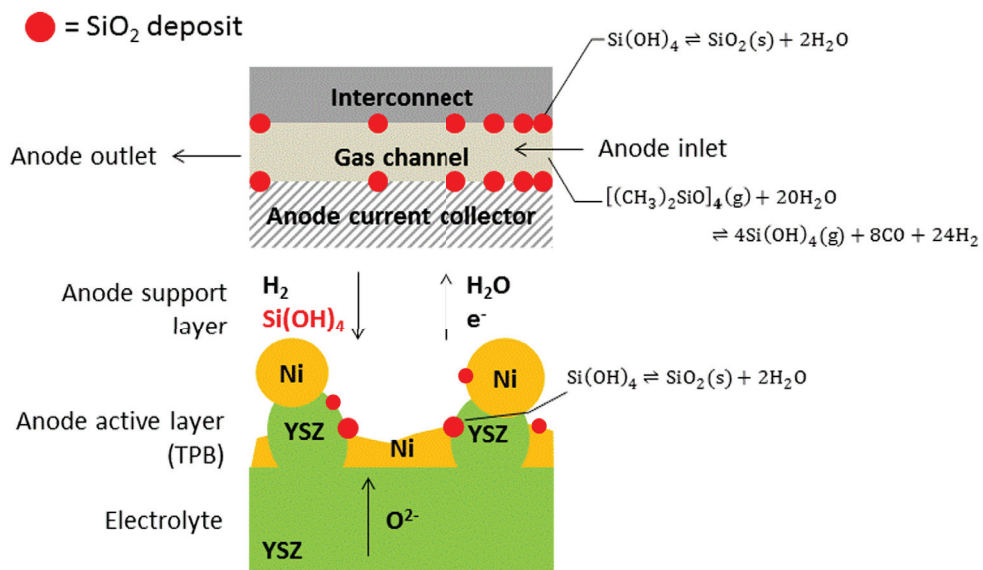
Figure 4.13 – Schematic representation of the proposed degradation mechanism.

In fact, Si is more abundant in the anode contact layer and the interconnect rather than in the inner anode region; nonetheless the Si contamination extends also to the anode region interfacing the electrolyte, thus affecting the TPB.

Electrochemical impedance spectroscopy results suggest that both the anode charge transfer and gas diffusion are affected by the formed Si-deposits. If silica keeps on depositing on the interconnect, an insulating layer would form that is expected to increase the ohmic resistance of the stack repeating unit.

Siloxanes have to be removed in the most complete possible way from biogas feed to SOFCs. Even trace contamination of the fuel feed at ppb level can affect the SOFC Ni anode, leading to fast degradation.

5 Siloxane Poisoning- Part B: Recovery Assessment

Contribution of H. Madi: literature review, thermodynamic calculations, single cell testing and characterizations, data evaluation and conclusion.

This chapter continues the poisoning effect of siloxanes and potential ways of recovery after exposure. Experiments focus on the degradation and recovery of AS Ni-YSZ fed with H_2, co-feeding 5 ppmv D4-siloxane as representative compound for the organic silicon species, at 800 °C.

5.1 Introduction

The previous chapter examined the effect of D4 on the performance of anode supported Ni-YSZ, single cells and short stacks and concluded that the degradation is related to condensation-type processes. Deposited $SiO_2(s)$ was found everywhere from the interconnect deep into the anode supported structure until the electrolyte interface.

This chapter evaluates the regeneration behavior of SOFC anodes single cells upon addition of siloxane D4 to the main fuel stream. First, experiments were performed with H_2 fuel at 800°C for duration of 100 h. The main objective was to evaluate the impact of D4 on the SOFC performance, when operated on H_2 fuel, and the possibility of performance recovery. IV characterization was performed before and after each level of impurity concentration, and EIS measurements taken periodically.

5.2 Experimental

For this study, commercial Ni-YSZ anode-supported SOFC discs of 60 mm diameter from SOLIDpower with cathode active area of 3 cm^2 were used. The test cells were heated at a rate of 100 °C/h up to 800 °C. For the reduction of NiO to Ni metal, a diluted flow of H$_2$ in Ar (20% H$_2$) was used. The total fuel flow rate was held at 100 sccm (standard cubic centimeters per minute) and the air (synthetic air, 79% N$_2$ and 21% O$_2$) flow rate to the cathode was kept constant at 250 sccm.

Experiments were designed to evaluate the cell regeneration behavior after exposure to the impurity. Fig. 5.1 shows the experimental plan. In cases 1, 2 and 3, the cells were fed with H$_2$ at 800 °C under 0.25 A/cm^2 current density. After 25 h of stabilization, D4 was added to the main fuel stream for the duration of 20 h. For case 1, the cell was kept under polarization at the same current density (0.25 A/cm^2) after stopping the impurity feed. For case 2, the cell was reset to OCV (open circuit voltage) condition and for case 3, the cell was operated at higher current density (0.65 A/cm^2) after stopping the impurity feed. The reason for these 3 experiments was to study cell recovery after exposure to siloxane poisoning.
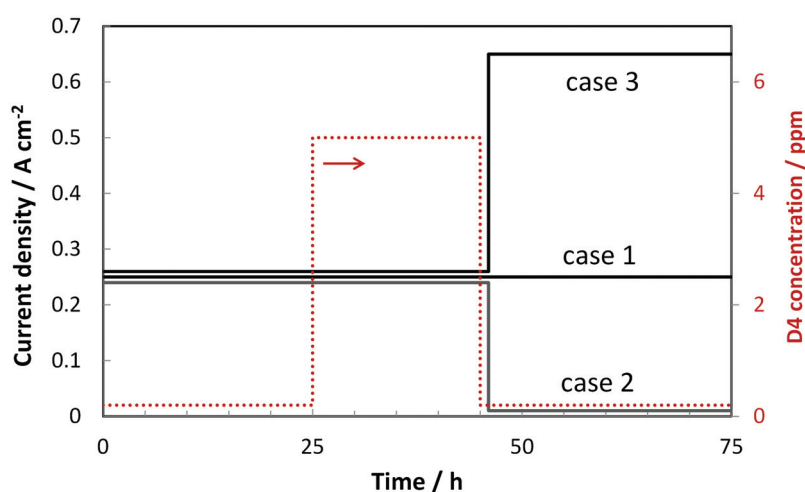
Figure 5.1 – Experiments plan. Performance recovery was compared under polarisation and at OCV.

5.2.1 Electrochemical Measurements

EIS was performed with an IM6 electrochemical workstation. All EIS measurements were performed with 20 mA perturbation amplitude in the frequency range from 100 kHz to 20 mHz at a current bias of 0.15 A/cm^2. The IVs were recorded using an EL 3160-60 electronic load. The cell voltage and temperature (K-type thermocouple) during the steady-state polarization phases were monitored with an Agilent 34970A data acquisition system.

5.2.2 Post-mortem Analysis

After cell fracturing, samples were polished with a Ilion 3 (Gatan) cross section polisher for several hours (depending on the sample), at 5 or 6 keV, at an angle of 85° without inclination of the gun. Up to several tens of microns were removed this way. For this step, the sample was glued on a mask to allow the beam to polish a flat surface. Silver paint was used for glueing the sample and then for covering the external surface of the sample to make its surface conductive to avoid charging problems during SEM observation.

A Zeiss Merlin scanning electron microscope 1-30 kV Schottky was used to take surface and cross-section images at low acceleration voltage. EDX spectroscopy was used for an elemental analysis approximation of the studied zones of the exposed samples.

Rectangular zones parallel to the electrolyte were analyzed, to give average elemental distributions as a function of the distance from the electrolyte (or from the gas interface, depending on the point of view), Fig. 5.2. The thinner and closer-spaced the rectangles in a wide array, the better the results.
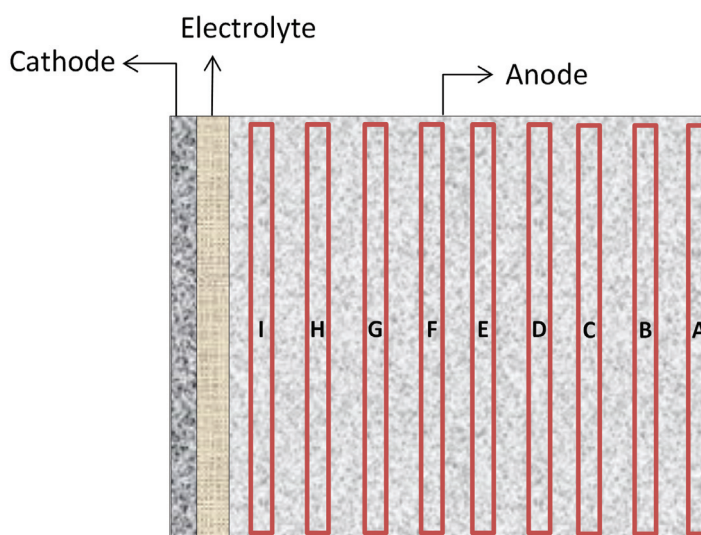
Figure 5.2 – Schematic of anode cross section. Rectangular areas of observation (A to I). Thinner and higher number of these areas will increase the accuracy of the results.

5.3 Results and Discussion

5.3.1 Thermodynamic Calculations

In order to reveal the poisoning mechanism of siloxanes, it is important to first identify the stable form of impurity species in the fuel gas and also its possible interaction with anode materials under SOFC operational conditions. HSC Chemistry (version 7.1, Outokumpu Research Oy, Finland) as a thermodynamical calculation program was used to generate equilibrium

compositions of fuel gases containing the impurity at relevant temperatures. The calculated phase diagram indicates that $SiO_2(s)$ can be formed at high temperature. The calculations also indicated that, even at such low concentration of siloxanes, Si could affect Ni-based anodes via the formation of NiSi and Ni_2Si as shown in the previous chapter. According to Haga et al. [80], SOFC performance degradation is associated with the formation of $SiO_2(s)$ according to the following reactions:

$$[(CH_3)_2SiO]_5(g) + 25\,H_2O \rightleftharpoons 5\,Si(OH)_4(g) + 10\,CO + 30\,H_2 \tag{5.1}$$

$$Si(OH)_4(g) \rightleftharpoons SiO_2(s) + 2\,H_2O \tag{5.2}$$

The previous chapter showed that $SiO_2(s)$ was deposited on the outer anode surface, inside the anode pores and even close to the anode/electrolyte interface. In reducing atmospheres and at high temperatures, $SiO_2(s)$ can be reduced into gaseous $SiO(g)$ by losing oxygen to the atmosphere [117]. If we consider the gas composition of the previous chapter, the reformed biogas composition of H_2, CO, H_2O and CO_2, the overall chemical reaction and the reduction of $SiO_2(s)$ can be expressed as Eq. 5.3. However, the formed gaseous $SiO(g)$ can be entrained into the fuel stream and anode and electrochemically oxidized to $SiO_2(s)$ at the triple phase boundaries by O^{2-} transported through the electrolyte. The reactions of reduction and of electrochemical oxidation of $SiO_2(s)$ are expressed by Eqs. 5.3 and 5.4.

$$2\,SiO_2(s) + H_2(g) + CO(g) \longrightarrow 2\,SiO(g) + H_2O(g) + CO_2(g) \tag{5.3}$$

$$SiO(g)(an) + \tfrac{1}{2}O_2(g)(air) \longrightarrow SiO_2(s)(an) \tag{5.4}$$
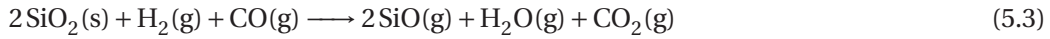
$P_{SiO(g)}$ in Eq. 5.3 and the Nernst potential (E) of Eq. 5.4 are calculated based on the method proposed in [117]. The calculated logarithmic $P_{SiO(g)}$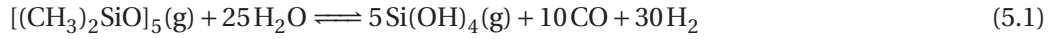 as a function of reciprocal temperature, with the considered reformed biogas mixture, is shown in Fig. 5.3. This figure indicates that $P_{SiO(g)}$ increases with increasing temperature, therefore, one of the potential ways to remove $SiO_2(s)$ would be to increase the temperature.

The calculated E value as a function of temperature for the reformed biogas mixture is shown in Fig. 5.4. According to this graph, operating the cell at OCV after exposure to siloxane prevents electrochemical reoxidation of $SiO(g)$ to solid phase $SiO_2(s)$.

In summary, thermodynamic calculations suggest that the recovery is possible if we increase the temperature and operate the cell at OCV, for a duration long enough. Increasing the operating temperature was not tried due to limitation of the setup. For this reason, the cells

after Si exposure were subjected to different current densities, i.e. operation under the same current density as during exposure, under higher current density and at OCV, with the more likely conditions for recovery expected for the latter case.
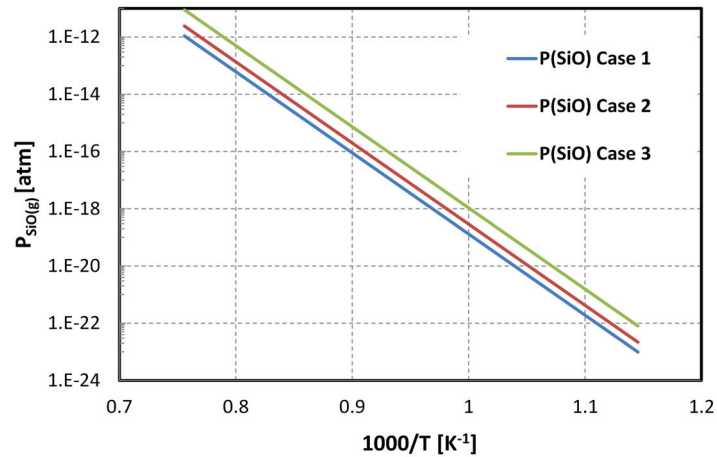
Figure 5.3 – Partial pressure of SiO(g) over 600-1000 °C. $P_{SiO(g)}$ increases with increasing temperature.
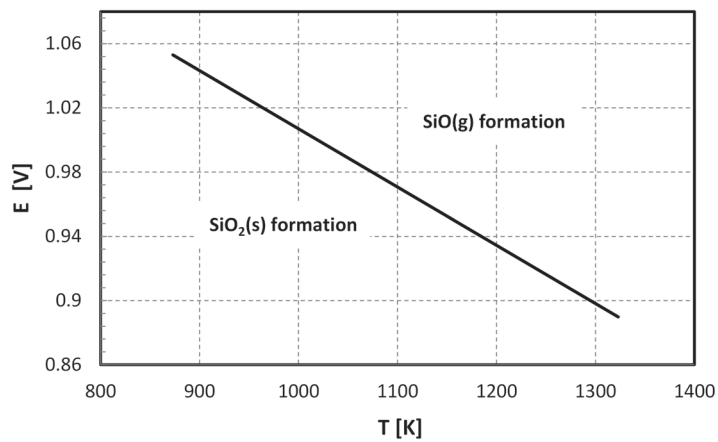
Figure 5.4 – Calculated E value (Eq. 5.4) as a function of temperature for the reformed biogas mixture.

5.3.2 Cell Voltage vs. Time

Figs. 5.5 (A-C) show the cell voltage as a function of time for siloxane D4 (5 ppmv) poisoning at 800 °C. Degradation behavior is similar to what has been previously observed by Haga et al. [80]. Exposure to siloxane D4 reveals a prompt degradation over a short period of time at this concentration. The cell was exposed to siloxane D4 for 20 h; afterwards the cell regeneration behavior was examined by stopping the impurity feed.

63

Interestingly, after initial degradation the performance of the cell could be partially restored. For cases 2 and 3, similar degradation rates during poisoning were observed as with case 1. We will compare the results for the 3 tests through IVs, EISs and post-mortem analysis.

5.3.3 Characterization

IV characterization is performed before injection of siloxane, at the end of injection and 48 h later (recovery) (Figs. 5.6 (A-C)). Fig. 5.6 (A) indicates an increase in the total ASR (18%) after injection of the impurity. This figure shows recovery of the cell is partly possible (6% reduction in the total ASR of the freshly poisoned anode). However, for case 2 (Fig. 5.6 (B)), maintaining the cell at OCV after impurity exposure did not lead to performance recovery and the total ASR in fact further increased (by 1.5%).

Comparison of Figs. 5.6 (A) and (B) indicates that results are contrary to the thermodynamic prediction, as we would expect a potential recovery of the sample by operating at OCV, due to revolatilisation of deposited SiO_2(s) to SiO(g). This lead to the third experiment (case 3) to evaluate the cell regeneration behaviour by operating at higher current density as shown in the experimental plan (Fig. 5.1).

Fig. 5.6 (C) also shows a further increase in ASR by operating the cell at higher current density (0.65 A/cm^2) after the D4 exposure. However, operating at higher current density may increase the degradation rate [118] due to additional processes, like the agglomeration of nickel particles, which leads to a decrease of the amount of TPB, resulting in an increase in the anode losses. From case 3, it cannot be concluded that the cell performance could recover from the impurity exposure as it can be masked by such overlapping phenomena.
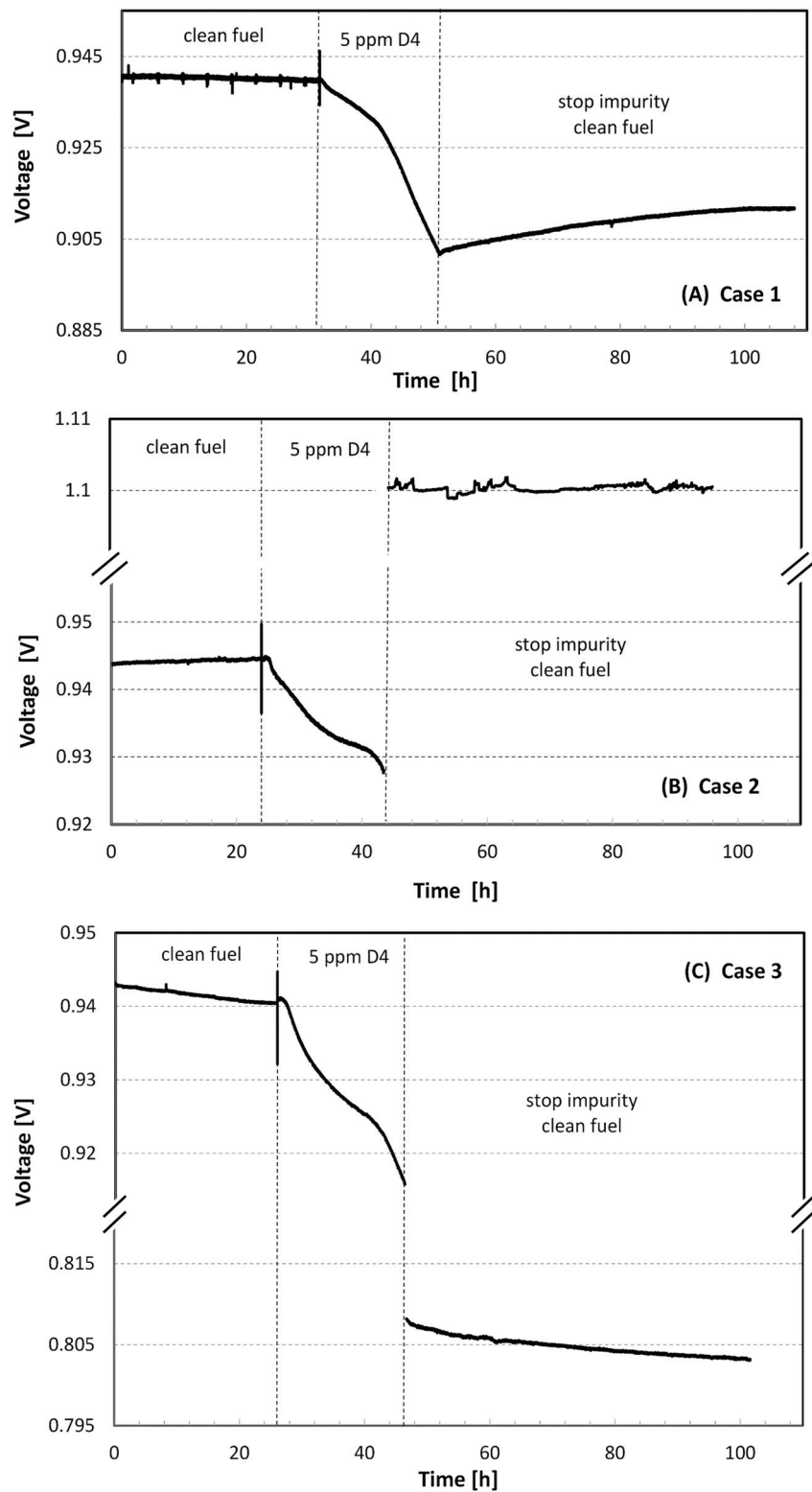
Figure 5.5 – Effect of 5 ppmv siloxane D4 at 800 °C and regeneration of the cell A)case 1, B) case 2, C) case 3.
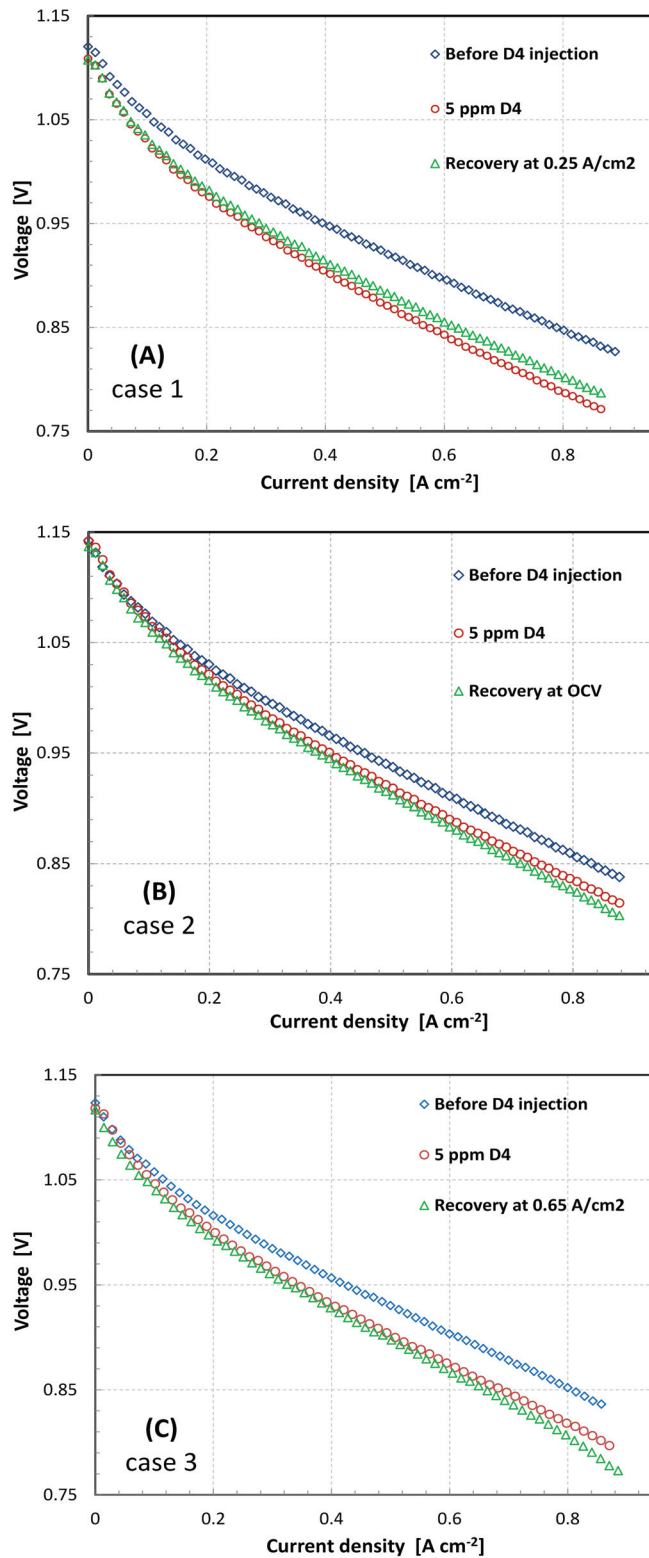
Figure 5.6 – IVs recorded A) cases 1: recovery at the same current density (0.25 A cm^2), B) case 2: recovery at OCV. C) case 3: recovery at higher current density (0.65 A/cm^2). Test conditions: 800 °C, inlet anode gas H$_2$ and air to the cathode.

EIS measurements are performed before the injection of siloxane, at the end of injection and 48 h later (Figs. 5.7 (A-C)). The Nyquist plots show that the degradation corresponds to an increase in the polarization resistance. A slight decrease in the ohmic resistance is observed after injecting the impurity, which could be due to carbon deposits from D4 decomposition. According to the EIS measurements of case 1 (Fig. 5.7 (A)), there is an increase of 16.5% in the total cell resistance (ohmic + polarization) which corresponds to the value obtained from IV curves (18% cf above). Recovery of the cell leads to a restoring of the original ohmic resistance but the total resistance remained constant due to a small reduction in the polarization resistance (5%). It must be said that all EIS were performed at the current density of 0.15 A/cm^2 and therefore its results are representing that operating point on the IV curves. Cell recovery in case 2 (Fig. 5.7 (B)) shows, as with the previous case, restoring of the ohmic resistance but now a 10% reduction in polarization resistance. These results suggest that the recovery in polarization resistance is slightly better if the cell is left at OCV than when polarized after exposure to siloxane D4.
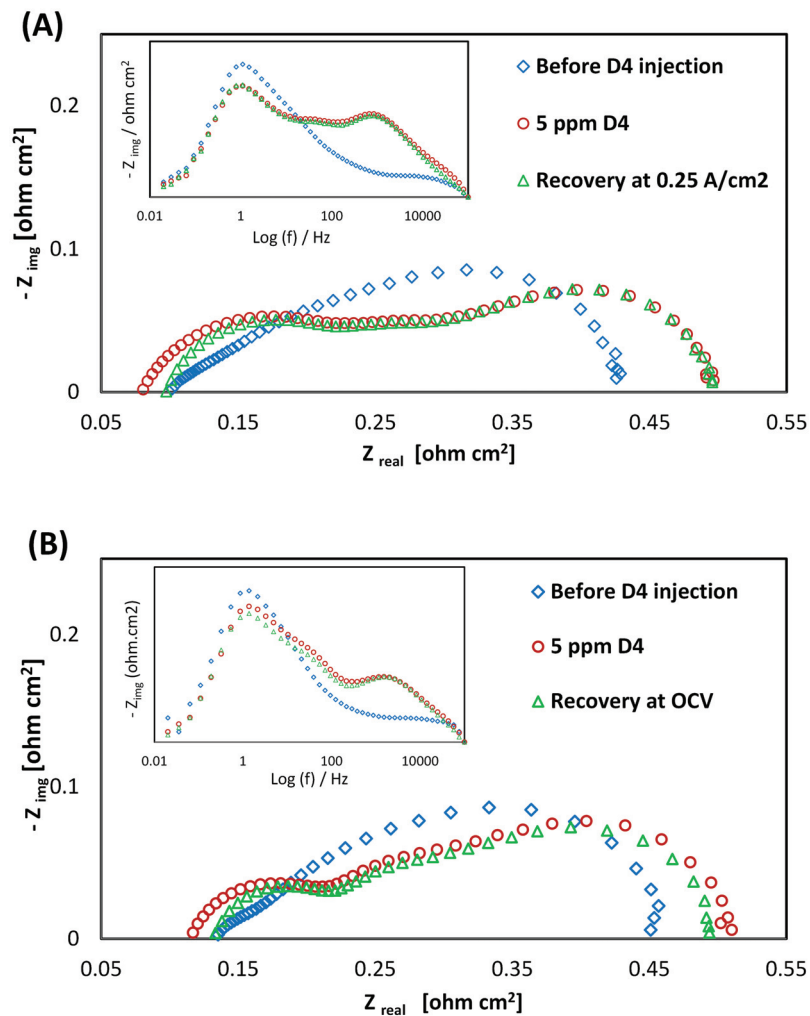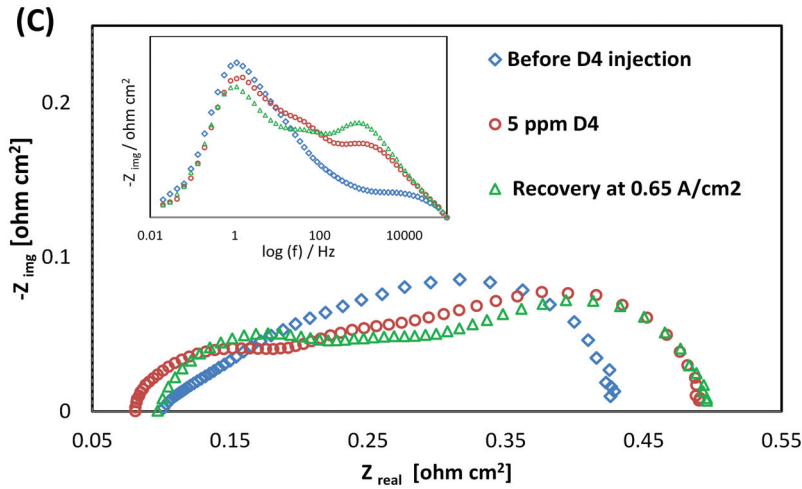
Figure 5.7 – EIS measurements a) case 1, b) case 2 c) case 3. Test conditions: 800 °C, inlet anode gas H_2 and air to the cathode.

5.3.4 Post-mortem Analysis

EDX was used for the elemental analysis of the exposed samples. Based on the explained method, a cross-section of the anode was divided in an array of 20 rectangles and the composition inside each rectangle was analyzed. Fig. 5.8 presents the EDX analyses for cases 1 and 2. It clearly indicates that Si is deposited everywhere and with a gradient from the anode surface towards the interface with the electrolyte. A higher amount of Si is deposited at the anode-gas surface than close to the electrolyte interface. A similar trend in Si distribution over the anode cross-section is observed for both cases; due to the measurement error it cannot be concluded whether the difference between the two plots is significant. The revolatilisation of $SiO_2(s)$ to $SiO(g)$ might occur at a slow rate. Possibly, if the cell were left at OCV for a longer duration, a higher amount of $SiO_2(s)$ could be removed from the TPB. Further experiments are required to verify this.

5.4 Conclusion

The chemical degradation of anode supported Ni-YSZ SOFC single cells by siloxane D4 as a common biogas impurity was evaluated by electrochemical characterization, thermodynamical calculations and micro-structural analysis.

Thermodynamic calculations predict the decomposition of D4 to $SiO_2(s)$ followed by chemical reduction of $SiO_2(s)$ to $SiO(g)$, which can diffuse into the pores and reach the TPBs where it is reoxidized electrochemically to $SiO_2(s)$.
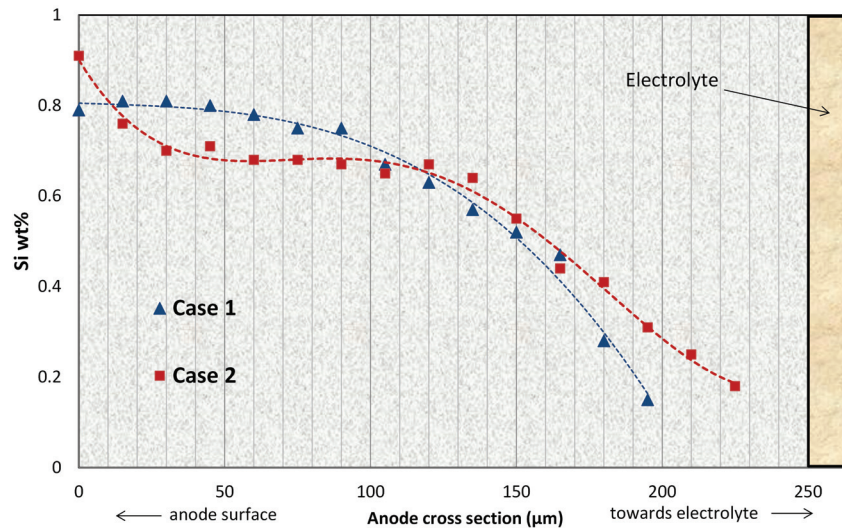
Figure 5.8 – Si distribution over the anode cross-section. Higher amount of Si is deposited towards the anode surface than in areas close to the electrolyte.

The IV result of the case 1 test study (D4 in H_2-fuel only) showed a partial recovery of the cell performance, after contamination, by maintaining cell polarization at the same current density (0.25 A/cm^2) rather than operating in OCV mode or high current densities. Yet analysis of EIS measurements (at 0.15 A/cm^2) suggested that the recovery in polarization resistance, after exposure to siloxane D4 is slightly better if the cell is left at OCV rather than when kept polarized. SEM-EDX analyses clearly indicate that Si is deposited everywhere with a gradient from the anode surface towards the interface with the electrolyte.

This study confirmed that siloxanes have to be removed completely from biogas feed to SOFCs. Even trace contamination of the fuel feed at ppb level can affect the SOFC Ni anode, leading to fast degradation.

6 | Chlorine Poisoning

(partly taken from: H. Madi, A. Lanzini, D. Papurello et al. Solid Oxide Fuel Cell Anode Degradation by the Effect of Hydrogen Chloride in Stack and Single Cell environments. Journal of Power Sources, 326, 349-356, 2016.)

Contribution of H. Madi: literature review, design of experiments, single cell testing, post-test analysis, data evaluation and conclusion.

This chapter evaluates the poisoning effect of hydrogen chloride (HCl) on state-of-the-art Ni anode-supported SOFCs at 750 °C in either hydrogen or reformed biogas fuel. Experiments were performed on both single cells and short stacks. The HCl concentration in the fuel gas was increased from 1 ppmv up to 500 ppmv and the cell performance was evaluated at different current densities.

6.1   Introduction

Syngas derived from biomass or coal via gasification contains chlorine, e.g. HCl, Cl_2 and CH_3Cl. Several ppmv of HCl can be present in the producer gas of biomass gasifiers, as high as up to 90 ppmv [119]. Also landfill biogas from municipal solid waste usually contains heavy loads of halogenated compounds [10, 68]. Landfills are still the largest biogas producers worldwide.

Chapter 2, section 2.4.3 provided a literature review on the state-of-the-art effect of chlorine compounds on the performance of SOFCs. In this chapter, the effect of HCl on the performance of the SOFC Ni anode is investigated. The main objective of this study is to evaluate the impact of HCl from low (1 ppmv) to high (1,000 ppmv) concentrations on the performance and durability of single cells and short stacks. The observed stack degradation is compared against single cell degradation. The tolerance threshold concentration of HCl in the fuel gas is evaluated and post-test characterization SEM-EDX is used for correlation with the observed degradation in electrochemical performance. The aim is to determine the need and the extent

of the removal of chlorine compounds from biofuel feeds in order to avoid significant irreversible SOFC degradation.

6.2 Experimental Methods

6.2.1 Single Cells

Commercial Ni-YSZ anode-supported SOFCs were received from Topsoe Fuel Cells (Denmark). The cells were circular with an active cathode area of 7.5 cm^2. All poisoning tests were conducted at 750 °C with 250 Nml/min air at the cathode and 100 sccm of hydrogen or reformed biogas containing a few ppmv contaminant (HCl) at the anode side. HCl impurity was prepared in gas bottles premixed with H_2. Electronic mass flow controllers (MFC, Bronkhorst) were employed to set the anode fuel composition.

Additional experiments on anode-supported single cells (80 mm diameter, 47 cm^2 active area) provided by SOLIDpower (Italy) were carried out with a set-up using ceramic housing. Experiments performed with this second type of set-up will be designated with the term 'Apparatus B' to distinguish it from the one that uses metallic housings ('Apparatus A'). Both test rigs were developed in different labs, and both types of anode supported cells use the same materials and are of similar thicknesses. Obtaining similar results with different test rigs and on similar cells from different suppliers should increase the confidence in them.

Experiments performed with the 'Apparatus A' were carried out at EPFL and the one on 'Apparatus B' at Politecnico di Torino (POLITO).

6.2.2 Short Stack

SOFC stacks consist of 11 Ni anode-supported cells were delivered by Topsoe Fuel Cell (Denmark). The nominal operating condition corresponds to a stack current of 20 A and FU of 60%. The feeding gas for stacks was a mixture that simulates steam-reformed biogas or H_2-rich syngas. The gas molar composition is 0.3% CH_4, 10% CO_2, 19.3% CO, 50.6% H_2 and 19.9% H_2O. The contaminant was directly fed at the stack inlet manifold avoiding its contact with the rest of the Balance of Plant (BoP[1]) (e.g., the fuel pre-heater). Dry filtered compressed air was fed to the cathode side. High-purity gases and demineralized water were used for the anode feed. A summary of the testing details is given in Table 6.1.

Experiments on short stacks A and B were carried out at EPFL and POLITO, respectively.

---

[1]The BoP contains all the direct stack support systems, reformer, compressors, pumps, and the recuperating heat exchangers

Table 6.1 – Details of test conditions for single cells or stacks.

Test type	Origin	Test bench	Conditions	HCl concentration (ppmv)
Single cell	TOFC	Aparatus A	H_2, 0.25 A/cm^2	10- 100
	TOFC	Aparatus A	H_2, 0.6 A/cm^2	10- 1000
	SOLIDpower	Aparatus B	H_2, 0.46 A/cm^2	1- 1000
	TOFC	Aparatus A	H_2, 0.62 A/cm^2	10
	TOFC	Aparatus A	reformed biogas, 0.62 A/cm^2	10- 90
Short stack	TOFC	Stack A	reformed biogas, 60% FU	up to 30
	TOFC	Stack B	reformed biogas, 60% FU	up to 500

6.2.3 Electrochemical Testing

All impedance spectra were measured in galvanostatic mode with a frequency range from 0.02 Hz to 100 kHz and a 20 mA AC perturbation at 0.25 A/cm^2, using a Zennium electrochemical workstation (Zahner, Germany).

6.2.4 SEM/EDX Imaging and Image Analysis

Pieces of the tested cells were prepared for SEM investigations using a Gatan Ilion II cross-section polisher. The sample was glued on a mask and an Ar beam used to polish a flat surface. A Zeiss Merlin scanning electron microscope 1-30 kV Schottky was used to take surface and cross-section images at low acceleration voltage. EDX spectroscopy was used for elemental analysis approximation of the studied zones of the exposed samples. To conduct EDX analysis also at higher acceleration voltage and thus to avoid charge accumulation, a carbon coating of 15 nm was sputtered on the samples.

6.3 Results

Several tests were performed to evaluate the effect of HCl on the performance of Ni-YSZ. Fuel composition, current density and fuel utilization were the variable parameters.

6.3.1 Operation on H_2– single cell

Fig. 6.1 (A) shows variation of cell voltage with time by exposure to 10–100 ppmv HCl at 750 °C and 0.25 A/cm^2 ('Apparatus A')– conditions of line 1 in Table 6.1. The cell was initially operated on clean hydrogen for a duration of 70 h. The 'baseline' voltage degradation rate under clean hydrogen was 1.9% per 1000 h, calculated from the ratio of voltage decrease to initial voltage (959 mV). Afterwards, 10 ppmv HCl was added to the fuel stream. A constant degradation in cell voltage was observed due to this exposure, with a higher slope than the baseline, 3.1% per 1000 h. The performance deterioration becomes ever more visible at higher concentrations of HCl. Recovery of the cell voltage was observed after exposure to 100 ppmv HCl.
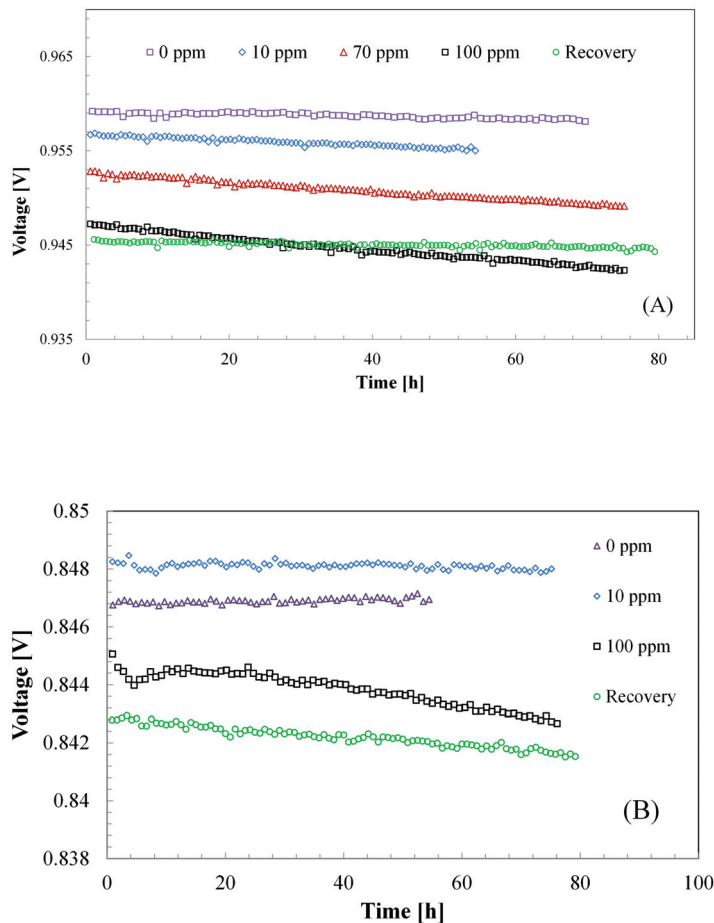
Figure 6.1 – Single cell operation on H_2 fuel gas, A) at 0.25 A/cm^2 with HCl from 10 to 100 ppmv in the fuel feed (FU= 13%). B) At 0.6 A/cm^2 (FU= 31%).

Fig. 6.1 (B) exhibits the effect of the impurity on the performance at higher current density (0.6 A/cm^2) ('Apparatus A')– conditions of line 2 in Table 6.1. The cell was first operated for 50 h on HCl-free fuel gas and afterwards different amounts of HCl were added. There was no regeneration step in between each level of HCl concentration. The degradation trend is constant, similar to what was observed with operation at lower current density (Fig. 6.1 (A)). In the case of 100 ppmv HCl, the performance drop observed at 0.6 A/cm^2 is larger than the degradation effect at 0.25 A/cm^2 (13% per 1000 h), indicating that operating at higher current density can aggravate the poisoning effect. Switching back to HCl-free fuel gas did not restore the initial cell performance on the short term; the degradation rate was nevertheless reduced, to 7.5% per 1000 h.

The effect of HCl with H_2 was further explored at intermediate current between the previous two cases, by varying the HCl concentration from 1 to 1000 ppmv using 'Apparatus B'– conditions of line 3 in Table 6.1. Between each exposure level, a regeneration step in HCl-free H_2 was allowed. Results are shown in Fig. 6.2. A non-linear degradation trend was observed

for the cell voltage with increasing HCl concentration. Below 20 ppmv of HCl, degradation remained modest, in line with the trends found in the Figs. 6.1 (A) and (B). Once exposure levels of 200 ppmv and more were used, no more recovery in cell voltage could be observed.
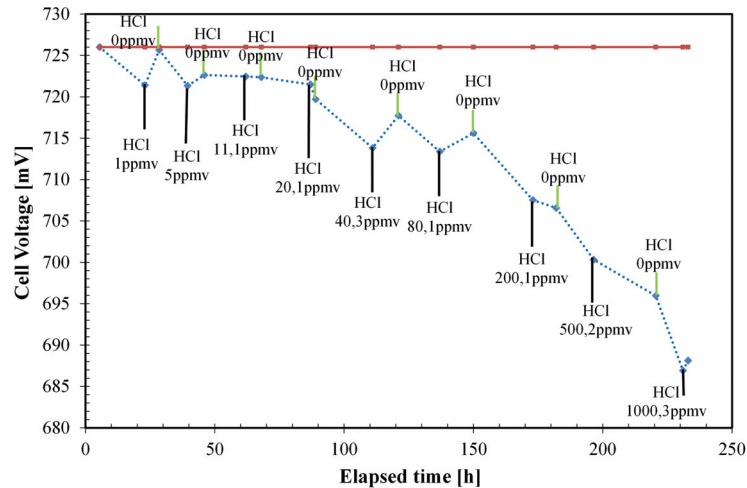
Figure 6.2 – Single cell operation on H_2 fuel gas, at 0.46 A/cm^2 and FU = 30% (active area 47 cm^2, 'Apparatus B').
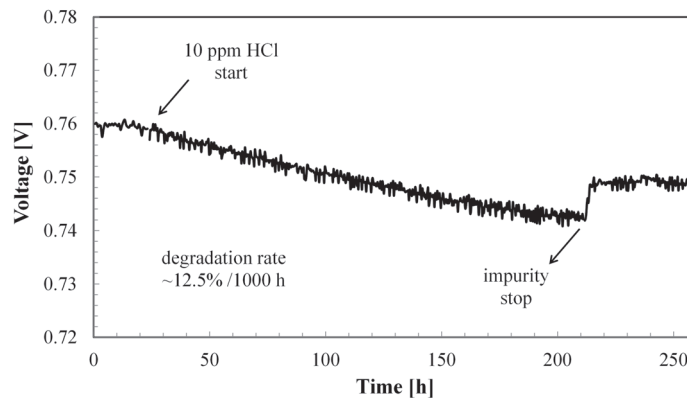
Figure 6.3 – Single cell operation on H_2 fuel gas at 62% FU for the duration of 250 h, 'Apparatus A'.

Durability was evaluated in 'Apparatus A' when exposed to an amount of HCl at reasonable fuel utilization (FU 62%) (Fig. 6.3)– conditions of line 4 in Table 6.1. A constant HCl concentration of 10 ppmv was added for around 200 h. The resulting degradation rate during this testing period was linear, at 12.5% per 1000 h, higher than the observed degradation rate at the same impurity concentration (10 ppmv) but operating at lower FU. Cell voltage partially recovered within a few hours after switching off the HCl flow. According to the experiments shown, at higher current densities or higher fuel utilisation, concentration polarization plays a role in the degradation.

75

6.3.2   Operation on Reformed Biogas- Single Cell

More important is to evaluate the effect of HCl on the performance of SOFC operated on reformed biogas. Fig. 6.4 shows its polarization behavior, with 'Apparatus A'– conditions of line 5 in Table 6.1. The exposure duration for each HCl concentration was about 25 h. Degradation behavior is constant with time, like what was seen for the cell fed with H_2. Degradation is limited with fuel gas containing 10 ppmv HCl (1.1% per 1000 h). It increases to 5.5%/kh with increasing HCl concentration to 90 ppmv.
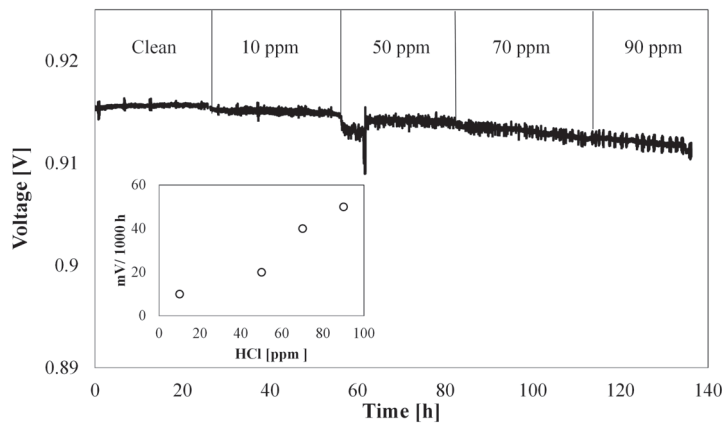
Figure 6.4 – Single cell operation on reformed biogas at 750°C and 0.25 A/cm^2

The effect of HCl on the performance of SOFCs fed with hydrogen or reformed biogas at the same current densities (0.25 A/cm^2) is summarized in Fig 6.5. Results indicate that HCl addition causes a slightly larger performance drop under hydrogen fuel than under reformed biogas fuel.
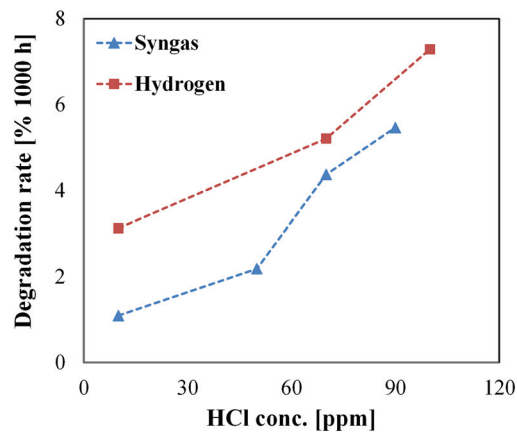
Figure 6.5 – Degradation rate vs. contaminant concentration for cells fed with hydrogen and reformed biogas.

6.3.3 Operation on Reformed Biogas- Short Stack

The effect of HCl on the short stack performance is shown in Figs. 6.6 and 6.7. In 'stack A' (line 6 in Table 6.1), the HCl concentration was varied from 2 to 30 ppmv added to the anode reformate feed and the stack was exposed to each concentration for around 100 h. No degradation in stack performance is seen up to 20 ppmv of HCl in the fuel stream. At 30 ppmv HCl a slight degradation sets in; however, analysing the test data showed a shortage of fuel due to a minor blockage of the fuel line during this period. Because of this issue, we are not able to state if the observed degradation after the injection of 30 ppmv HCl is due either to HCl contamination or the fuel shortage. The data reveal that at least up to 20 ppmv, HCl did not cause any measurable degradation in stack performance under the used test conditions.
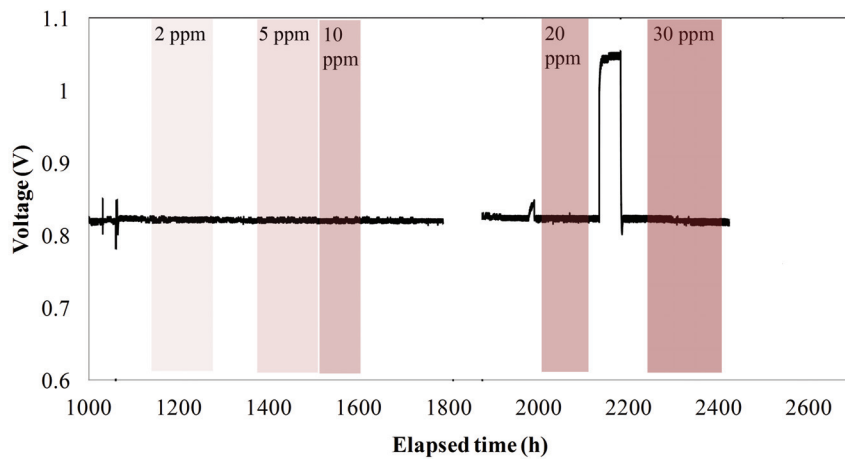
Figure 6.6 – 'Stack A' poisoning by HCl from 2 to 30 ppmv at 750 °C and 60% FU with reformed biogas fuel
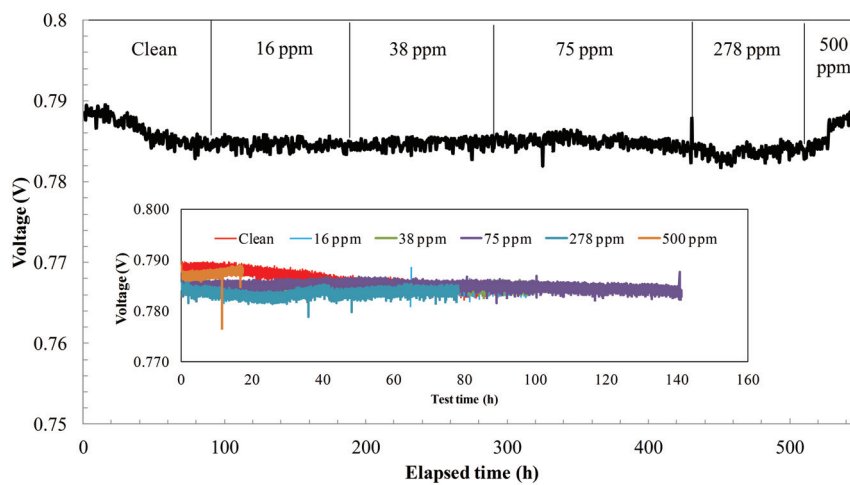
Figure 6.7 – 'Stack B' HCl poisoning from 16 to 500 ppmv. (Courtesy of POLITO)

A second experiment ('stack B'- line 7 in Table 6.1) was carried out to further clarify the impact of HCl on the stack performance. Fig. 6.7 depicts the results, with a variable HCl concentration up to 500 ppmv. The various traces at constant HCl concentration are superimposed to better show relative differences among the tested concentrations. No obvious stack voltage degradation is observed. However, severe corrosion of the anode exhaust pipe was seen in the region where the gas is cooled down before feeding a water-cooled condenser. This indirectly confirms that HCl did indeed pass through the entire stack.

The stack experiments suggest that the role of interconnects and additional feeding piping play a part in determining – and more specifically, limiting – the impact of HCl on the electrochemical performance of the single cells. The HCl adsorption capacity of stack components appears able to mask and potentially significantly delay the anode contamination. At the same time, the visible corrosion of exhaust piping in 'Stack B', suggests that some of the HCl must exit the stack environment without being adsorbed.

6.4   Discussion

6.4.1   Electrochemical Characterization

In order to examine degradation, IV and EIS measurements were performed regularly. Fig. 6.8 shows IV curves recorded before and after each poisoning test of Fig. 6.1 (B). According to this figure, the OCV remains constant over the entire experiment duration. The area specific resistance (ASR) is used to characterize the cell performance. There is a slight change in ASR after poisoning with 10 ppmv HCl; the increase in total ASR is more pronounced when a higher amount of HCl (100 ppmv) is added to the fuel stream. According to this figure, at high current density the concentration polarization results are more affected by the presence of 100 ppmv HCl in the fuel stream.

EIS measurements were used to characterize the cell and obtain more detailed information on degradation processes. The Nyquist (-Z_{img} vs. Z_{real}) and Bode (-Z_{img} vs. f) plots of the impedance data are reported in Fig. 6.9 (A) and (B), respectively. The first observation is that the impedance increased with increasing HCl concentration. The total impedance was increased by 15% from 0 to 100 ppm HCl. Evaluating the impedance at different concentrations of HCl, the serial resistance, R_s (mainly attributed to the resistance of the electrolyte) remained unchanged as HCl concentration increased. However, the polarization resistance R_p, which is attributed to electrode processes, increased. This plot shows two arcs with both of them affected by the addition of HCl.
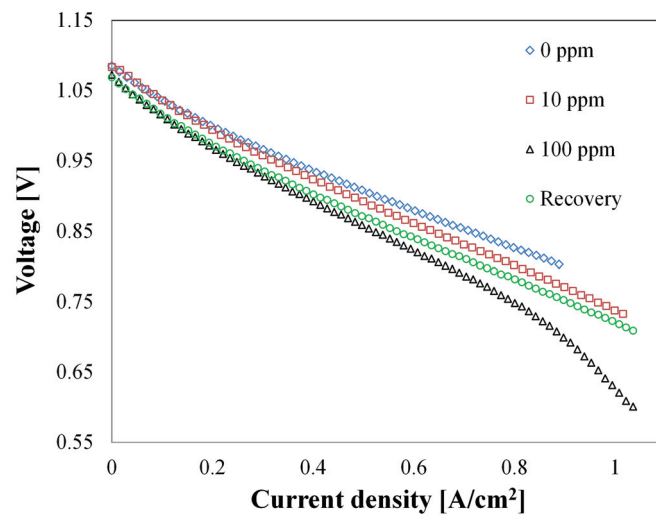
Figure 6.8 – IV curves corresponding to the test of Fig. 6.1 (B).
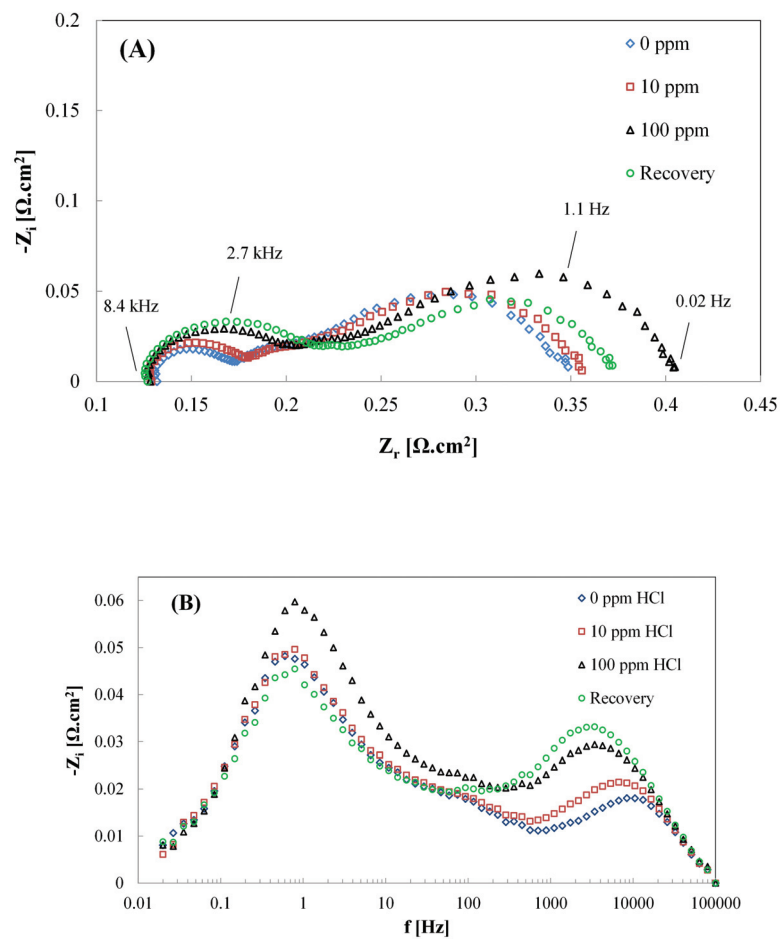
Figure 6.9 – A) Nyquist plot and B) Bode plot corresponding to the test Fig. 6.1 (B).

According to the Bode plot (Fig. 6.9 (B)), there is a peak at high to medium frequencies (5-10 kHz) and another one at low frequencies (1 Hz). There might be several processes which are overlapping but a general trend states peaks at high to medium frequencies correspond to activation polarization which are related to the electrochemical reactions at electrolyte/electrode interfaces. Concentration polarization at low frequencies (below 10 Hz) refers instead mainly to mass transport of the fuel and oxidant through the electrodes. Therefore, a more detailed impedance analysis is needed to separate the contributions from each electrode.

DRT enables the identification of the number of processes and their nature involved in electrochemical cells [120, 121]. DRT calculations were performed using impedance transforms in the software Ravdav [105]. The DRT transforms calculated from the spectra of Fig. 6.8 (B) are shown in Fig. 6.10 (A). The inspection of the DRT plot gives considerably more insight into the system than the raw impedance plot. Four separated peaks with different time constants, which correspond to four different processes, ranging from <10 Hz to several kHz are recognized by the DRT analysis. High frequency peaks (above 1 kHz) are related to ionic conductivity and electrochemical reactions at the TPB [122]. Gas diffusion and conversion processes appear at low frequencies below 20 Hz.

The detailed equivalent circuit resulting from the analysis of the DRTs consists of 6 serial impedance elements, each characteristic of one loss mechanism. The equivalent circuit model used in this work is as follows: L- R_s- RQ_{ionic}- RQ_{TPB}- G- RQ_{diff}- RQ_{conv}. In the fitted model, L is the high frequency inductance and R_s is the ohmic resistance. 2 RQ circuits (a parallel connection of resistance and a constant phase element) representing the anode high-frequency processes (RQ_{ionic} and RQ_{TPB}) and the Gerischer element (G) represents the activation polarization of the cathode. The total activation polarization is the sum of RQ_{ionic}, RQ_{TPB} and G. Further, 2 RQ circuits were used for the low frequency processes (RQ_{diff} and RQ_{conv}). These resistances are most likely connected with the gas conversion and diffusion loss inside the anode substrate. The results from the complex non-linear least squares (CNLS) fitting with the impedance spectra to the above described model are shown in Fig. 6.10 (B).

(A)
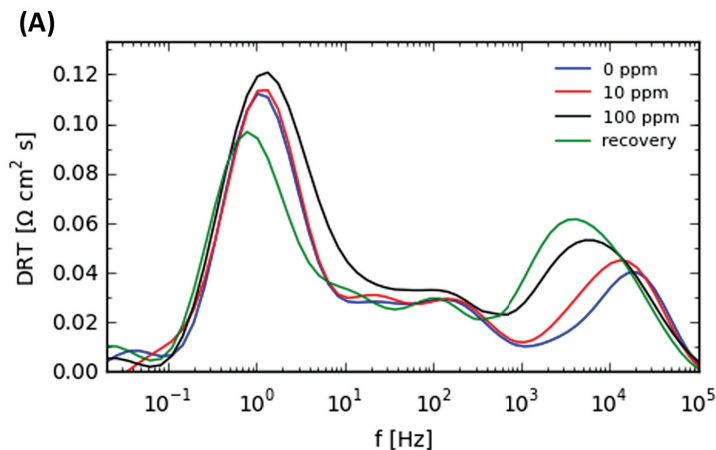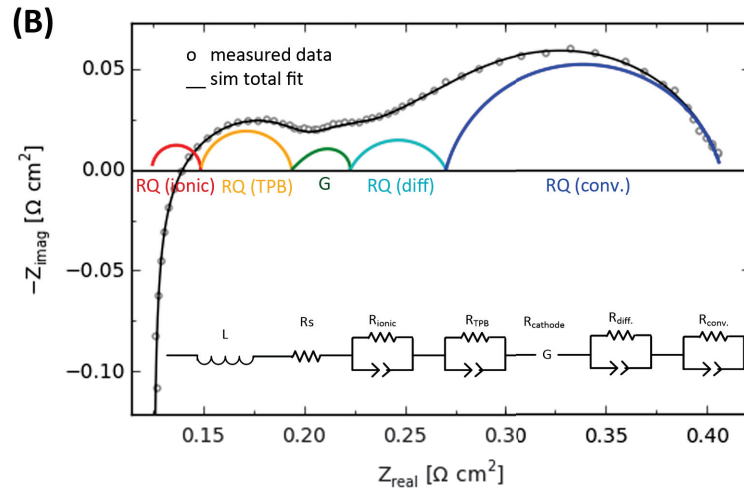
Figure 6.10 – A) DRT calculations of the cell of test Fig. 6.1 (B), exposed to 10 and 100 ppmv HCl. B) Equivalent circuit model of impedance measured during the test, in this case 100 ppmv HCl. The CNLS with a Boukamp goodness [106] of fit of $9e^{-4}$.

Fig. 6.11 shows the fitted values as determined by the model. The results from fitting the impedance data to an equivalent circuit model show, in agreement with the DRT analysis, that exposure to HCl causes degradations at the TPBs (2-4 kHz) and fuel conversion impedance (below 1 Hz), whereas its contribution to the other processes is fairly small. According to this graph, the increase in gas diffusion impedance (10-20 Hz) as the HCl concentration increases, is negligible compared to the other two processes. It can be derived that the increase in cell resistance with exposure to HCl can be due to the presence of electronegative atoms such as Cl which hinder the adsorption of H_2 on Ni surfaces (Eq. 6.1) [123] and also to the formation of $NiCl_2$ (g) via Eq. 6.2, which blocks the reaction sites at the TPBs. Switching to HCl-free fuel gas enables a partial recovery of the initial performance. The recovery occurs for low frequency processes, related to the gas conversion, whereas the impedance response did not recover for processes related to the TPB. An irreversible modification / reconstruction of the TPB is consistent with the findings from the EIS experiments.

$$HCl(g) \rightleftharpoons Cl(ad) + 0.5H_2(g) \tag{6.1}$$

$$Ni(s) + 2HCl(g) \rightleftharpoons NiCl_2(g) + H_2(g) \tag{6.2}$$
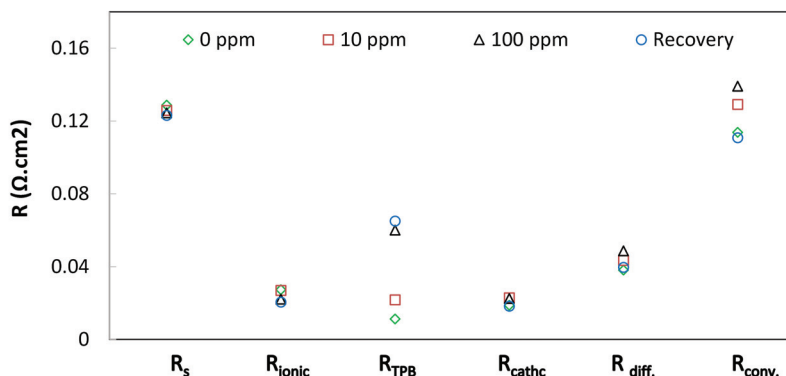
Figure 6.11 – Contribution from each resistance based on the equivalent circuit model.

6.4.2 Post-test Analysis

Post-test characterization of a sample which was operated on H_2 fuel and exposed to 100 ppmv HCl was performed using SEM/EDX analysis. For comparison, a similar analysis was performed on a Ni/YSZ anode tested in clean H_2 fuel. No obvious change in microstructure due to the HCl exposure was observed. Haga et al. [82] found a significant microstructural change of the cermet anode surface and a lower Ni-to-Zr ratio after poisoning by 1000 ppmv Cl_2. This lower Ni-to-Zr ratio was explained by the sublimation of $NiCl_2$. Although our experimental conditions are different and we used a different chlorine compound at lower concentration, we were not able to observe by HRSEM any small size (<100 nm) deposited Ni particle, that could indicate Ni sublimation via $NiCl_2(g)$. Line scan cross section EDX analysis from the anode surface towards the electrolyte was conducted, to evaluate the elemental ratios; no difference in Ni-to-Zr ratio from anode surface towards the electrolyte was apparent.

Interestingly, EDX mapping of the anode cross section showed traces of Cl, at the peripheries of Ni grains (Fig. 6.12). Investigation of Xu et al. [85] by XPS analysis showed traces of Cl at the anode cross-section and the anode surface. According to Trembly et al. [84], the formation of a secondary nickel phase, $NiCl_2(s)$, is not feasible. Combining our results with the previous investigations suggests that chlorine is present in the form of adsorbed species, rather than as a chlorine nickel compound.

6.4.3 Poisoning Mechanism

The effect of foreign atoms on the adsorption kinetics of gases on the Ni surface is of considerable interest in view of explaining the role of poisons in heterogeneous catalysis [123]. According to Coute et al. [124], Ni-based commercial catalysts are effective in the destruction of trichloroethane, trichloroethylene and perchloroethylene by steam reforming. Nonetheless, the prolonged exposure of the catalyst to HCl is able to deactivate it.
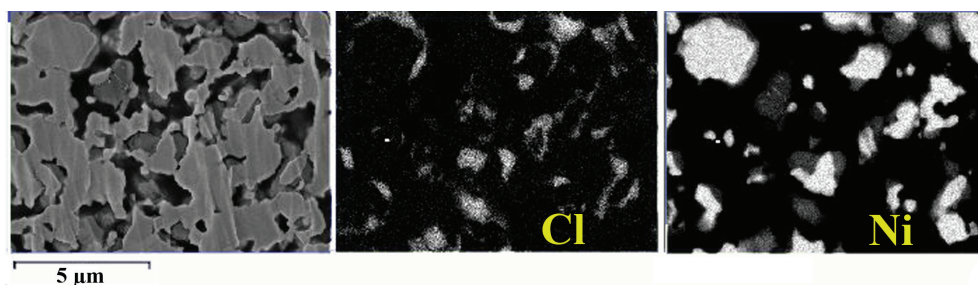
Figure 6.12 – SEM/EDX of the cermet anode poisoning test by 100 ppmv HCl at 750°C.

Marina et al. [95] thermodynamically evaluated $NiCl_2(s)$ evaporation from the Ni surface as the potential degradation mechanism, Eq. 6.3. Their calculations show that formation of solid $NiCl_2(s)$ is not practically possible except maybe for high concentrations of HCl as high as 500 ppmv. The formation of $NiCl_2(g)$ is even more unlikely.

$$Ni(s) + 2\,HCl \longrightarrow NiCl_2(s) + H_2 \tag{6.3}$$

So the expected degradation mechanism for catalyst deactivation is thought to involve adsorbed Cl (or Cl-containing species) onto the Ni surface. However, a clear deactivation mechanism could not be identified in the work of Coute et al.; according to Richardson et al. [125] strong Cl chemisorption most certainly takes place on the Ni catalyst, and even in the presence of H_2, an equilibrium coverage of Cl could be established. However, not clear is the impact of adsorbed Cl on steam-reforming and WGS reactions. Also, reversible type deactivation is reported once Cl contamination is stopped.

Marina et al. [95] investigated the impact of HCl on Ni-YSZ cells. Cl adsorption on Ni surface was the proposed explanation for the reversible performance degradation they observed. According to their findings and related discussion, adsorption-type degradation is consistent with the fact that above a certain HCl concentration in the feeding gas, degradation no further increases (i.e. saturation coverage is achieved) and the ASR relative increase reduces at higher temperatures.

Investigations of Xu et al. [85] on the effect of HCl at the concentration of 100 ppm on a Ni-YSZ anode supported cell showed a slight degradation (1.6% of overall voltage loss) after continuous exposure to HCl for about 300 h. However, the first 100 h showed no degradation at all. EIS experiments neither showed degradation. Post-mortem analysis revealed instead how the HCl-poisoned cell changed the Ni surface morphology. Ni particles all over the exposed area acquired a distinctive rough texture (at the sub-micron scale), showing a more accidental surface than clean samples. This feature showed also a gradient from the gas channel region - where it was more pronounced - towards the electrolyte interface. Hence, Ni-Cl ad atoms seem to possess a larger mobility than Ni particles alone and are responsible of an overall redistribution of Ni particles on the surface of the electrode. Interestingly, this phenomenon can either enhance or reduce the TPB of the fuel cell depending on the specific morphology of

the Ni surface and the degree of penetration of this re-texturizing effect. As proposed by Xu et al., the adsorbed Ni-Cl species might also possess a lower melting point and thus higher volatility compared to Ni, thus causing a gradual sublimation and then redistribution of Ni particles over the long run. A similar phenomenon was observed also by Haga et al., even though their explanation involved the formation of $NiCl_2(s,g)$, which seems more unlikely (according to thermodynamic equilibrium calculations) than the formation of adsorbed Ni-Cl species.

The Ni-Cl species block active sites needed for the electrochemical reactions. As current increases, the impact of having a reduced TPB gets more pronounced and so the HCl-poisoning effect is enhanced. This work showed that degradation rates vary by operating single cells at low (13%, Fig. 6.1 (A)) and high (62%, Fig. 6.3) fuel utilization, with higher loss rate at the higher FU. This is an indication that Ni coverage by the Cl species and increase in the activation polarization play the major role in the performance degradation.

A possible explanation for the reduced poisoning of cells operated with reformed biogas compared to H_2 fuel is that CO is highly competitive with respect to Cl adsorption on Ni atoms. CO coverage would thus provide protection toward Cl contamination. At the same time, adsorbed CO does not behave as a poison since it is either electrochemically oxidized to CO_2, or it reacts with H_2O to form H_2 and CO_2 (through WGS reaction). Hence, CO presence might be a key to prevent Cl adsorption on the Ni surface.

For the stack experiment, where no voltage degradation was observed even for high HCl concentrations in the fuel gas up to 500 ppm – actually voltage improved over the time as HCl concentration increased –the most probable explanation is that Ni surface coverage might actually occur but without really limiting the TPB activity due to reduced coverage compared to the overall available Ni sites. More importantly, Ni changes are expected to take place being responsible of a redistribution of Ni particles that enhances TPB rather than reducing it. So an overall performance improved is observed that is consistent, or at least foreseeable, with the observations reported by Xu et al. and Haga et al..

6.5   Conclusion

The effect of HCl from 1 to 1000 ppmv in the fuel stream on the performance and durability of commercial Ni-YSZ anode-supported SOFC, single cells and short stacks was investigated. Polarisation curves reveal that:

- HCl affects the cell performance more severely when operated at higher current density, mainly due to diffusion limitations.

- Performance drop is larger when the cell is fed with hydrogen than reformed biogas.

- In the case of short stacks, no degradation is observed, except severe corrosion of the anode exhaust pipe.

DRT analysis and an equivalent circuit model were used to analyse the cell impedance response and investigate in more detail the affected processes.

- The following model, which was in good fit with the impedance data was used: L- Rs- RQ_{ionic}- RQ_{TPB}- G- $RQ_{diff.}$ - $RQ_{conv.}$.

- The model showed that HCl causes degradation at the TPB (2-4 kHz) and fuel conversion impedance (below 1 Hz).

- The partial recovery was related to the low frequencies. In fact the activation polarisation at the TPB did not recover.

Post-test analysis of the anode cross section showed traces of Cl element, where Ni is located. Combing these results of this work with the investigations of Trembly et al. [84], we suggest that chlorine is present in the anode in the form of an adsorbed species, rather than as a solid nickel chloride.

The total amount of chlorine compounds in biogas are typically low, as shown in chapter 2 no gas clean up for these compounds is required.

7 Sulfur Poisoning

(partly published in: H. Madi, S. Diethelm, Ch. Ludwig and J. Van herle. Organic-Sulfur Poisoning of Solid Oxide Fuel Cell Operated on Reformed Biogas. International Journal of Hydrogen Energy, 41, 12231-12241, 2016.)

This chapter analyzes the performance and degradation of an AS Ni-YSZ SOFC exposed to H_2S and thiophene (C_4H_4S). Extensive investigations have previously been made on the effect of hydrogen sulfide as an inorganic sulfur compound on the performance of SOFCs but much less on complex sulfur-containing molecules like thiophene. The impact of this organic sulfur compound on the performance of SOFC Ni-YSZ anodes is reported as a function of temperature and the impurity concentration.

7.1   Introduction

Biomass-derived fuels such as gasified biomass for SOFCs have been addressed in several articles [126, 127]. Impurities in the biomass-derived fuel e.g. sulfur compounds, chlorines and tars can poison both the reforming and electrochemical activities of the anode. Among these impurities, sulfur is notorious. The interaction between sulfur-containing molecules and Ni-based anode materials is an important research topic in SOFCs. Even in small amounts, they deactivate steam-reforming and water gas shift reactions. Ni-YSZ anode supported SOFCs have limited tolerance towards sulfur compounds [43, 83, 128].

In most of the investigations, H_2S is chosen as the sulfur model compound as it is by far the most frequent sulfur based molecule in biogas and gasified biomass or coal. However, a variety of S-containing hydrocarbons are also found in biomass gasifiers [129]. The most abundant of these S-containing hydrocarbons are thiophenes (0.9-11.4 ppmv) and benzothiophenes (0.14- 4.4 ppmv) [93]. Their concentrations depend on the type of gasifier and also the source of biomass. In the case of natural gas, as it is odorless and colorless, sulfur compounds are

added for safety reasons. Tetrahydrothiophene (THT) is a commonly used odorant additive to natural gas in Europe [130]. The limits are documented in Marcogas GI-OD-04-01 and range from 2.5 to 10.2 ppmv.

This chapter investigates the effect of thiophene on the performance of AS Ni-YSZ SOFCs. Experiments are performed to evaluate the impact of this impurity on SOFC performance at a constant (5 ppmv), and at variable concentrations ranging from 1-15 ppmv in the fuel stream. The first set of experiments compared operation at 750 °C and 700 °C. The second set of experiments evaluates the cell performance at a constant concentration of the impurity (5 ppmv) for a minimal useful time (100 h). The degradation mechanism of this sulfur compound on the Ni anode is interpreted based on these experiments using an EIS analytical method.

7.2 Materials and Methods

7.2.1 Methane-free Biogas

Direct feeding of biogas to SOFCs has been proven to be feasible for multiple SOFC designs and materials by several experimental studies [6, 43, 44, 131]. However, carbon may form during the operation of a direct-biogas SOFC and this will gradually deactivate the anode catalyst and consequently affect the electrochemical reactions.

A way to overcome this problem (carbon formation) is to modify the conventional biological path of the biogas production [132]. In this approach a methane-free biogas is produced by inhibition of the methanogenic activities, creating a high quality fuel, consisting mainly of CO_2 (70 to 50%), H_2 (30 to 50%), and traces of CO and H_2S. There are some advantages in using methane-free biogas [132] such as the endothermic behavior of the reverse water gas shift reaction (rWGS) and self-cooling of the stack that increases the efficiency of the system. This self-cooling is less excessive than in the case of dry reforming and therefore prevents additional thermal stress to the cell due to the large temperature drop from the endothermicity of the reforming reaction. Using methane-free biogas is anticipated to reduce the effect of H_2S poisoning as sulfur highly affects the methane reforming process.

A reference reformed biogas composition of 50, 20, 10 and 20 (vol.%) for H_2, CO, CO_2 and H_2O, respectively at chemical equilibrium was considered. The equilibrium gas composition was calculated with the thermodynamic database HSC Chemistry (version 7.1, Outokumpu Research Oy, Finland). Afterwards, this equilibrium gas composition was replaced by a mixture of H_2 and CO_2 to obtain the same equilibrium gas composition at high temperatures. This proper gas composition was 70 vol.% H_2 and 30 vol.% CO_2. Fig. 7.1 presents the equilibrium gas composition for this mixture from 300 to 800 °C. The figure also indicates the formation of C(s). The last section of this chapter investigates the carbon formation by post analysis of the samples.
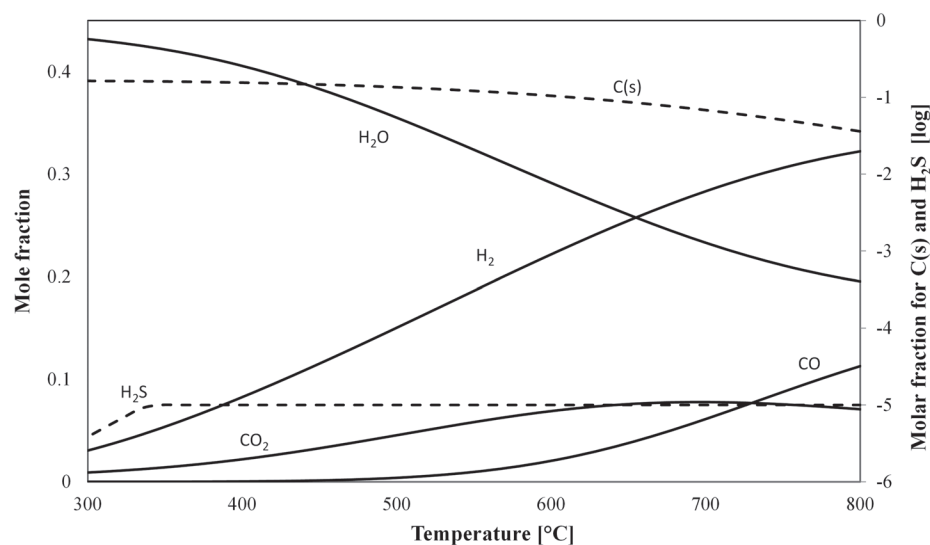
Figure 7.1 – Equilibrium gas composition vs. temperature (left axes). The right axes shows C(s) formation and decomposition of thiophene to H_2S.

7.2.2 Experimental

The SOFC single cells used for this experiment were commercial AS Ni-YSZ SOFCs, with an active cathode area of 3.1 cm^2, produced by SOLIDPower. Cathode and anode were contacted by gold mesh and nickel foam, respectively. A commercial glass was used for sealing. Simulated reformed biogas of 70 vol.% H_2 and 30 vol.% CO_2 was used. A trace level of thiophene (50 ppmv) was prepared in gas bottles premixed with H_2. Bronkhorst mass flow controllers were employed to control the gas feeds. The total anode and cathode gas flow rates were maintained constant at 75 sccm and 200 sccm, respectively. The poisoning test was carried out by replacing the pure H_2 flow in the mixture with impurity-containing H_2 gas (premix of 50 ppmv C_4H_4S in H_2). Cell voltage was measured at a constant current density of 0.25 A/cm^2.

Before focusing on the poisoning effect of thiophene, a test was accomplished in order to investigate the H_2S impact on the cell performance with a fix concentration (3 ppmv). The test was performed at 750 °C under 0.25 A/cm^2 and the reference reformed biogas composition (50, 20, 10 and 20 (vol.%) for H_2, CO, CO_2 and H_2O, respectively) was used.

Several experiments were performed evaluating the effect of thiophene. In Test #1, the cell was operated at 750 °C and then the temperature was reduced to 700 °C (Test #2). The thiophene concentration was varied between 1 ppmv and 15 ppmv. The objective was to evaluate the impact of thiophene on the performance of the Ni-YSZ anode at different concentrations. Test #3 focused on the cell performance degradation at a constant concentration of the impurity (5 ppmv) during 100 h of exposure at 700 °C.

Impedance spectra were recorded by a IM6 electrochemical workstation with ac-amplitude of 20 mA at DC current density of 0.25 A/cm^2. A low impedance cable set (LoZ, provided by Zahner) was used to reduce the inductance. The test frequency range was 100 kHz to 20 mHz. Electrochemical measurements were made before and after every change in thiophene concentration. Steady-state polarization was measured by the same workstation in order to avoid disruption of the test during polarization.

7.2.3 SEM Imaging and Image Analysis

SEM-EDX was used for elemental analysis of the samples exposed to this impurity. We investigated carbon formations due to decomposition of the aromatic sulfur compound by a method described as follows. The sample was broken with tweezers and polished with a Ilion 3 (Gatan) cross section polisher for several hours (depending on the sample), at 5 or 6 keV, over an angle of 85° without inclination of the gun. Tens of microns were removed. For this step, the sample had to be glued onto a mask to allow the beam to polish a flat surface. Silver paint was used to glue the sample and cover the external surface of the sample to make its surface conductive thereby avoiding charging during observation.

A Merlin Zeiss scanning electron microscope, 1-30 kV Schottky was used to take surface and cross-section images at low acceleration voltage. EDX analysis was used for the elemental distribution of the exposed samples. Rectangular arrays (45 in number) parallel to the electrolyte were drawn and the area inside these rectangles was analysed by EDX. This approach gives average compositions depending on the distance from the electrolyte (or from the gas interface, depending on the point of view). The more closely spaced the array rectangles, the more precise the results.

7.3 Results and Discussions

7.3.1 Electrochemical Polarization Behavior

Poisoning effect of H$_2$S

Fig.7.2 clearly shows how introducing H$_2$S to the fuel stream affects the cell performance. It is possible to observe the fast initial degradation followed by a quasi-stable voltage as it was explained in the literature review chapter. Sulfur poisoning of the Ni-anode is partially reversible. Once the H$_2$S is stopped, a voltage increase is observed that suggests S desorption form the Ni sites. The desorption trends are quite similar to corresponding adsorption ones. However, the performance recovery is not full. It is likely that some sulfur remains trapped in the TPBs thus permanently increasing the anode polarization.
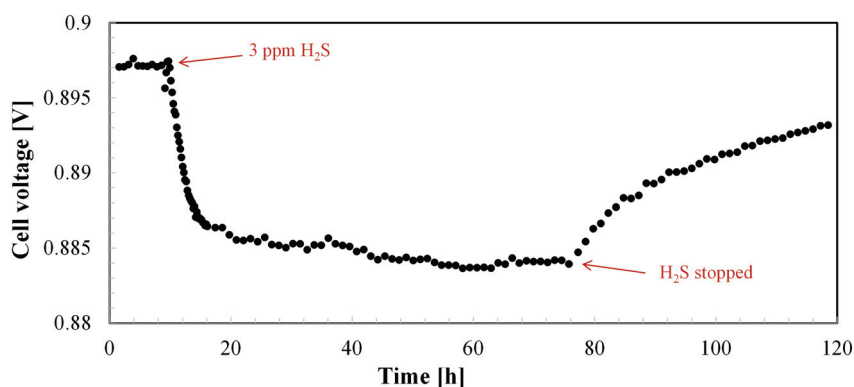
Figure 7.2 – Polarization behavior of the Ni-YSZ anode measured in the fuel containing 3 ppmv H_2S at 750 °C under 0.25 A/cm^2.

Variable concentration- thiophene

Figs. 7.3 (a) and (b) show the polarization behavior of the Ni-YSZ anode measured in fuel containing thiophene at 0.25 A/cm^2 at 750 °C and 700 °C, respectively. The thiophene concentration was increased from 1 ppmv to 15 ppmv and then recovery of the cell was examined by stopping the impurity flow. These two runs were performed on the same cell. Initially the cell was operated at 750 °C (Test #1) and after 40 h of stabilization under the reformed biogas, 1 ppmv of thiophene was added to the fuel flow.

As shown in Fig. 7.3, the initial cell voltage was 900 mV and decreased to 879 mV when exposed to the fuel containing 1 ppmv thiophene. The figure shows that the cell potential was stabilized after around 15 h. This behavior is similar to what is known from Ni-YSZ exposure to H_2S (initial steep degradation followed by slow gradual degradation) [88]. Interestingly, an increase in thiophene concentration did not affect the cell performance further and stopping the impurity flow even caused an additional drop in the cell voltage. The experiment was repeated to confirm this behavior.

Indeed, the cell voltage showed slight improvement at higher impurity concentration (Fig. 7.3 (a)). The fuel gas composition is believed to cause the deactivation of the rWGS [132], Eq. 7.1 and therefore explain this observation, and the one that removing the impurity feed at t=130 h leads to a small decrease in cell performance. Feeding the cell with the H_2/CO_2 composition obviously first promotes the rWGS; deactivation of the Ni catalyst by thiophene then reduces the rWGS reaction rate which consequently produces less steam. This increases the voltage through the Nernst equilibrium. By removing the impurity flow, the catalyst recovers and the rWGS reactivates, producing again more steam and CO. This in turn re-decreases the voltage through the Nernst equilibrium. Thus the variation in steam content explains the cell voltage alteration in Fig. 7.3.
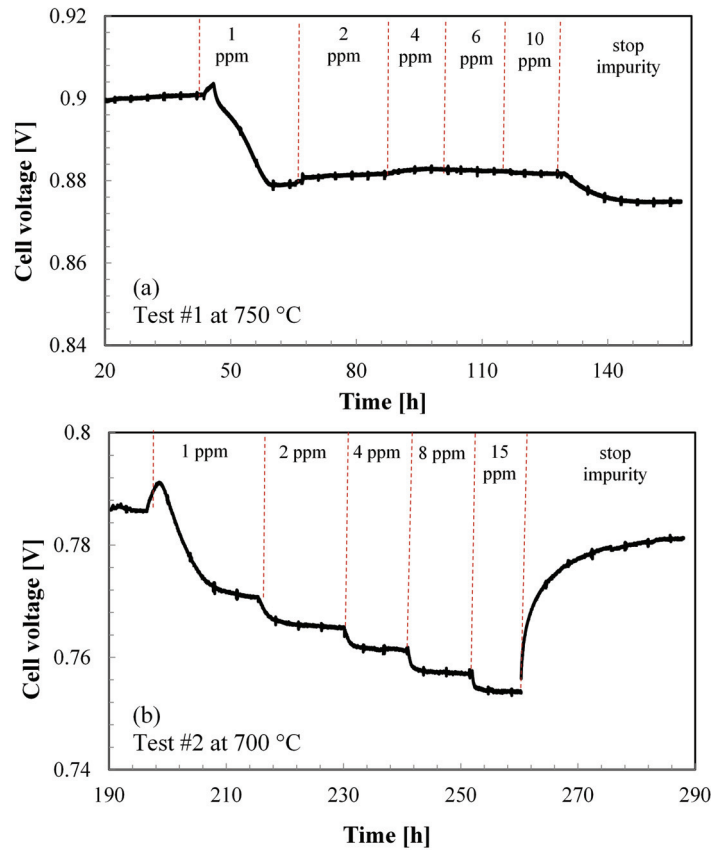
Figure 7.3 – Polarization over time for different concentration of thiophene, a) Test #1 at 750 °C b) Test #2 at 700 °C.

$$CO_2 + H_2 \rightleftharpoons H_2O + CO \qquad (7.1)$$

The test was continued at 700 °C to evaluate the effect of thiophene on the performance of Ni-YSZ at lower temperatures (Test #2). Addition of 1 ppmv thiophene to the fuel caused an initial increase in the voltage followed by a 16 mV decrease in cell potential. Further step decreases in the cell potential were observed with each higher thiophene concentration (Fig. 7.3 (b)). After this exposure to different levels of thiophene concentration, an almost full recovery was observed after 25 h of operation in clean fuel.

Prolonged exposure with fixed impurity concentration- thiophene

Test #3 was designed to evaluate the SOFC with a constant concentration feed (5 ppmv) of thiophene. The cell was first operated at 750 °C with 1, 2 and 4 ppmv of thiopene to reconfirm the data from Test #1. Afterwards, temperature was decreased to 700 °C and injection of 5 ppmv was started after 90 h of operation. Fig. 7.4 represents the cell voltage under 0.25 A/cm^2

polarisation for a duration of 100 h. By addition of 5 ppmv C_4H_4S, the cell voltage dropped steeply within a few hours from 0.824 V to 0.815 V, followed by a gradual only slight further degradation in cell voltage under this poisoning condition. After stopping the impurity flow, the cell voltage recovered to its initial level in approximately 6 h.
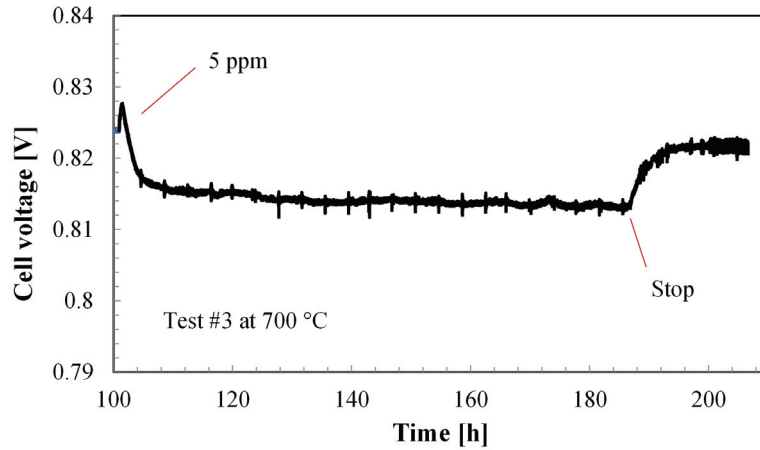
Figure 7.4 – Polarization over time at constant concentration of thiophene (5 ppmv) at 700 °C. Test #3

7.3.2 Sulfur Coverage on Nickel

The electrochemical reactions occur at the TPB active sites which results in the production of current at a certain cell potential. According to thermodynamical calculations, when thiophene is introduced to the system, it decomposes to H_2S which blocks the TPB active sites and covers the Ni surfaces that the fuel must access for the electrochemical and reforming reactions. The resulting decrease in reaction surface area (Eq. 7.2) consequently decreases the produced power.

$$A_{TPB} = A_{TPB}^{\circ}(1 - \theta_s) \tag{7.2}$$

A_{TPB} and A_{TPB}° are active TPB area (m^2/m^3) after and before exposure to sulfur, respectively. Hansen [133] explained the behavior of H_2S adsorption on Ni using a Temkin-like isotherm (Eq. 7.3). The enthalpy of formation (ΔH_f°) in Eq. 7.3 is 280 kJ/mol and the entropy of formation (ΔS_0) is -19 J/mol K and α=0.69. Rearranging this equation, results in Eq. 7.4

$$\frac{P_{H_2S}}{P_{H_2}} = \exp\left(\frac{\Delta H_f^{\circ}(1 - \alpha\theta_s)}{RT} - \frac{\Delta S_0}{R}\right) \tag{7.3}$$

93

$$\theta_s = 1.45 - 9.53 \times 10^{-5} T + 4.17 \times 10^{-5} ln[\frac{P_{H_2S}}{P_{H_2}}] \tag{7.4}$$

where θ_s is the equilibrium sulfur coverage. Eq. 7.4 is not accurate for θ_s close to zero and close to 1 [133].

Similar to Hansen's approach for H_2S, experimental data of Test #2 is now used to derive a relationship between sulfur coverage, originating from the thiophene feed, and the cell performance drop. The latter is calculated using the difference in cell voltage at steady state, before introducing thiophene, and the point where cell voltage stabilized during poisoning. In Fig. 7.5 (a), this cell performance drop (P), expressed in percent, is plotted vs θ_s determined from Eq. 7.4. A very good correlation was found between the performance drop and sulfur coverage. The correlation can be given as in Eq. 7.5. These results are in full agreement with Hansen [133] with a coefficient of correlation of 0.99.

$$P = k \cdot (\theta_s - \theta_{min}) \tag{7.5}$$
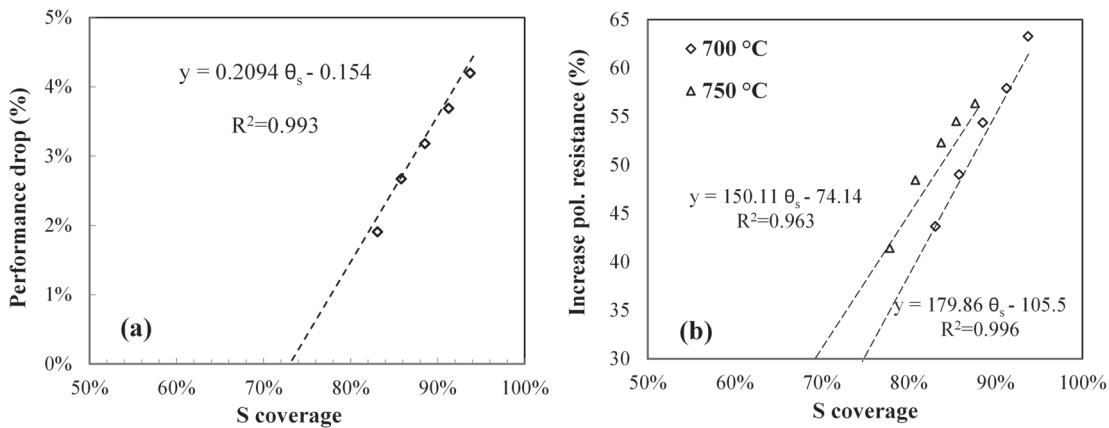
Figure 7.5 – Hansen isotherm, a) performance drop and b) increase in polarization resistance vs. sulfur coverage, respectively.

Experimental data shows that the x-axis intercept (θ_{min}) is not at zero coverage, but rather at 60-70%. This indicates a minimum coverage is required (72% in this study) to have a decrease in the cell performance. θ_{min} depends on the experimental condition such as the fuel gas composition, anode material, temperature and current density. θ_{min} increases with increased current density and increased temperature. The slope of the curve (0.209) is similar to what has been observed by Papurello et al. [87] for short stack test exposure to H_2S up to 25 ppmv, which is 0.191. This slope depends on the current density and temperature. It decreases with increased temperature and decreased current density.

Results reported in [90,99] showed that poisoning by H_2S is lower at higher current density and suggested that adsorbed sulfur atoms are oxidized electrochemically at the TPB (Eq. 7.6) due to the higher flux of O_2 and thus a higher rate of sulfur desorption. However, other studies have reported that higher current loads resulted in a greater deactivation of SOFC performance during sulfur poisoning. For example, Hagen et al. [134], using a Ni-ScYSZ based anode, showed that the sulfur related performance drop was more severe at higher current density such as $1 \, A/cm^2$, due to the deactivation of fuel reforming reactions in the anode, leading to less available fuel and higher local fuel utilization.

$$S(ads) + 2\,O^{2-} \rightleftharpoons SO_2(g) + 4\,e^- \qquad (7.6)$$

Using the recorded impedance response data presented in detail in section 7.3.3, the increase in the cell polarization resistance as a function of sulfur coverage was calculated and plotted in Fig. 7.5 (b). Again a linear dependence of cell resistance with the sulfur coverage was observed in both cases (at temperatures 700 °C and 750 °C). Figs. 7.5 (a) and (b) indicate a direct relation between the number of available sites and the electrochemical activity. In other words, increasing the concentration of sulfur increases the coverage of the available sites. This leads to an increased polarization resistance and consequently to a decrease in cell performance.

7.3.3 EIS measurements

Impedance spectroscopy measurements were recorded before sulfur was introduced into the anode fuel and then during the sulfur poisoning period at each thiophene concentration level tested. Figs. 7.6 (a-c) show the Nyquist plots ($-Z_{img}$ vs. Z_{real}) of the impedance spectra for the Tests # 1, 2 and 3, respectively. The high frequency intercept remained unchanged as the thiophene concentration increased. These figures show two principal depressed arcs, which are overlapped. Due to constant conditions at the cathode, the change in impedance response spectra is caused by the anode following sulfur exposure. Increasing the thiophene concentration mainly affects the first, high frequency, arc while the second, lower frequency, arc changes only slightly. For Test #1, initially there are three arcs but adding 1 ppmv thiophene merged the first two and increased the total polarization resistance considerably. The latter then changed comparatively less (+ ca. 10%) by adding higher amounts of thiophene. The cell resistance partly recovered after removing the impurity, even though the polarization curve of Fig. 7.3 (a) had shown a decrease in cell voltage, for which an explanation was proposed higher.

Fig. 7.6 (c) shows the Nyquist plot for Test #3, at the constant concentration of thiophene (5 ppmv) at 700 °C for 100 h. The polarization resistance increased considerably (23%) by introducing thiophene to the system, with virtually no further change recorded during the 90 h of exposure. The response at time 210 h (20 h after stopping the impurity flow) shows near full recovery of the cell behavior.
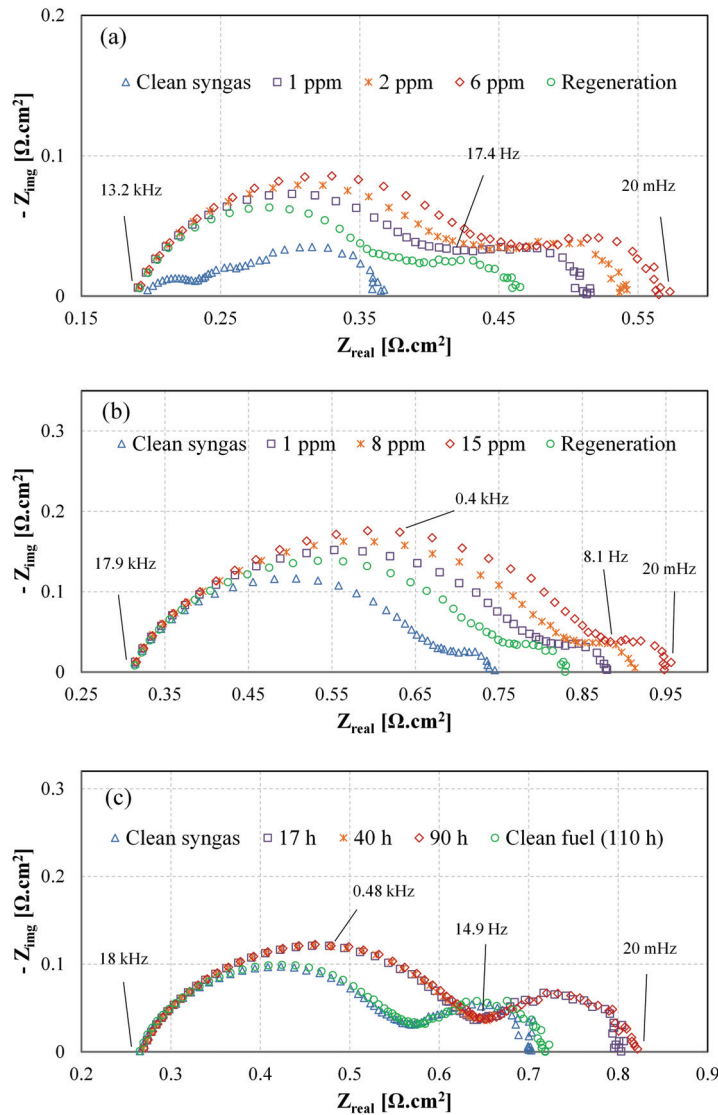
Figure 7.6 – Nyquest plots of a) Test #1 b) Test #2 c)Test #3

To determine the frequencies at which the impedance response is affected most by the addition of thiophene, differential impedance analysis (ADIS) is used. A high-quality ADIS spectrum can be obtained only when the recorded impedance data comply with the Kramers-Krönig transformation, which in practice requires a very smooth data set. This method excludes all processes that remained unchanged by variation of a particular operating parameter.

Fig. 7.7 (a) shows the ADIS transforms from the impedance spectra of Test #1. The response under 1 ppmv thiophene is chosen as the base line as the one before sulfur poisoning had a different shape (3 arcs). This figure focuses on the evolution of the response by increasing the thiophene concentration. The first peak is located in the frequency range of 100-1000 Hz, which is related to the charge transfer reaction. A small peak appears in the frequency range of

10-50 Hz, related to the diffusion of the fuel in the anode substrate. Sulfur poisoning leads to a marked deactivation of the gas conversion as the 3rd peak (0.1-2 Hz) height increases with increased C_4H_4S concentration. Sulfur poisoning is more severe at the lower temperatures (Test #2); the peaks appeared in the same frequency range but the peak height is higher which indicates a higher resistance, for the charge transfer process. The response after the regeneration step indicates recovery at higher frequencies rather than at lower frequencies.

The ADIS calculation of Test #3 aims to evaluate changes in the spectrum over time during exposure to the sulfur compounds. The base line is the spectrum recorded at 17 h of exposure to sulfur. The calculated ADIS indicates no change at high frequencies; however, small changes appeared in the low frequency range, related to gas conversion.
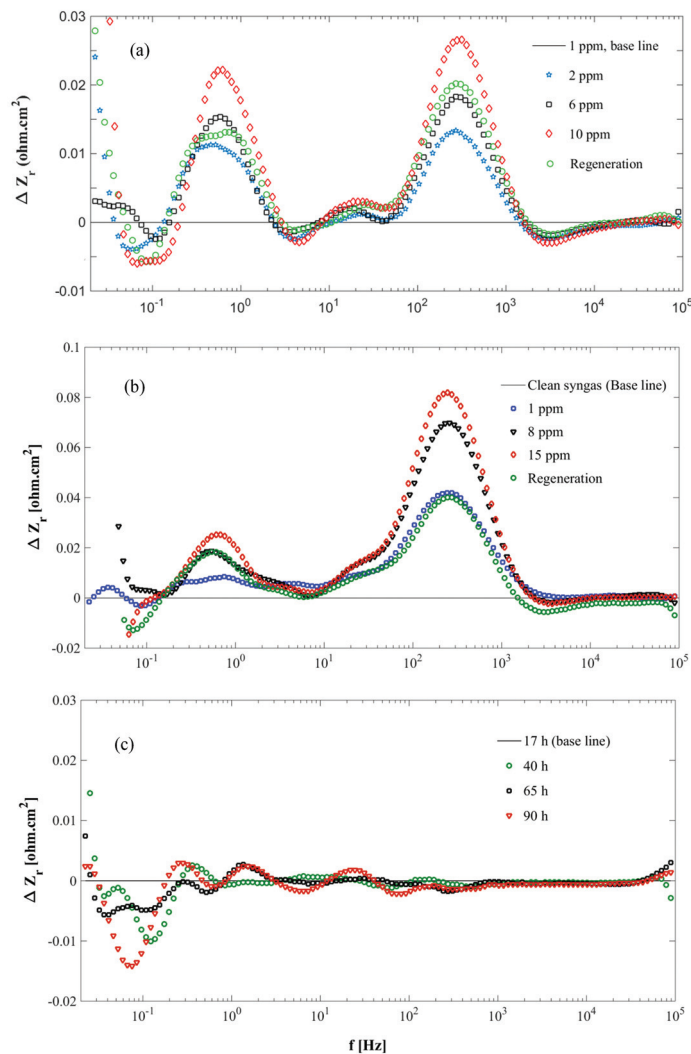
Figure 7.7 – ADIS calculation. a) Test #1, b) Test #2 and c) Test #3.

7.3.4 Post-mortem Analysis

SEM-EDX was used for elemental distribution analysis of the Test #3 sample. The result is compared with a sample, which was operated at the same experimental condition without the impurity (clean fuel), for 200 h. Based on the explained method (section 7.2.3), a cross-section of the anode was divided in an array of 45 narrow rectangles and the composition (S and C) inside each rectangle was analyzed.

No S-compounds, which could be related to the presence of thiophene in the fuel, were found in post-mortem EDX studies. However, the measurement resolution of the instrument used for post-test analysis may be too low. Fig. 7.8 shows the EDX analyses for the sample exposed to clean biogas for 200 h and the sample of Test #3, exposed to 5 ppmv thiophene for 90 h. This figure reveals that carbon is present at a constant concentration along the anode for the sample exposed to clean fuel. Earlier, thermodynamic calculation of Fig. 7.1 showed that C(s) can be produced using 70 vol.% H_2 and 30 vol.% CO_2 fuel composition. Carbon deposition has to occur by dissociation of CO_2 via rWGS and Boudouard reactions.

Same EDX analysis was performed on the sample of Test #3, as shown in Fig. 7.8. Solid carbon is deposited along the anode with a gradient going from the anode surface towards the interface with the electrolyte. A higher amount of C(s) is deposited at the anode-gas surface than close to the electrolyte interface. Carbon deposition rate cannot be increased by poisoning of rWGS; it rather would lead to less carbon. Therefore, one could assume that rather the regeneration (hydrogasification or reforming) of carbon already present is hindered by the presence of sulfur, either by blocking sites necessary for the adsorption of steam or hydrogen, or due to a lower local steam concentration (due to the deactivation of rWGS). Decomposition of thiophene to C(s) can also increase the amount of deposited carbon.
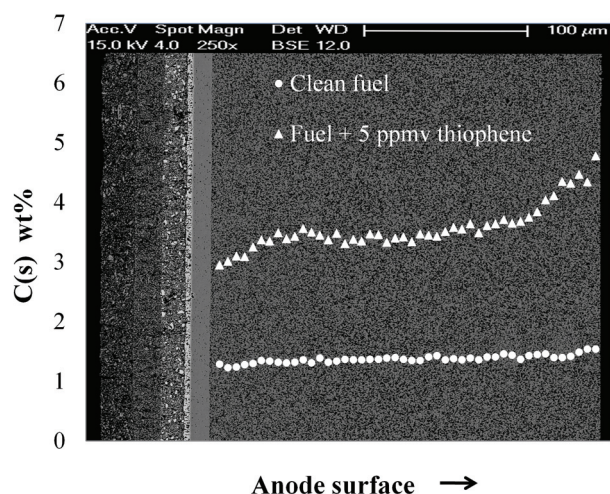
Figure 7.8 – C(s) distribution at the anode cross-section. Higher amount of solid carbons are deposited at the anode surface than areas close to the electrolyte.

7.3.5 rWGS Deactivation

An experiment is designed to further explain the deactivation and activation of rWGS reaction and to confirm the data presented in the section 7.3.1. In Fig. 7.3 (a), the cell voltage showed a slight improvement, when higher amount of the impurity was added to the fuel. Afterwards, stopping the impurity (at 130 h) led to a decrease in the cell performance. We suggested that this is due to the fuel gas composition and can be explained by deactivation of the rWGS, Eq. 7.1.

The cell in this experiment was polarized at 0.25 A/cm^2 and 750 °C (same condition as the Test #1). The cell was operated at 750 °C and after 25 h of stabilization under the reformed biogas composition, 1 ppmv of thiophene was added to the fuel flow. As shown in Fig. 7.9, the initial cell voltage is around 840 mV and it decreases to 825 mV when the Ni-YSZ anode was exposed to the fuel containing 1 ppmv thiophene. Thiophene concentration was increased to 5 ppmv and the cell response (voltage) is shown in this figure. Stopping the impurity flow caused a drop in the cell voltage as in Test #1. This step (poisoning by thiophene and recovery) is repeated several times and results are shown here.
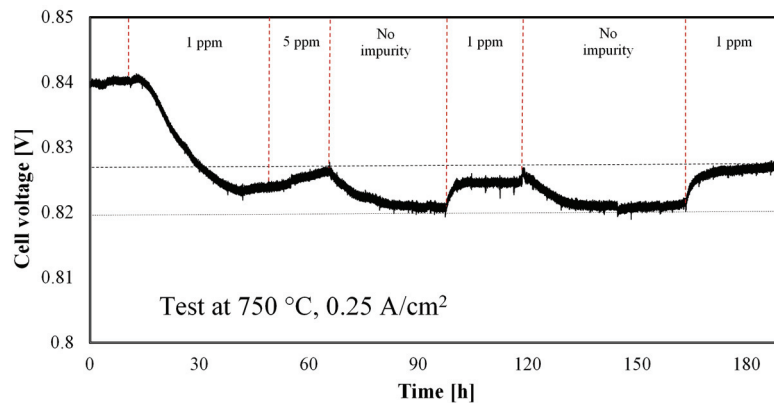
Figure 7.9 – Deactivation and reactivation of rWGS due to the sulfur poisoning.

Qualitative analysis has been performed using a continuum composite electrode model of the anode. The governing equations and the details of the calibration are provided in [135, 136]. The computational domain is one-dimensional and discretized along the thickness of the electrode. The charge transport and transfer are solved in the Ni and YSZ phases and coupled with gas-phase transport and chemical reactions. Only hydrogen is electrochemically converted at the triple-phase boundaries, following the set of elementary steps proposed by Zhu et al. [137]. The dusty-gas model is solved in the pore phase, with steam-methane reforming and the water-gas shift reaction. The local rate of the steam-methane reforming reaction is computed using the kinetic approach of Achenbach and Riensche [138]. The equilibrium of the water-gas shift is approximated locally [139].

The model is sensitive to variations in operating conditions under syngas, even though the electrode behavior under the studied experimental conditions is simplified. The effect of sulfur poisoning on the water-gas shift reaction has been implemented following the Maxed model approach (Eq. 7.7) [140].

$$R = R_0 (1 - \theta_s)^3 \tag{7.7}$$

The reaction rate of the water-gas shift R is provided as function of the rate in the absence of sulfur R_0, and the surface coverage of sulfur on the Ni surface, computed by Hansen isotherm.

The simulation results indicate a change in the Nernst potential of about 5 mV, indirectly caused by the deactivation of WGS reaction. This prediction is in line with the voltage increase observed in Fig. 7.9. This result suggests that the deactivation of the Ni catalyst by thiophene reduces the WGS reaction rate and consequently decreases the production of steam. By stopping the impurity flow, the catalyst recovers and the WGS reactivates, producing steam and CO, which affects the Nernst voltage.

7.3.6 Transient Response to the Contaminant Exposure

Poisoning by thiophene shows an initial transitory improvement in cell voltage (Figs. 7.3 (a-c)). An explanation is the fact that thiophene is an organic sulfur compound which can act as a fuel source. At high temperatures and in presence of fresh Ni catalyst, thiophene decomposes to H_2S and lighter hydrocarbons, Eq. 7.8. Dry reforming (Eq. 7.9) of these hydrocarbons due to the existence of CO_2 increases the concentration of H_2 and CO and consequently the voltage increases. Once the Ni active sites are partially covered by sulfur, the rates of the reforming and electrochemical reactions decrease and then lead to a decrease in voltage. This idea can be rejected because the complete decomposition of thiophene at that low concentration leads to few ppm increase in H_2 and CO concentration, which of course cannot cause the observed 4-5 mV increase in voltage. A more accurate explanation is deactivation of rWGS as explained already in the section 7.3.1.

$$C_4H_4S + H_2 \rightleftharpoons C_xH_y + H_2S \qquad x \leq 4 \tag{7.8}$$

$$C_xH_y + xCO_2 \rightleftharpoons \frac{y}{2}H_2 + 2xCO \tag{7.9}$$

To further examine this transient response, experiments were designed with a varying concentration of CO_2 (Table 7.1). The purpose was to remove CO_2 from Eq. 7.9 and slow down the rWGS reaction. The total fuel flow rate was kept constant with Ar injected to compensate

Table 7.1 – Fuel compositions to evaluate the initial peak.

Fuel composition	H_2 vol.%	CO_2 vol.%	Ar vol.%
1	70	30	0
2	70	10	20
3	70	0	30

for the CO_2 flow. 1 ppmv of thiophene was injected to the fuel gas in all cases. Fig. 7.10 (a) shows the experimental results for different concentrations of CO_2 in the fuel. No increase in the cell voltage is observed with fuel composition 3. Removing CO_2 from the fuel gas (fuel composition 3), eliminates the rWGS. In the case of 10% CO_2 (fuel composition 2) a smaller transient improvement in the cell voltage could be seen as shown in this figure, intermediate between the compositions 1 and 3.
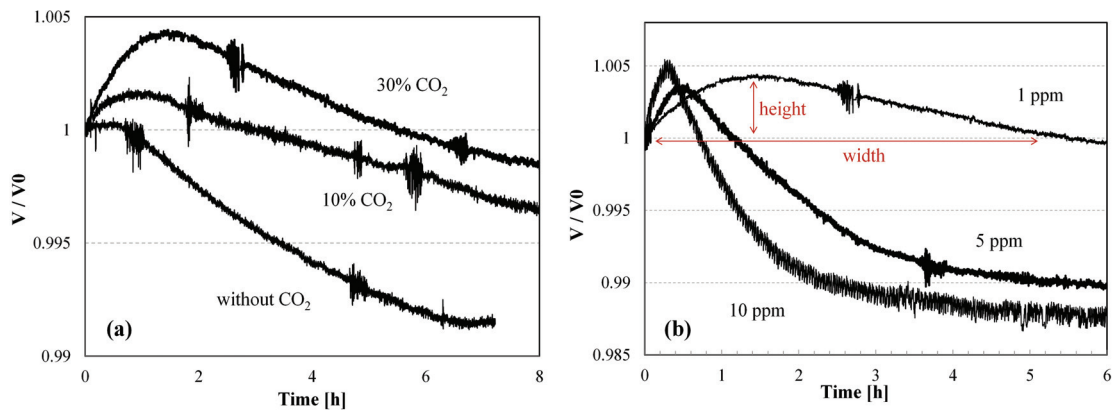
Figure 7.10 – a) The effect of CO_2 content on the initial peak. b) The effect of thiophene concentration on the peak height and length. Normalized cell voltage value.

Further experiments were designed to evaluate the transient peak height and width and their dependence on the thiophene concentration. Fig. 7.10 (b) represents the effect of thiophene concentration on the initial peak height and width. Injection of 5 and 10 ppmv lead to a narrower peak but the height remained nearly constant in all the experiments. Papurello et al. [87] evaluated time-to-coverage (the time needed to reach full sulfur saturation) for variation of H_2S concentration on the Ni anode. Results reveal that higher concentration of H_2S requires less time to cover the surface. This indicates that an increase in the sulfur inlet concentration leads to a faster Ni surface coverage which slows down the rWGS reaction.

7.4 Conclusions

The degradation of organic-sulfur poisoning of the Ni-YSZ cermet anode is described using polarization curves, EIS data and post-test analysis. Experimental results of Test #1 at 750 °C showed a voltage drop of ca. 20 mV (2%) within 10 h following exposure to the sulfur com-

pound. However, increasing the impurity concentration further did not decrease the cell voltage further, although EIS data showed a further slight increase in polarization resistance. The irreversible degradation in Test #1 is suggested to be due to the existence of S-containing compounds and the accompanied change in the microstructure, even though we could not corroborate this by SEM analysis. Results of Test #2 at lower temperature 700 °C (continuation of Test #1) showed that the cell performance drop, determined from both EIS data and cell voltage has a linear dependency on the thiophene concentration and this trend is similar to what has been observed with H_2S poisoning.

The ADIS spectra of exposed samples were compared to identify the affected processes. According to these measurements, thiophene mainly affects the anode charge transfer, specifically at lower temperatures such as those of Test #2. Gas conversion impedance was also affected by the presence of thiophene.

Exposure for a prolonged period of 90 h at this lower temperature (700 °C) with constant thiophene concentration (5 ppmv) did not cause degradation beyond the initial drop. EDX studies identified no S, which could be explained with the proposed adsorption isotherm pathway, where the adsorbed S-species, after feed interruption of the contaminant, revolalitises – which correlates with the observed restoration in cell voltage at this temperature. In general, the observed degradation behavior is similar to that observed with H_2S.

8 SOFC Degradation by the Effect of Tars

This chapter presents an experimental study on the impact of toluene on the performance of AS Ni-YSZ SOFC operating at 800 °C, 0.25 A/cm^2 fed with H$_2$ and biosyngas. Toluene was added to the fuel stream and its concentration increased from tens to thousands of ppm. Each poisoning test was followed by a recovery step. The main goal of this work is to define a concentration threshold of toluene as a model tar compound and to identify the degradation mechanism caused by this tar compound.

8.1 Introduction

In literature "tar" is used as a general expression for all higher hydrocarbon substances with more than 6 carbon atoms, condensible at room temperature and with different properties. Tars are one of the major contaminant present in wood gasification biosyngas, but less pronounced in biogas.

Depending on the gasification technology used, tar contents can be as high as several hundred g/Nm^3 for updraft gasifiers, however they are less present with fluidized bed and downdraft gasifiers, 15 g/Nm^3 and less than 2 g/Nm^3, respectively [141]. Their composition is highly dependent on the reaction conditions, especially temperature during the gasification process [142]. A typical composition of biomass gasification tars are benzene (37.9 wt.%), toluene (14.3 wt.%), other one-ring aromatic hydrocarbons (13.9 wt.%), naphthalene (9.6 wt.%), the remainder being other two-, three- or four-ring aromatic hydrocarbons [142].

In SOFCs, the primary effect of tars is the formation of solid carbon on the anode, especially on the Ni catalyst. Carbon deposition can result in catalyst deactivation by blocking the active sites, plugging the micro- and macro-pores, and build-up of carbon filaments that could potentially destroy the support of the catalyst. Carbon deposits can lead to mechanical stress and finally break-down of the cells due to difference in the thermal expansion coefficient from the one of the ceramic/metal composition of the anode [140]. Carbon deposition effects are strongly dependent on operating parameters of the cell. It is favored especially at low steam-to-carbon ratios [4] and low current densities, because on the contrary high steam and/or oxygen content will lead to oxidation of the carbon and thus consume the deposit.

Singh et al. [143] theoretically investigated the risk of carbon deposition in SOFCs fed by tar-containing biosyngas. They performed thermodynamic calculations in order to predict carbon deposition formation for various operating conditions such as current density, steam and temperature. Tar was represented by a mixture of toluene, naphthalene, phenol and pyrene. Results showed the amount of carbon deposition was suppressed by increasing temperature and the amount of steam in the fuel gas. Also increasing the current density has a positive effect on the removal of deposited carbon and after a critical current density no deposited carbon was observed.

Table 8.1 summarize the studies concerning exposure to tar compounds, short and long time exposure. Recently, Liu et al. [144] studied the interaction between toluene as the model tar and Ni-GDC anode SOFCs at different temperatures fed with syngas (dry and wet conditions). Dry condition is considered as $16\%H_2$, $1.5\%CH_4$, $46.5\%N_2$, $16\%CO_2$, $20\%CO$. The cell did not suffer from carbon deposition at the wet condition and when the cell was loaded with mild current load at the dry condition. Operation with the dry gas composition at OCV might induce carbon formation.

Table 8.1 – Summary of studies involving tar-containing fuels.

References	Anode	Fuel gas	T (°C)	Tar concentration	Duration	Observations
Aravind et al. [145]	Ni-GDC	Humidified H_2 with 4.2% H_2O	750, 850	56- 110 ppm naphtalene	2 h	No significant degradation in performance when the anodes are fed for short time periods H_2 containing naphtalene up to around 110 ppm level.
Kim et al. [146]	Cu-ceria-YSZ	Humidified H_2 with 3% H_2O	700	n-decane and toluene	24 h	Formation of polymeric compound by gas-phase via free-radical reactions at temperatures above 700 °C, which can be removed by steam.
Mermelstein et al. [147]	Ni-GDC, Ni-YSZ	40% H_2, 5%H_2O, balance N_2	765	15 g/Nm^3 Benzene	30 min	structure and composition of the anode and the operational condition have significant role in suppression of carbon formation. Ni-CGO anode is more resilient to carbon formation.
Liu et al. [148]	Ni-YSZ	$16H_2$,1.5 CH_4, 46.5 N_2,16 CO_2, 20 CO with variable H_2O (0-10%)	750, 850	6.3 g/Nm^3 Toluene	40- 300 min	Higher steam and higher current reduce degradation rate. Even with 10% steam carbon can form if the cell is operating at OCV. Threshold can be defined only by considering combination of factors.

In this study, toluene was chosen as the model tar compound since (i) lighter aromatic tars are more difficult to remove than heavier ones [149] and (ii) research showed that the order of reactivity of a single-ring aromatic tar is much superior to that of two- and higher ring aromatics such as pyrene and naphthalene [150]. The literature review showed that most experiments are short tests under humidified conditions and less attention is paid to dry conditions. Here the effects of toluene on the performance of AS Ni-YSZ SOFCs fed with hydrogen and biosyngas are compared for longer tests. The main objective is to evaluate the impact of toluene from tens of ppm to thousands ppm on the anode performance and durability at 800 °C and 0.25 A/cm^2.

8.2 Experimental

8.2.1 SOFC Test Station

In this study, commercial Ni-YSZ anode-supported SOFCs, with active cathode area of 8 cm^2, produced by Topsoe Fuel Cell were used. A test station has been developed to evaluate the carbon deposition characteristics of artificially added biomass gasification tars on SOFCs. Liquid toluene (99.9% purity, 34866 Sigma-Aldrich) was injected into a home-built evaporator (set to 140 °C) using a syringe pump (NE-1000 Series, Syringe Pumps). Deionized water was fed using a peristaltic pump (Ismatec® Reglo ICC) into a second temperature-controlled evaporator, to adjust the steam addition. The anode fuel transfer lines were heated to prevent water condensation between the evaporator and furnace.

8.2.2 Operational Procedure

Two experiments were performed with different fuels (see Fig. 8.1). The total fuel flow rate was held at 100 sccm. Synthetic air 79%N_2 with 21%O_2 was used at the cathode side with a flow rate of 250 sccm. Fig. 8.1 shows the experimental plan and conditions for the two experiments. For the first experiment (Exp. 1), the cell was fed with H_2 and toluene was injected to the fuel stream when the voltage was stable. The concentration level of toluene was increased from 48 to 1960 ppm and each poisoning test followed by a recovering step (no toluene in the fuel stream) for the duration of 25 h. The cell in the second test (Exp. 2) was fed with reformed biosyngas made from a feed of 65%H_2 with 25%CO_2, 5%CO and 5% H_2O.

Thermodynamic calculations have been performed to illustrate the chemical equilibrium behavior of a C-H-O system under SOFC operation conditions. Fig. 8.2 shows that both gas compositions are in carbon deposition-free region at 800 °C, which suggests carbon deposition is not thermodynamically favored if the SOFC is operated with the tar-free biosyngas. Adding the tar compound to the feed stream will change slightly the points location but the change is negligible and no deposited carbon is expected. In these experiments, cells were operated at 0.25 A/cm^2, which will further withdraw the points from the boundary and into the thermodynamic carbon-free region.
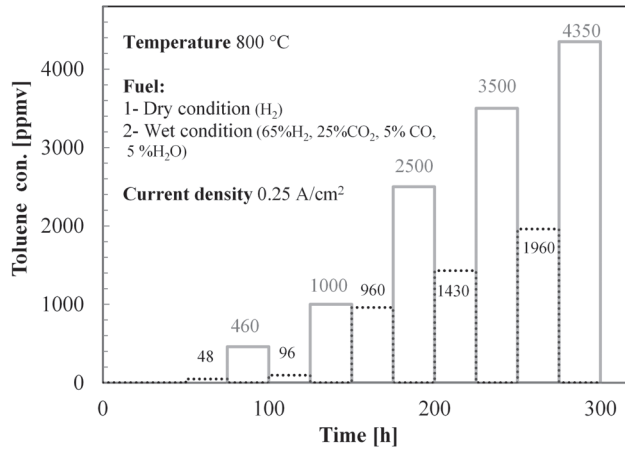
Figure 8.1 – Experimental plan and the test conditions, dry fuel feed condition (black dotted lines) and wet fuel feed condition (gray full line)
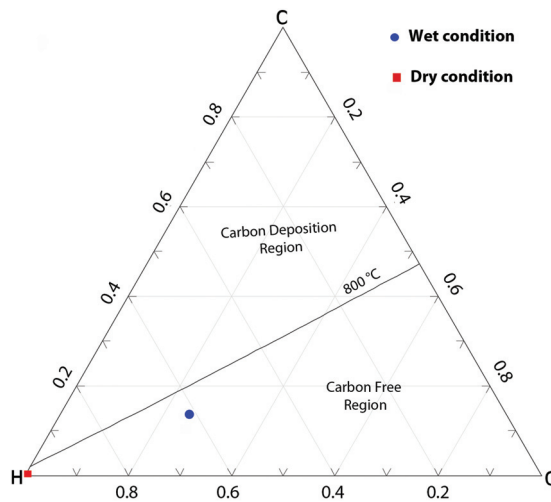
Figure 8.2 – C-H-O diagram indicating the thermodynamic region of carbon deposition. Red and blue points represent the tar-free H_2 (dry) and tar-free biosyngas (wet) composition at open circuit, respectively.

8.3 Results and Discussions

8.3.1 Operation on H_2

The cell was kept under polarisation at 0.25 A/cm^2 and 800 °C for a duration of 50 h to activate the cell. After voltage stabilization, 48 ppm of toluene was added to the main fuel flow for a duration of 25 h. In order to compare the degradation rate for each contaminant concentration, a regeneration step was necessary and achieved by stopping the flow of toluene. The recovery step was operated for 25 h as well.

Fig. 8.3 shows the performance of the cell at various concentrations of toluene. Degradation rates are compared in this figure for the concentration ranging from 48 ppm up to almost 2000 ppm. The degradation trend (voltage decrease over time) is 4 mV/100 h for the first 150 h of the test. Adding 960 and 1440 ppm toluene increased the degradation rate to 20 and 61 mV/100 h, respectively. A critical degradation is observed in the case of 1960 ppm. After 20 h of exposure to 1960 ppm, a severe drop in voltage occurred which was due to carbon formation at the fuel inlet and blockage of the line.
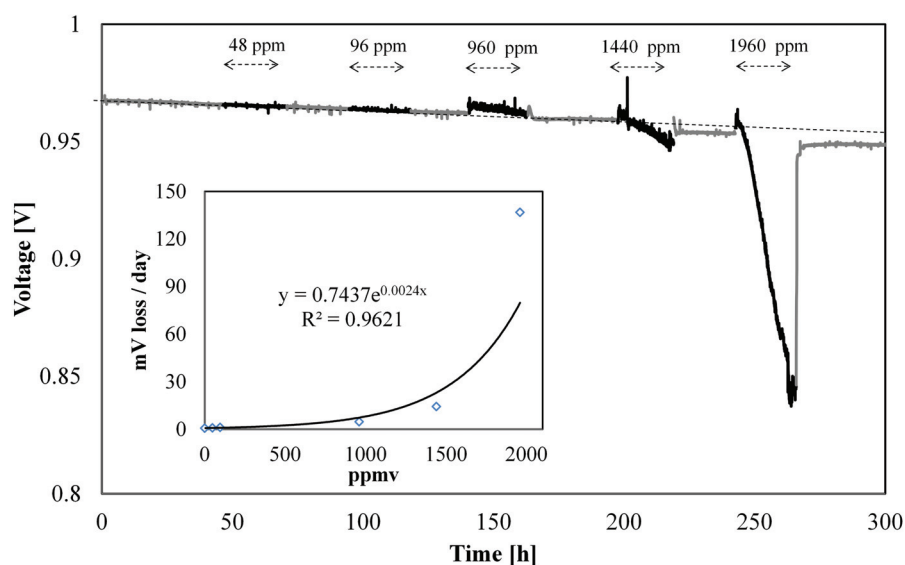
Figure 8.3 – Overview of cell performance and degradation caused by toluene (Exp. 1 operation on H_2). Black and gray colors are indicating condition with toluene and without toluene, respectively. The dashed line is the expected performance without toluene in the fuel.

IV curves

Consecutive IVs were performed at the beginning and end of a change in the conditions, i.e. before and after adding toluene, and after regeneration. Fig. 8.4 shows IVs recorded after adding toluene. ASR is increasing with increased tar concentration. In the case of 1960 ppm, there is a drop in OCV and the ASR is higher than other cases. This could be due to carbon formation at the fuel inlet. At elevated temperatures toluene decomposes to solid carbon via Eq. 8.1 and as no carbon reforming agent (i.e. H_2O or CO_2) is present, this solid carbon accumulates and blocks the fuel inlet.

$$C_7H_8 \longleftrightarrow 7\,C + 4\,H_2 \qquad \Delta H^\circ_{298K} = -50\,kJ/mol \qquad (8.1)$$

107
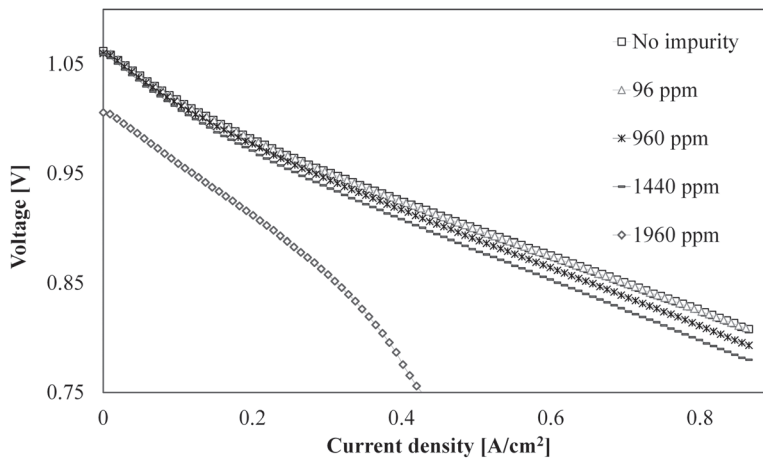
Figure 8.4 – IV curves for dry H_2 feed at different concentrations of toluene.

Impedance spectroscopy

EIS is used to characterize the impact of carbon deposits on the cell performance. They were measured at 0.25 A/cm^2, before tar loading and 25 h after exposure. EIS spectra confirm the IV curves, that indicates no change in the high frequency ohmic intercept but a slight change in the low frequency polarisation resistance. Fig. 8.5 shows the evolution of impedance spectra measured for the case of exposure to 960 and 1960 ppm. The Nyquist plot shows two main depressed arcs, which are overlapping. There is a slight reduction in the ohmic resistance after exposure to toluene in both cases. This is an indication for slight carbon deposition at the anode side, because carbon deposits increase the conductivity, therefore a decrease in ohmic resistance can be expected. Exposure to toluene enlarges the low frequency arc. In fact, carbon deposition on the other hand can cover the active sites and increase the activation polarisation resistance and on the other hand these deposits can block the pores and cause the increase in concentration polarisation due to fuel shortage. However, the Nyquist plot can not distinguish between these polarisation resistances, but the existence of such deposits is inevitable.

Recovery

Recovery of the cell was examined for the different exposure steps to toluene. The degradation rate during the recovery phase stayed constant (4 mV/100h) until 200 h (before adding 1440 ppm), as shown with the dashed line in Fig. 8.3. Switching to toluene-free H_2 after the 1440 ppm and 1960 ppm exposure steps, shows lower voltages than expected. It is interesting to mention that the degradation rate during the recovery phase after both 1440 ppm and 1960 ppm exposure steps is only 2 mV/100h. This is not in contradiction with the existence of deposited carbon, as carbon deposits can enhance the anode conductivity leading to a temporary increase in performance [151]. Carbon removal in this case is due to the direct
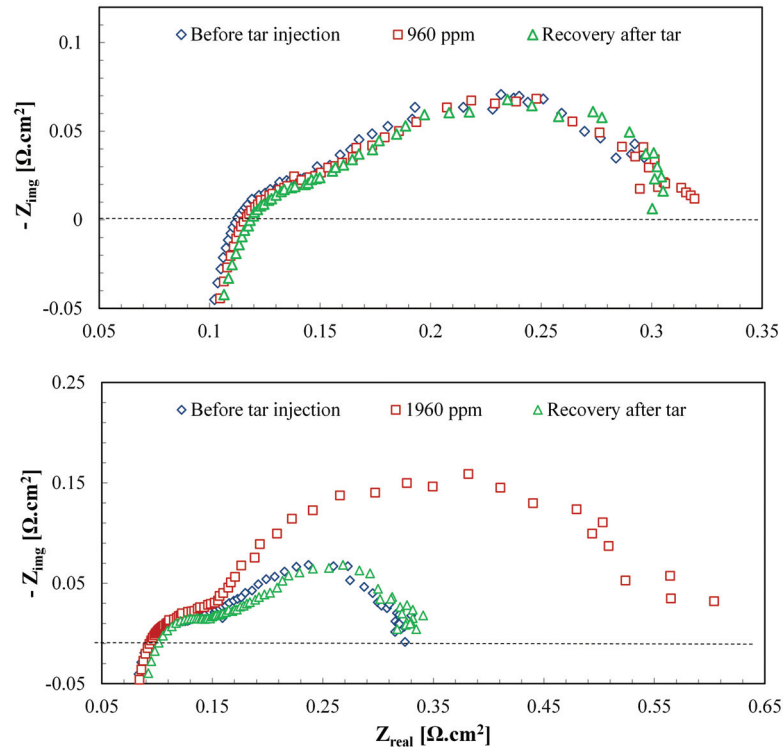
Figure 8.5 – EIS spectra for the case of 960 and 1960 ppm toluene in the fuel feed, before, after exposure and after recovery.

reaction of carbon with oxygen ions (Eq. 8.2). Carbon in this case needs to be located near the TPB lines to generate electrical current.

$$C + O^{2-} \longrightarrow CO + 2\,^{e-} \qquad \Delta H = -111\,\text{kJ/mol} \tag{8.2}$$

8.3.2 Operation on Biosyngas

Following the anode reduction, the cell was fed with H_2 under 0.25 A/cm^2 at 800 °C for a duration of 50 h to ensure that the anode surface is carbon-free. Afterwards the fuel feed was switched to the biosyngas and operated for 25 h under tar-free condition as shown in Fig. 8.1. As no degradation was observed with low concentrations of toluene in the previous test, tar loading was started at a 10-fold concentration in this test. Fig. 8.6 shows cell voltage over time for the case of 460 ppm, 1500 ppm and 4350 ppm exposure, corresponding to 1.87, 6.08 and 17.65 g/m^3, respectively of toluene in the fuel. No significant degradation was observed at concentrations lower than 3500 ppm (14.2 g/Nm^3). A linear degradation is observed at 4350 ppm (around 7% per 100 h) for at least the 40 h of exposure to this concentration level.

8.3.3   Tar Reforming

Toluene is expected to reform with H_2O on the nickel catalyst via steam reforming (Eq. 8.3) or CO_2 dry reforming (Eq. 8.4). H_2 and CO are produced due to these reforming reactions, therefore providing more fuel at the anode which consequently leads to an increased open circuit voltage (OCV). Assuming conversion by reforming of 1000 ppm of toluene (0.1%) would raise the H_2/CO concentration by 1.8%, making the effect non-negligible. In this experiment, cell operation at OCV is avoided due to possible anode delamination from the electrolyte and irreversible degradation [28]. The initial increase in cell voltage is shown in Fig. 8.7. Data in this figure has been normalized for a better comparison of increase in voltage. The cell voltage increases when increasing the feeding tar concentration, indicating that tar reforming occurs under the SOFC conditions.
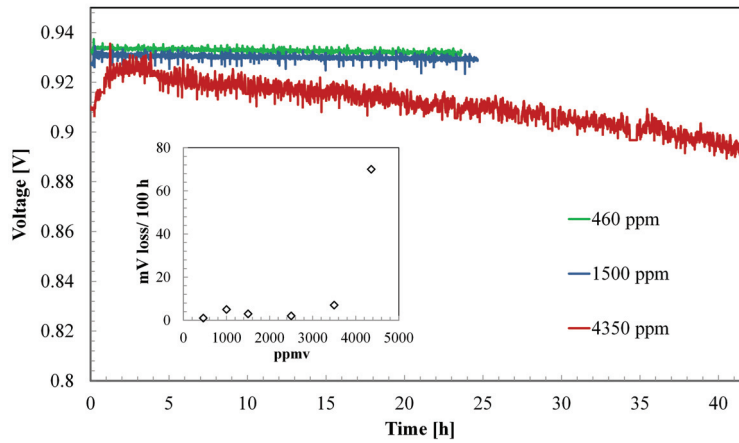
Figure 8.6 – Polarisation over time for the wet fuel condition test (800°C, 0.25 A/cm^2). Degradation rate for different levels of toluene is compared.
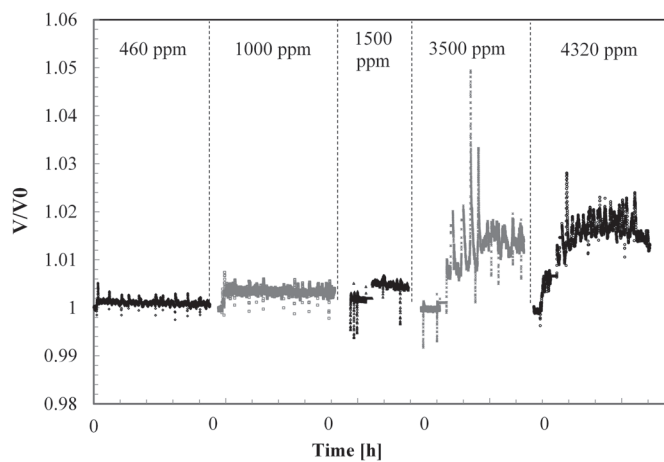
Figure 8.7 – Initial increase in the cell voltage for different concentration of toluene (normalized values). The time of injection is labeled 0.

$$C_7H_8 + 7H_2O \longrightarrow 7CO + 11H_2 \qquad \Delta H^{\circ}_{298K} = 869\,\text{kJ/mol} \tag{8.3}$$

$$C_7H_8 + 7CO_2 \longrightarrow 14CO + 4H_2 \qquad \Delta H^{\circ}_{298K} = 1157\,\text{kJ/mol} \tag{8.4}$$
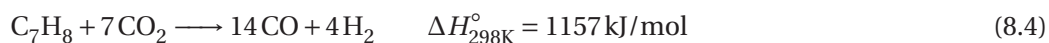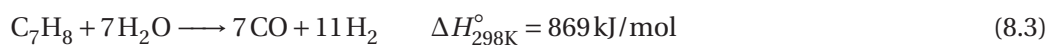
IV curves

Similar to the previous test, consecutive IVs were performed before and after changing the toluene concentration and also after recovery. Fig. 8.8 shows IVs recorded for different concentrations of toluene. Increasing the concentration leads to an increase in ASR.
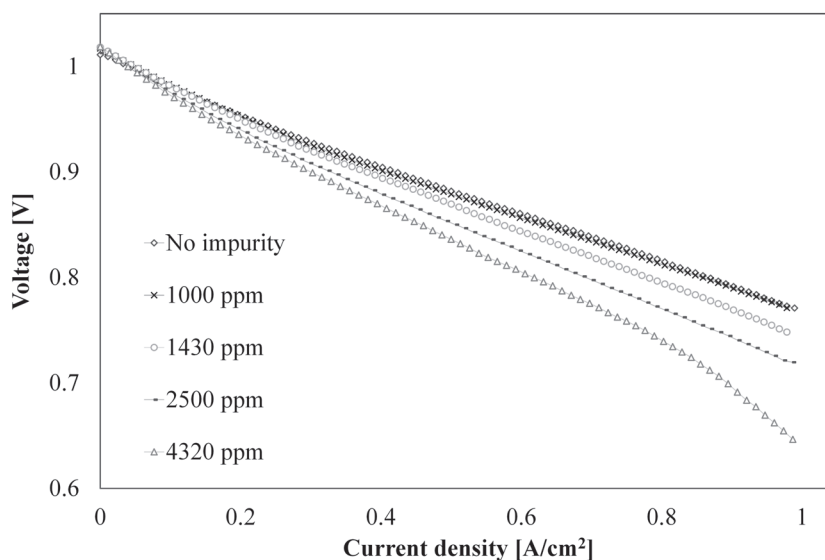
Figure 8.8 – IV curves for the wet fuel condition test. Some of the data are not shown here for better reading.

Impedance spectroscopy

Impedance of the SOFC was measured before, during and after each toluene cycle, all under current load (0.25 A/cm^2). The Nyquist plots for the case of 3500 and 4350 ppm are shown in Fig. 8.9. At 4350 ppm, there is a slight improvement in the ohmic resistance, as explained, it could be due to some deposited carbon. The plots show an increase in the total polarisation resistance. This increase is more visible at the higher concentration of the tar compound. In addition, reversible degradation is observed for all the exposures.
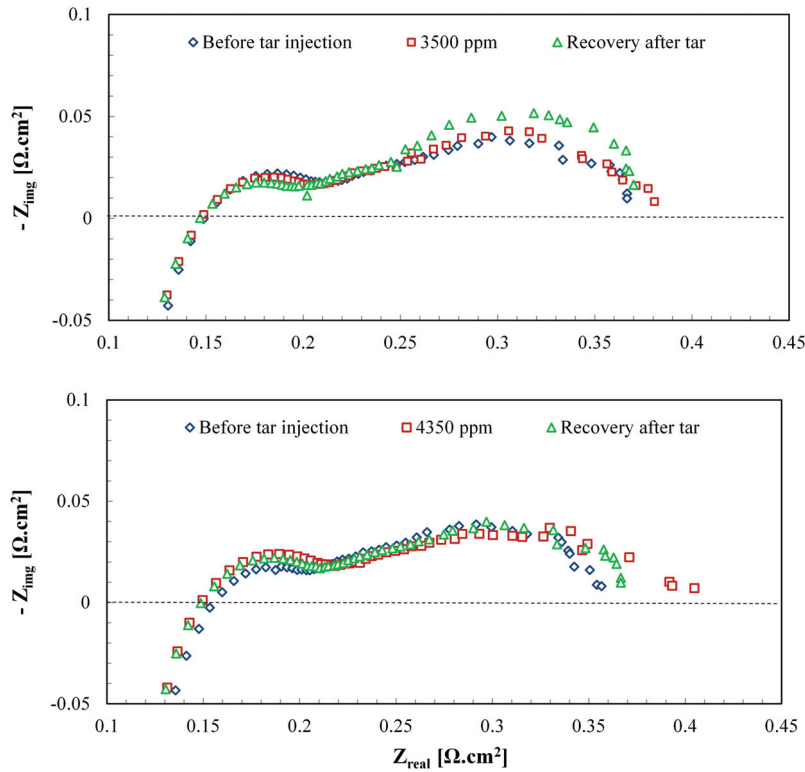
Figure 8.9 – EIS spectra for the cases of 3500 and 4350 ppm, before, during and after recovery.

8.3.4 Damages due to Dry Corrosion

Fig. 8.10 shows the cell and Ni mesh current collector that were used for the experiment of Fig. 8.3. The central parts of the cells are damaged and the Ni mesh current collector is partly disintegrated. This process is also known as metal dusting or dry corrosion. Metal dusting comprises the disintegration of bulk metal into metal particles at high temperatures (300-850 °C) in environments that are supersaturated with carbon. The dusting mechanism [152] is as follows:

- initially carbon deposits (due to exposure to toluene) on the metal surface,

- dissolution of the carbon into the bulk of the metal.

- precipitation of carbon as a graphite fiber within the metal whereby the metal mechanically breaks up.

Figure 8.10 – Anode-supported cell after operation for 350 h under H_2 plus toluene, Ni mesh current collector used at the anode side after the test.

8.4   Conclusion

The impact of a tar (toluene as a model compound), on the performance of AS Ni-YSZ SOFC fed with different fuels (H_2 and biosyngas) was studied. The polarisation behavior, current-voltage and electrochemical impedance were measured to analyze the performance evolution. Results show that degradation due to exposure to tar compounds highly depends on the fuel composition. A linear degradation is observed at concentrations above 1000 ppm for a feed with only H_2. In contrast, toluene even up to 3500 ppm (for exposure durations of a day) did not cause significant added degradation when the cell was fed with biosyngas.

9 Concluding Remarks and Outlook

9.1 Conclusions

Due to their high operating temperatures, SOFCs exhibit a high fuel flexibility as they do not require pure hydrogen as fuel. This constitutes a major advantage due to the high cost of hydrogen production and operation of SOFCs on various fuels such as natural gas, biogas, and biosyngas is therefore gaining of interest. Among the various biofuels, biogas is considered a promising raw fuel to be used as syngas source for SOFC applications. The conversion routes of biomass (thermochemical and biochemical) to biosyngas and biogas were therefore described and compared in this work. Their main compositions and trace elements were presented. In addition to the main components (i.e. methane and carbon dioxide), biogas contains various harmful trace compounds such as hydrogen sulfide, halogenated compounds and siloxanes which were also detailed.

The scope of this thesis was to find the tolerable limits of contaminants within the anode feed for SOFC single cells and short stacks to operate. The analysis started from micro-contaminants that are contained in a biogas from a WWTP, then was extended to other contaminants that are mostly found in biosyngas from lignocellulosic biomass gasification. The performance of anode supported SOFCs under a wide range of trace compounds was thus studied by identifying the degradation mechanisms.

The following contaminants were tested : siloxane D4, HCl, C_4H_4S, H_2S and C_7H_8. Anode fuel gas composition was varied between hydrogen and reformed biogas, including contaminants and the cell performances were compared. The impact of siloxanes on SOFC performance was studied with a D4 concentration ranging from 70 ppbv to 5 ppmv. The effects of chlorine were tested using HCl with a variable concentration ranging from 1 to 1000 ppmv. Sulfur compound (organic and inorganic) effects were tested using hydrogen sulfide and thiophene with variable operating temperatures and variable concentrations up to 10 ppm. The impacts of toluene (C_7H_8) on SOFC performance were tested in the same way.

A summary of the main findings and conclusions is given below:

- Siloxanes were the most detrimental compounds due to silicon dioxide formation in the anode which irreversibly blocked the fuel channels, even at ppbv levels. This phenomenon causes porosity reduction and TPB contamination of the anode structure and the SOFC performance thus irreversibly decreases. Irreversible effects are already witnessed at 70 ppbv. Siloxane quickly decomposes into $SiO_2(s)$ as it reaches the fuel cell anode chamber, thus depositing silica both on the interconnect and anode current collector. Some Si remains in the vapour phase as $Si(OH)_4(g)$ and further diffuses to the TPB region where it eventually precipitates as well. These impurities must be completely purged from biogas feed to SOFCs.

- Chapter 5 evaluated the recovery potential of SOFC anode single cells upon exposure to siloxanes based on thermodynamic calculations. These calculations proposed two pathways to volatilize the deposited $SiO_2(s)$ to $SiO(g)$, increasing temperature or operating the cell at OCV after exposure to siloxanes. Performance recovery was examined by designing three experiments i.e. to operate the cell at OCV, maintaining at the same current density or at higher current density. Results were contrary to the thermodynamic prediction. Partial recovery of the cell performance was observed by maintaining cell polarization at the same current density rather than operating in OCV mode or high current densities.

- A linear degradation was observed as a result to HCl exposure. Single cell experiments revealed that the degradation is not severe if there are some ppm of HCl in the fuel gas. Even short stack tests showed no performance degradation at high concentrations. The total amount of chlorine compounds in biogas are typically low, as shown in chapter 2 no gas clean up for these compounds is required.

- The degradation mechanism by chlorine compounds was not clear. The prior proposed mechanisms were as follows: (i) formation of nickel chloride, an unstable phase, and changes in the microstructure of Ni-YSZ anode (ii) adsorption of chlorine on the Ni surface, reducing the active TPBs. Based on the findings of this thesis, the degradation is due to adsorption of chlorine on the Ni surface. Based on the DRT calculation and the equivalent circuit model, exposure to HCl causes degradation at the TPBs (2-4 kHz impedance) and the fuel conversion impedance (below 1 Hz). SEM-EDX analysis of the anode cross section showed traces of Cl element, where Ni is located. This study suggests that chlorine is present in the form of the adsorbed species, rather than as a chlorine nickel compound.

- Exposure to thiophene as an organic sulfur compound causes a fast drop in the cell performance followed by a gradual slow degradation. Results showed that thiophene affects both the anode charge transfer impedance (100-1000 Hz), specifically at the low temperatures and gas conversion impedance (0.1-2 Hz). In general, the observed degradation behavior is similar to that observed with H_2S.

- Exposure to toluene resulted in a linear degradation at concentrations above 1000 ppm for the dry condition (H_2 fuel). In contrast, toluene even up to 3500 ppm did not cause significant added degradation when the cell was fed with biosyngas. Biogas contains low amount of tars as shown in chapter 2 and it is not necessary to remove them from the biogas. Existence of high tar load could be problematic in the case of product gas from wood gasification, specifically with up-draft gasifiers.

The following research questions have been proposed and answered in this thesis:

- **RQ.1:** *Do we need to remove the impurities from biogas and biosyngas?*

- **RQ.2:** *If an impurity causes a degradation, what is the potential single cell/stack threshold tolerance limit towards that contaminant?*

- **RQ.3:** *What is the degradation mechanism of the relevant contaminants?*

- **RQ.4:** *Do single cell and stack behave in the same manner towards a specific impurity?*

Table 9.1 – Response to the research questions

Impurity	RQ.1	RQ.2	RQ.3	RQ.4
Siloxanes	Yes	complete removal	$SiO_2(s)$ deposition on the interconnect, anode support structure and at TPBs	Stacks degraded slightly higher than single cells
HCl	No	10 ppm	Ni coverage by the Cl species and increase in the activation polarization	A linear degradation for single cells but no degradation for short stacks even at higher concentrations
H_2S	Yes	0.5 ppm [†]	Ni coverage by S due to dissociative chemisorption of H_2S on nickel active sites and blocking of TPBs	Based on the European SOFCOM project results, similar behavior
Thiophene	Yes	0.5 ppm	It decomposes to H_2S and the degradation mechanism is similar to the one of H_2S	n.a.
Toluene	No	3500 ppm for biosyngas	Carbon deposition at the TPBs, damages of current collector due to dry corrosion	n.a.

[†] This value has been suggested based on reforming catalyst experiments and short stacks tests of the European SOFCOM project. Results are not published yet.

9.2 Further Research

- Ni-YSZ anode material is very sensitive to sulfur, its performance dropping systematically within minutes when H_2S is contained in the fuel. It is thus advantageous to find a new SOFC anode catalyst with high catalytic activity for the oxidation of the fuel and chemical stability when facing S-containing fuels. Self-Regenerating Anodes (SERAN) is an ongoing project funded by the Competence Center Energy and Mobility (CCEM) that focuses on a novel smart, sulfur tolerant catalyst with an additional self-regenerating effect of the catalytic phase. Such a smart material minimizes poisoning effects caused by sulfur contaminants. In addition this material concept will lead to a reversibility and self-regeneration of the temperature induced microstructural degradation. As an alternative to the standard nickel-zirconia or nickel-ceria anode materials, the novel catalyst based on a conducting $LaSrTiO_3$ perovskite ceramic (i.e. made from cheap elements), is much less prone to sulfur poisoning and reoxidation damage, while maintaining adequate electrochemical performance.

- Naphthalene is a tar compound that can be found in the product gases from wood gasifiers. There were difficulties in preparing a proper setup to inject naphthalenes into the main anode fuel stream. An evaporator is under design and a mass spectrometer has been purchased to monitor the inlet concentration. The effect of this tar compound has to be evaluated on the steam-reforming of methane and water-gas shift reaction.

- Real biogases or product gases contain several impurities, however less attention is paid to the combination effect of these impurities. Hence, it would be required to evaluate the crossing effect of impurities on the performance of SOFCs. The crossing effect can be more or less harmful. For instance a trial test was performed on the crossing effect of siloxane D4 and H_2S as shown in Fig. 9.1. The cumulative effects of sulfur and D4 is worse than the poisoning effect of each of these impurities individually. For instance, the degradation slope with 1 ppm D4 + 3 ppm H_2S (40%/1000h) is steeper than with 1 ppm D4 alone (32%/1000h).
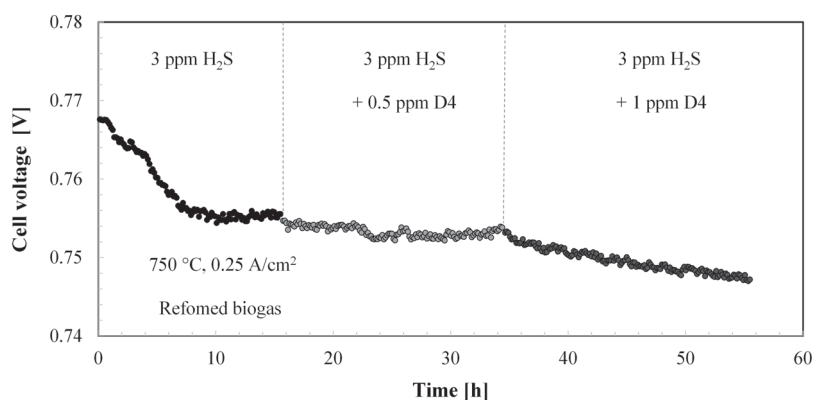

Figure 9.1 – Crossing effect of siloxane D4 and H_2S. Concentration of H_2S was kept constant at 3 ppm and then D4 was added.

- The DRT tool was used to deconvolute EIS spectra in chapter 6, the poisoning effect of HCl. This tool is very powerful in the identification of individual processes. Unfortunately, the tool can only process high quality spectra, meaning that EIS spectra in other chapters could not benefit from the DRT method. Efforts have been made to achieve high quality spectra, such as shortening the measurement wires, twisting the cables and modifying the test bench though there is still a need to improve the resulting quality.

9.3 Recommendations and Outlook

The effects of various biogas impurities on the performance of AS Ni-YSZ SOFCs have been shown in this study. This provided guidelines regarding the maximum impurity concentrations which can be tolerated in biogases after cleaning for SOFC operations. Biogas cleaning is proven to be essential for SOFC applications. Several desulfurization methods exist such as chemical absorption in aqueous solutions containing metallic cations or alkaline reactants, chemical adsorption on metal oxides (e.g., ZnO) or impregnated activated carbon. Siloxanes can be removed using adsorption methods, for instance activated carbon. However there are difficulties in co-adsorption of these impurities. Low-cost and high-capacity sorbents that can remove sulfur and siloxane simultaneously, need to be developed. Yet a minimal level of sulfur, on the order of 1 ppm, can be tolerated. Its effect is recoverable.

The provision of biogas from organic residues and wastes as well as its use as a renewable source of energy for electricity generation is gaining more interest. The EPFL campus may evaluate the installation of a small scale SOFC system fed by biogas. The idea is to use the campus food wastes, generate biogas on site and produce electricity using highly efficient SOFCs. Preliminary investigations [153] showed that an average of 228 tons/year of food waste are collected, which could feed a SOFC in the range of 6.5-17.2 kW, generating 50 to 147 MWh electricity per year. So far, no integrated SOFC-biogas installations of such scale exist in Switzerland.

Recently, Biosweet (Biomass for Swiss Energy Future) a large coordinated SCCER (Swiss Competence Center for Energy Research) project, started to evaluate the feasibility of electricity production from manure using SOFC systems at medium scale (10-75 kWe). This study is covering the manure resources availability in Switzerland, the feasibility of an anaerobic digester at small scale, the choice of gas cleaning and the size of the SOFC system.

In the continuation of the European SOFCOM project, the European project DEMOSOFC focuses on larger scales with the installation of the first European high efficiency cogeneration plant with a medium size fuel cell fed by biogas. The main challenge for this project is to install a CHP system with an electrical efficiency of 53%, that would generate approximately 175 kW electrical power and 90 kW of thermal power.

Bibliography

[1] Wikipedia. Global warming [online], May 2016. Available: http://en.wikipedia.org/wiki/Global-warming.

[2] Tanseem Abbasi and S. A. Abbasi. *Renewable Energy Sources: Their Impact on Global Warming and Pollution.* PHI Learning Pvt. Ltd., February 2012.

[3] Dimitris K. Niakolas, Maria Daletou, Stylianos G. Neophytides, and Constantinos G. Vayenas. Fuel cells are a commercially viable alternative for the production of "clean" energy. *Ambio,* 45(Suppl 1):32–37, January 2016.

[4] Hossein Madi, Andrea Lanzini, Stefan Diethelm, Davide Papurello, Jan Van herle, Matteo Lualdi, Jørgen Gutzon Larsen, and Massimo Santarelli. Solid oxide fuel cell anode degradation by the effect of siloxanes. *Journal of Power Sources,* 279:460–471, April 2015.

[5] World Bioenergy Association. Biogas An important renewable energy source, 2014.

[6] Jan Van herle, Yves Membrez, and Olivier Bucheli. Biogas as a fuel source for SOFC co-generators. *Journal of Power Sources,* 127(1–2):300–312, March 2004.

[7] Jan Van herle, F. Maréchal, S. Leuenberger, and D. Favrat. Energy balance model of a SOFC cogenerator operated with biogas. *Journal of Power Sources,* 118(1-2):375–383, May 2003.

[8] J Van herle, F Maréchal, S Leuenberger, Y Membrez, O Bucheli, and D Favrat. Process flow model of solid oxide fuel cell system supplied with sewage biogas. *Journal of Power Sources,* 131(1–2):127–141, May 2004.

[9] F. Curletti, M. Gandiglio, A. Lanzini, M. Santarelli, and F. Maréchal. Large size biogas-fed Solid Oxide Fuel Cell power plants with carbon dioxide management: Technical and economic optimization. *Journal of Power Sources,* 294:669–690, October 2015.

[10] Dionissios D. Papadias, Shabbir Ahmed, and Romesh Kumar. Fuel quality issues with biogas energy – An economic analysis for a stationary fuel cell system. *Energy,* 44(1):257–277, August 2012.

[11] *Fuel Cell Handbook.* U.S. Department of Energy, 7th edition edition, November 2004.

Bibliography

[12] H. Yokokawa and N. Sakai. Part 4. fuel cell principle, systems and applications, chapter 13 history of high temperature fuel cell development. *Handbook of Fuel Cells Fundamentals Technology and Application*, 1:219–266, 2003.

[13] Omar Z. Sharaf and Mehmet F. Orhan. An overview of fuel cell technology: Fundamentals and applications. *Renewable and Sustainable Energy Reviews*, 32:810–853, April 2014.

[14] Harumi Yokokawa, Hengyong Tu, Boris Iwanschitz, and Andreas Mai. Fundamental mechanisms limiting solid oxide fuel cell durability. *Journal of Power Sources*, 182(2):400–412, August 2008.

[15] A. Lanzini, P. Leone, C. Guerra, F. Smeacetto, N.P. Brandon, and M. Santarelli. Durability of anode supported Solid Oxides Fuel Cells (SOFC) under direct dry-reforming of methane. *Chemical Engineering Journal*, 220:254–263, 2013.

[16] A. Lanzini and P. Leone. Experimental investigation of direct internal reforming of biogas in solid oxide fuel cells. *International Journal of Hydrogen Energy*, 35(6):2463–2476, 2010.

[17] A. Lanzini, P. Leone, M. Pieroni, M. Santarelli, D. Beretta, and S. Ginocchio. Experimental investigations and modeling of direct internal reforming of biogases in tubular solid oxide fuel cells. *Fuel Cells*, 11(5):697–710, 2011.

[18] P. Leone, A. Lanzini, G.A. Ortigoza-Villalba, and R. Borchiellini. Operation of a solid oxide fuel cell under direct internal reforming of liquid fuels. *Chemical Engineering Journal*, 191:349–355, 2012.

[19] R. Mukundan, E.L. Brosha, and F.H. Garzon. Sulfur Tolerant Anodes for SOFCs. *Electrochemical and Solid-State Letters*, 7(1):A5–A7, 2004.

[20] Z. Cheng, J.-H. Wang, Y. Choi, L. Yang, M.C. Lin, and M. Liu. From Ni-YSZ to sulfur-tolerant anode materials for SOFCs: Electrochemical behavior, in situ characterization, modeling, and future perspectives. *Energy and Environmental Science*, 4(11):4380–4409, 2011.

[21] B. Shri Prakash, S. Senthil Kumar, and S. T. Aruna. Properties and development of Ni/YSZ as an anode material in solid oxide fuel cell: A review. *Renewable and Sustainable Energy Reviews*, 36:149–179, August 2014.

[22] A. Faes, A. Hessler-Wyser, D. Presvytes, C. G. Vayenas, and J. Van herle. Nickel–Zirconia Anode Degradation and Triple Phase Boundary Quantification from Microstructural Analysis. *Fuel Cells*, 9(6):841–851, December 2009.

[23] San Ping Jiang and Siew Hwa Chan. A review of anode materials development in solid oxide fuel cells. *Journal of Materials Science*, 39(14):4405–4439, July 2004.

[24] Chunwen Sun, Rob Hui, and Justin Roller. Cathode materials for solid oxide fuel cells: a review. *Journal of Solid State Electrochemistry*, 14(7):1125–1144, October 2009.

[25] Anil V Virkar, Jong Chen, Cameron W Tanner, and Jai-Woh Kim. The role of electrode microstructure on activation and concentration polarizations in solid oxide fuel cells. *Solid State Ionics*, 131(1–2):189–198, June 2000.

[26] Kirk Gerdes, Mark C. Williams, Randall Gemmen, and Briggs White. A Global Framework for Examination of Degradation in SOFC. *ECS Transactions*, 57(1):289–297, October 2013.

[27] J. Laurencin, G. Delette, F. Lefebvre-Joud, and M. Dupeux. A numerical tool to estimate SOFC mechanical degradation: Case of the planar cell configuration. *Journal of the European Ceramic Society*, 28(9):1857–1869, 2008.

[28] Vanesa Alzate-Restrepo and Josephine M. Hill. Carbon deposition on Ni/YSZ anodes exposed to CO/H2 feeds. *Journal of Power Sources*, 195(5):1344–1351, March 2010.

[29] William M. Harris, Jeffrey J. Lombardo, George J. Nelson, Barry Lai, Steve Wang, Joan Vila-Comamala, Mingfei Liu, Meilin Liu, and Wilson K. S. Chiu. Three-Dimensional Microstructural Imaging of Sulfur Poisoning-Induced Degradation in a Ni-YSZ Anode of Solid Oxide Fuel Cells. *Scientific Reports*, 4, June 2014.

[30] Anke Hagen, Jens F. B. Rasmussen, and Karl Thydén. Durability of solid oxide fuel cells using sulfur containing fuels. *Journal of Power Sources*, 196(17):7271–7276, September 2011.

[31] Antonin Faes. *RedOx Stability of Anode Supported Solid Oxide Fuel Cells*. PhD thesis, EPFL, 2011.

[32] Khairul Anam and Chih Kuang Lin. Thermal Stress Intensity Factors of Crack in Solid Oxide Fuel Cells. *Applied Mechanics and Materials*, 493:331–336, January 2014.

[33] D Simwonis, F Tietz, and D Stöver. Nickel coarsening in annealed Ni/8ysz anode substrates for solid oxide fuel cells. *Solid State Ionics*, 132(3–4):241–251, July 2000.

[34] Omar M. Pecho, Andreas Mai, Beat Münch, Thomas Hocker, Robert J. Flatt, and Lorenz Holzer. 3d Microstructure Effects in Ni-YSZ Anodes: Influence of TPB Lengths on the Electrochemical Performance. *Materials*, 8(10):7129–7144, October 2015.

[35] A. Lanzini, P. Leone, C. Guerra, F. Smeacetto, N. P. Brandon, and M. Santarelli. Durability of anode supported Solid Oxides Fuel Cells (SOFC) under direct dry-reforming of methane. *Chemical Engineering Journal*, 220:254–263, March 2013.

[36] Tatsuya Takeguchi, Yukimune Kani, Tatsuya Yano, Ryuji Kikuchi, Koichi Eguchi, Keigo Tsujimoto, Yoshitaka Uchida, Akira Ueno, Koiji Omoshiki, and Masanobu Aizawa. Study on steam reforming of CH4 and C2 hydrocarbons and carbon deposition on Ni-YSZ cermets. *Journal of Power Sources*, 112(2):588–595, November 2002.

[37] G. Rabenstein and V. Hacker. Hydrogen for fuel cells from ethanol by steam-reforming, partial-oxidation and combined auto-thermal reforming: A thermodynamic analysis. *Journal of Power Sources*, 185(2):1293–1304, 2008.

[38] Amal Elleuch, Kamel Halouani, and Yongdan Li. Bio-methanol fueled intermediate temperature solid oxide fuel cell: A future solution as component in auxiliary power unit for eco-transportation. *Materials & Design*, 97:331–340, May 2016.

[39] N. Laosiripojana and S. Assabumrungrat. Catalytic steam reforming of methane, methanol, and ethanol over Ni/YSZ: The possible use of these fuels in internal reforming SOFC. *Journal of Power Sources*, 163(2):943–951, January 2007.

[40] C. Strazza, A. Del Borghi, P. Costamagna, A. Traverso, and M. Santin. Comparative LCA of methanol-fuelled SOFCs as auxiliary power systems on-board ships. *Applied Energy*, 87(5):1670–1678, May 2010.

[41] D. Cocco and V. Tola. Externally reformed solid oxide fuel cell–micro-gas turbine (SOFC–MGT) hybrid systems fueled by methanol and di-methyl-ether (DME). *Energy*, 34(12):2124–2130, December 2009.

[42] Brittany Farrell and Suljo Linic. Direct electrochemical oxidation of ethanol on SOFCs: Improved carbon tolerance of Ni anode by alloying. *Applied Catalysis B: Environmental*, 183:386–393, April 2016.

[43] Y. Shiratori, T. Oshima, and K. Sasaki. Feasibility of direct-biogas SOFC. *International Journal of Hydrogen Energy*, 33(21):6316–6321, November 2008.

[44] Y. Shiratori, T. Ijichi, T. Oshima, and K. Sasaki. Internal reforming SOFC running on biogas. *International Journal of Hydrogen Energy*, 35(15):7905–7912, August 2010.

[45] A. Lanzini, P. Leone, C. Guerra, F. Smeacetto, N. P. Brandon, and M. Santarelli. Durability of anode supported Solid Oxides Fuel Cells (SOFC) under direct dry-reforming of methane. *Chemical Engineering Journal*, 220:254–263, March 2013.

[46] European Commission. Directive 2009/28/EC on the promotion of the use of energy from renewable sources., 2009.

[47] Peter McKendry. Energy production from biomass (part 1): overview of biomass. *Bioresource Technology*, 83(1):37–46, May 2002.

[48] Prabir Basu. Chapter 1 - Introduction. In Prabir Basu, editor, *Biomass Gasification and Pyrolysis*, pages 1–25. Academic Press, Boston, 2010.

[49] Mathew Michael Pickett. *Modeling the Performance and Emissions of British Gas_lurgi-based Integrated Gasification Combined Cycle Systems.* PhD thesis, 2005.

[50] H.A.M. Knoef. *Handbook Biomass Gasification.* BTG Publisher, 2005.

[51] I Olofsson, A Nordin, and Ulf Söderlind. *Initial Review and Evaluation of Process Technologies and Systems Suitable for Cost-Efficient Medium-Scale Gasification for Biomass to Liquid Fuels.* Umeå Universitet, Umeå, 2005.

[52] Son Ich Ngo, Thanh D. B. Nguyen, Young-Il Lim, Byung-Ho Song, Uen-Do Lee, Young-Tai Choi, and Jae-Hun Song. Performance evaluation for dual circulating fluidized-bed steam gasifier of biomass using quasi-equilibrium three-stage gasification model. *Applied Energy*, 88(12):5208–5220, December 2011.

[53] L. F. Calvo, M. V. Gil, M. Otero, A. Morán, and A. I. García. Gasification of rice straw in a fluidized-bed gasifier for syngas application in close-coupled boiler-gasifier systems. *Bioresource Technology*, 109:206–214, April 2012.

[54] Salah H. Aljbour and Katsuya Kawamoto. Bench-scale gasification of cedar wood – Part II: Effect of Operational conditions on contaminant release. *Chemosphere*, 90(4):1501–1507, January 2013.

[55] Xiangmei Meng, Wiebren de Jong, Ningjie Fu, and Adrian H. M. Verkooijen. Biomass gasification in a 100 kwth steam-oxygen blown circulating fluidized bed gasifier: Effects of operational conditions on product gas distribution and tar formation. *Biomass and Bioenergy*, 35(7):2910–2924, July 2011.

[56] Pratik N. Sheth and B. V. Babu. Experimental studies on producer gas generation from wood waste in a downdraft biomass gasifier. *Bioresource Technology*, 100(12):3127–3133, June 2009.

[57] Hayati Olgun, Sibel Ozdogan, and Guzide Yinesor. Results with a bench scale downdraft biomass gasifier for agricultural and forestry residues. *Biomass and Bioenergy*, 35(1):572–580, January 2011.

[58] Keith W. Waldron. *Bioalcohol Production: Biochemical Conversion of Lignocellulosic Biomass.* Elsevier, May 2010.

[59] L. Appels, J. Baeyens, J. Degrève, and R. Dewil. Principles and potential of the anaerobic digestion of waste-activated sludge. *Progress in Energy and Combustion Science*, 34(6):755–781, 2008.

[60] Canos Corma, S. Iborra, and A. Velty. Chemical routes for the transformation of biomass into chemicals. *Chemical Reviews*, 107(6):2411–2502, 2007.

[61] Saija Rasi. *Biogas Composition and upgrading to Biomethane.* PhD thesis, 2009.

[62] EBA Biogas Report 2014 - European Biogas AssociationEuropean Biogas Association, 2014.

[63] Aebiom. A Biogas Road Map for Europe. *Aebiom*, page 22, 2009.

Bibliography

[64] G. Mininni, G. Laera, G. Bertanza, M. Canato, and A. Sbrilli. Mass and energy balances of sludge processing in reference and upgraded wastewater treatment plants. *Environmental Science and Pollution Research International*, 22(10):7203–7215, May 2015.

[65] A. Milbrandt. A Geographic Perspective on the Current Biomass Resource Availability in the United States. Technical Report, NREL/TP-560-39181, 2005.

[66] Manure production data, department of agriculture and fisheries, queensland government. https://www.daf.qld.gov.au/environment/intensive-livestock/cattle-feedlots/managing-environmental-impacts/manure-production-data, 2011. Accessed: 2016-03-30.

[67] Frankfurt School of Finance & Management (De). ObserveER, Renac (DE), Institute for Renewable Energy (IEO/ EC BREC, PL), Jožef Stefan Institute (SI), ECN (NL) and Co-funded. The state of renewable energies in europe. 33(0):1–103, 2013.

[68] B. Tjaden, M. Gandiglio, A. Lanzini, M. Santarelli, and M. Järvinen. Small-Scale Biogas-SOFC Plant: Technical Analysis and Assessment of Different Fuel Reforming Options. *Energy & Fuels*, 28(6):4216–4232, June 2014.

[69] A. Lanzini, T. G. Kreutz, E. Martelli, and M. Santarelli. Energy and economic performance of novel integrated gasifier fuel cell (IGFC) cycles with carbon capture. *International Journal of Greenhouse Gas Control*, 26:169–184, July 2014.

[70] Marta Gandiglio, Andrea Lanzini, Massimo Santarelli, and Pierluigi Leone. Design and Balance-of-Plant of a Demonstration Plant With a Solid Oxide Fuel Cell Fed by Biogas From Waste-Water and Exhaust Carbon Recycling for Algae Growth. *Journal of Fuel Cell Science and Technology*, 11(3):031003–031003, January 2014.

[71] Argonne National Laboratory. Gas Clean-Up for Fuel Cell Applications Workshop. Technical report, 2014.

[72] N. de Arespacochaga, C. Valderrama, C. Mesa, L. Bouchy, and J. L. Cortina. Biogas biological desulphurisation under extremely acidic conditions for energetic valorisation in Solid Oxide Fuel Cells. *Chemical Engineering Journal*, 255:677–685, November 2014.

[73] Dennis Papadias. Biogas Impurities and Cleanup for Fuel Cells, Fuel Cell Seminar and Exposition,Uncasville, CT, 2012.

[74] M. D. Rey, R. Font, and I. Aracil. Biogas from MSW landfill: Composition and determination of chlorine content with the AOX (adsorbable organically bound halogens) technique. *Energy*, 63:161–167, December 2013.

[75] Orhan Sevimoğlu and Berrin Tansel. Effect of persistent trace compounds in landfill gas on engine performance during energy recovery: A case study. *Waste Management*, 33(1):74–80, January 2013.

[76] Nicolas Abatzoglou and Steve Boivin. A review of biogas purification processes. *Biofuels, Bioproducts and Biorefining*, 3(1):42–71, January 2009.

[77] M. Arnold and T. Kajolinna. Development of on-line measurement techniques for siloxanes and other trace compounds in biogas. *Waste Management*, 30(6):1011–1017, 2010.

[78] D.D. Papadias, S. Ahmed, and R. Kumar. Fuel Quality Issues in Stationary Fuel Cell Systems. Technical Report ANL/CSE/FCT/FQ-2011-11, Argonne National Laboratory, 2011.

[79] Michael Marsh, Chief Executive Officer, Ken Krich, Don Augenstein, John Benemann, Brad Rutledge, and Dara Salour. Biomethane from Dairy Waste A Sourcebook for the Production and Use of. *Prepared for Western United Dairymen. Funded part through USDA Rural Dev*, (July):1–282, 2005.

[80] Kengo Haga, Yusuke Shiratori, Kohei Ito, and Kazunari Sasaki. Chemical Degradation and Poisoning Mechanism of Cermet Anodes in Solid Oxide Fuel Cells. *ECS Transactions*, 25(2):2031–2038, September 2009.

[81] Ting Shuai Li, Cheng Xu, Tao Chen, He Miao, and Wei Guo Wang. Chlorine contaminants poisoning of solid oxide fuel cells. *Journal of Solid State Electrochemistry*, 15(6):1077–1085, August 2010.

[82] K. Haga, Y. Shiratori, K. Ito, and K. Sasaki. Chlorine Poisoning of SOFC Ni-Cermet Anodes. *Journal of The Electrochemical Society*, 155(12):B1233–B1239, December 2008.

[83] Kazunari Sasaki, Kengo Haga, Tomoo Yoshizumi, Daisuke Minematsu, Eiji Yuki, RunRu Liu, Chie Uryu, Toshihiro Oshima, Teppei Ogura, Yusuke Shiratori, Kohei Ito, Michihisa Koyama, and Katsumi Yokomoto. Chemical durability of Solid Oxide Fuel Cells: Influence of impurities on long-term performance. *Journal of Power Sources*, 196(22):9130–9140, November 2011.

[84] J. P. Trembly, R. S. Gemmen, and D. J. Bayless. The effect of coal syngas containing HCl on the performance of solid oxide fuel cells: Investigations into the effect of operational temperature and HCl concentration. *Journal of Power Sources*, 169(2):347–354, June 2007.

[85] Chunchuan Xu, Mingyang Gong, John W. Zondlo, XingBo Liu, and Harry O. Finklea. The effect of HCl in syngas on Ni–YSZ anode-supported solid oxide fuel cells. *Journal of Power Sources*, 195(8):2149–2158, April 2010.

[86] Alexander Kromp, Sebastian Dierickx, André Leonide, André Weber, and Ellen Ivers-Tiffée. Electrochemical Analysis of Sulphur-Poisoning in Anode-Supported SOFCs under Reformate Operation. *ECS Transactions*, 41(33):161–169, May 2012.

Bibliography

[87] Davide Papurello, Andrea Lanzini, Sonia Fiorilli, Federico Smeacetto, Rahul Singh, and Massimo Santarelli. Sulfur poisoning in Ni-anode solid oxide fuel cells (SOFCs): Deactivation in single cells and a stack. *Chemical Engineering Journal*, 283:1224–1233, January 2016.

[88] A. Hauch, A. Hagen, J. Hjelm, and T. Ramos. Sulfur Poisoning of SOFC Anodes: Effect of Overpotential on Long-Term Degradation. *Journal of The Electrochemical Society*, 161(6):F734–F743, January 2014.

[89] Shaowu Zha, Zhe Cheng, and Meilin Liu. Sulfur Poisoning and Regeneration of Ni-Based Anodes in Solid Oxide Fuel Cells. *Journal of The Electrochemical Society*, 154(2):B201–B206, February 2007.

[90] Zhe Cheng, Shaowu Zha, and Meilin Liu. Influence of cell voltage and current on sulfur poisoning behavior of solid oxide fuel cells. *Journal of Power Sources*, 172(2):688–693, October 2007.

[91] Zhe Cheng and Meilin Liu. Characterization of sulfur poisoning of Ni–YSZ anodes for solid oxide fuel cells using in situ Raman microspectroscopy. *Solid State Ionics*, 178(13–14):925–935, May 2007.

[92] Marcelo Kaufman Rechulski. *Catalysts for High Temperature Gas Cleaning in the Production of Synthetic Natural Gas from Biomass*. PhD thesis, EPFL, Lausanne, 2012.

[93] Urs Rhyner, Philip Edinger, Tilman J. Schildhauer, and Serge M. A. Biollaz. Experimental study on high temperature catalytic conversion of tars and organic sulfur compounds. *International Journal of Hydrogen Energy*, 39(10):4926–4937, March 2014.

[94] JianEr Bao, Gopala N. Krishnan, Palitha Jayaweera, Kai-Hung Lau, and Angel Sanjurjo. Effect of various coal contaminants on the performance of solid oxide fuel cells: Part II. ppm and sub-ppm level testing. *Journal of Power Sources*, 193(2):617–624, September 2009.

[95] O. A. Marina, L. R. Pederson, E. C. Thomsen, C. A. Coyle, and K. J. Yoon. Reversible poisoning of nickel/zirconia solid oxide fuel cell anodes by hydrogen chloride in coal gas. *Journal of Power Sources*, 195(20):7033–7037, October 2010.

[96] Akira Ishikura, Shinichi Sakuno, Norio Komiyama, Hiroshi Sasatsu, Naoto Masuyama, Hibiki Itoh, and Kenji Yasumoto. Influence of H2s Poisoning on Anode Layer of SOFC. *ECS Transactions*, 7(1):845–850, May 2007.

[97] Catherine M. Grgicak, Richard G. Green, and Javier B. Giorgi. SOFC anodes for direct oxidation of hydrogen and methane fuels containing H2s. *Journal of Power Sources*, 179(1):317–328, April 2008.

[98] Lan Zhang, San Ping Jiang, Hong Quan He, Xinbing Chen, Jan Ma, and Xiao Chao Song. A comparative study of H2s poisoning on electrode behavior of Ni/YSZ and Ni/GDC anodes of solid oxide fuel cells. *International Journal of Hydrogen Energy*, 35(22):12359–12368, November 2010.

[99] E. Brightman, D. G. Ivey, D. J. L. Brett, and N. P. Brandon. The effect of current density on H2s-poisoning of nickel-based solid oxide fuel cell anodes. *Journal of Power Sources*, 196(17):7182–7187, September 2011.

[100] Jason P. Trembly, Andres I. Marquez, Ted R. Ohrn, and David J. Bayless. Effects of coal syngas and H2s on the performance of solid oxide fuel cells: Single-cell tests. *Journal of Power Sources*, 158(1):263–273, July 2006.

[101] Yue Li, Tim Täffner, Michael Bischoff, Bernd Niemeyer, Yue Li, Tim Täffner, Michael Bischoff, and Bernd Niemeyer. Test Gas Generation from Pure Liquids: An Application-Oriented Overview of Methods in a Nutshell, Test Gas Generation from Pure Liquids: An Application-Oriented Overview of Methods in a Nutshell. *International Journal of Chemical Engineering, International Journal of Chemical Engineering*, 2012, 2012:e417029, February 2012.

[102] Yeqing Fu. *Theoretical and experimental study of solid oxide fuel cell (SOFC) using impedance spectra.* Thesis, Massachusetts Institute of Technology, 2014.

[103] Søren Højgaard Jensen, Anne Hauch, Peter Vang Hendriksen, Mogens Mogensen, Nikolaos Bonanos, and Torben Jacobsen. A Method to Separate Process Contributions in Impedance Spectra by Variation of Test Conditions. *Journal of The Electrochemical Society*, 154(12):B1325–B1330, December 2007.

[104] Jimmi Nielsen and Johan Hjelm. Impedance of SOFC electrodes: A review and a comprehensive case study on the impedance of LSM:YSZ cathodes. *Electrochimica Acta*, 115:31–45, January 2014.

[105] C. Graves. RAVDAV Data Analysis Software, 2012.

[106] Bernard A. Boukamp. A linear kronig?kramers transform test for immittance data validation. *Journal of The Electrochemical Society*, 142(6):1885–1894, June 1995.

[107] H. Schichlein, A. C. Müller, M. Voigts, A. Krügel, and E. Ivers-Tiffée. Deconvolution of electrochemical impedance spectra for the identification of electrode reaction mechanisms in solid oxide fuel cells. *Journal of Applied Electrochemistry*, 32(8):875–882, August 2002.

[108] Evgenij Barsoukov and J. Ross Macdonald. *Wiley: Impedance Spectroscopy: Theory, Experiment, and Applications, 2nd Edition.*

[109] André Leonide. *SOFC modelling and parameter identification by means of impedance spectroscopy.* KIT Scientific Publishing, 2010.

Bibliography

[110] Harumi Yokokawa, Katsuhiko Yamaji, M. E. Brito, Haruo Kishimoto, and Teruhisa Horita. General considerations on degradation of Solid Oxide Fuel Cell anodes and cathodes due to impurities in gases. *Journal of Power Sources*, 196(17):7070–7075, September 2011.

[111] Harumi Yokokawa. Report of Five-Year NEDO Project on Durability/Reliability of SOFC Stacks. *ECS Transactions*, 57(1):299–308, October 2013.

[112] M. Kymäläinen, K. Lähde, M. Arnold, J. M. Kurola, M. Romantschuk, and H. Kautola. Biogasification of biowaste and sewage sludge – Measurement of biogas quality. *Journal of Environmental Management*, 95, Supplement:S122–S127, March 2012.

[113] Matthew R. Allen, Alan Braithwaite, and Chris C. Hills. Trace Organic Compounds in Landfill Gas at Seven U.K. Waste Disposal Sites. *Environmental Science & Technology*, 31(4):1054–1061, April 1997.

[114] Kazunari Sasaki, Tomoo Yoshizumi, Kengo Haga, Hiroaki Yoshitomi, Takami Hosoi, Yusuke Shiratori, and Shunsuke Taniguchi. Chemical Degradation of SOFCs: External Impurity Poisoning and Internal Diffusion-Related Phenomena. *ECS Transactions*, 57(1):315–323, October 2013.

[115] A. Hauch, S. D. Ebbesen, S. H. Jensen, and M. Mogensen. Solid Oxide Electrolysis Cells: Microstructure and Degradation of the Ni/Yttria-Stabilized Zirconia Electrode. *Journal of The Electrochemical Society*, 155(11):B1184–B1193, November 2008.

[116] Bin Liu, Toshiaki Matsui, Hiroki Muroyama, Kazuo Tomida, Tatsuo Kabata, and Koichi Eguchi. Impedance Analysis of Practical Segmented-in-Series Tubular Solid Oxide Fuel Cells. *ECS Transactions*, 35(1):637–646, April 2011.

[117] Kevin Huang and John B. Goodenough. 11 - Poisoning of solid oxide fuel cell (SOFC) electrodes. In Kevin Huang and John B. Goodenough, editors, *Solid Oxide Fuel Cell Technology*, Woodhead Publishing Series in Energy, pages 197–219. Woodhead Publishing, 2009.

[118] G. J. Offer and N. P. Brandon. The effect of current density and temperature on the degradation of nickel cermet electrodes by carbon monoxide in solid oxide fuel cells. *Chemical Engineering Science*, 64(10):2291–2300, May 2009.

[119] P. Simell, P. Ståhlberg, Y. Solantausta, J. Hepola, and E. Kurkela. Gasification Gas Cleaning with Nickel Monolith Catalyst. In A. V. Bridgwater and D. G. B. Boocock, editors, *Developments in Thermochemical Biomass Conversion*, pages 1103–1116. Springer Netherlands, 1997.

[120] A. Leonide, S. Hansmann, André Weber, and E. Ivers-Tiffée. Performance simulation of current/voltage-characteristics for SOFC single cell by means of detailed impedance analysis. *Journal of Power Sources*, 196(17):7343–7346, September 2011.

[121] V. Sonn, A. Leonide, and E. Ivers-Tiffée. Combined Deconvolution and CNLS Fitting Approach Applied on the Impedance Response of Technical Ni 8ysz Cermet Electrodes. *Journal of The Electrochemical Society*, 155(7):B675–B679, July 2008.

[122] Per Hjalmarsson, Xiufu Sun, Yi-Lin Liu, and Ming Chen. Durability of high performance Ni–yttria stabilized zirconia supported solid oxide electrolysis cells at high current density. *Journal of Power Sources*, 262:316–322, September 2014.

[123] Maya Kiskinova and D. Wayne Goodman. Modification of chemisorption properties by electronegative adatoms: H2 and CO on chlorided, sulfided, and phosphided Ni(100). *Surface Science*, 108(1):64–76, June 1981.

[124] N. Coute, J. D. Ortego Jr., J. T. Richardson, and M. V. Twigg. Catalytic steam reforming of chlorocarbons: trichloroethane, trichloroethylene and perchloroethylene. *Applied Catalysis B: Environmental*, 19(3–4):175–187, December 1998.

[125] James T. Richardson, James D. Ortego Jr, Nicolas Coute, and Martyn V. Twigg. Chloride poisoning of water-gas shift activity in nickel catalysts during steam reforming. *Catalysis Letters*, 41(1-2):17–20, March 1996.

[126] Davide Papurello, Andrea Lanzini, Pierluigi Leone, Massimo Santarelli, and Silvia Silvestri. Biogas from the organic fraction of municipal solid waste: Dealing with contaminants for a solid oxide fuel cell energy generator. *Waste Management*, 34(11):2047–2056, November 2014.

[127] Ming Liu and P. V. Aravind. The fate of tars under solid oxide fuel cell conditions: A review. *Applied Thermal Engineering*, 70(1):687–693, September 2014.

[128] Florian P. Nagel, Tilman J. Schildhauer, Josef Sfeir, Alexander Schuler, and Serge M. A. Biollaz. The impact of sulfur on the performance of a solid oxide fuel cell (SOFC) system operated with hydrocarboneous fuel gas. *Journal of Power Sources*, 189(2):1127–1131, April 2009.

[129] M.D. Kaufman-Rechulski. Catalysts for high temperature gas cleaning in the production of synthetic natural gas from biomass. *EPFL*, page 270, 2012.

[130] Benoit Boulinguiez and Pierre Le Cloirec. Adsorption/Desorption of Tetrahydrothiophene from Natural Gas onto Granular and Fiber-Cloth Activated Carbon for Fuel Cell Applications. *Energy & Fuels*, 23(2):912–919, February 2009.

[131] Suranat Wongchanapai, Hiroshi Iwai, Motohiro Saito, and Hideo Yoshida. Performance evaluation of a direct-biogas solid oxide fuel cell-micro gas turbine (SOFC-MGT) hybrid combined heat and power (CHP) system. *Journal of Power Sources*, 223:9–17, February 2013.

[132] P. Leone, A. Lanzini, M. Santarelli, M. Calì, F. Sagnelli, A. Boulanger, A. Scaletta, and P. Zitella. Methane-free biogas for direct feeding of solid oxide fuel cells. *Journal of Power Sources*, 195(1):239–248, January 2010.

Bibliography

[133] John Bøgild Hansen. Correlating Sulfur Poisoning of SOFC Nickel Anodes by a Temkin Isotherm. *Electrochemical and Solid-State Letters*, 11(10):B178–B180, October 2008.

[134] Anke Hagen, Gregory B. Johnson, and Per Hjalmarsson. Electrochemical evaluation of sulfur poisoning in a methane-fuelled solid oxide fuel cell: Effect of current density and sulfur concentration. *Journal of Power Sources*, 272:776–785, December 2014.

[135] Arata Nakajo, Zacharie Wuillemin, Patrick Metzger, Stefan Diethelm, Günter Schiller, Jan Van Herle, and Daniel Favrat. Electrochemical Model of Solid Oxide Fuel Cell for Simulation at the Stack Scale I. Calibration Procedure on Experimental Data. *Journal of The Electrochemical Society*, 158(9):B1083–B1101, September 2011.

[136] Arata Nakajo, Pietro Tanasini, Stefan Diethelm, Jan Van Herle, and Daniel Favrat. Electrochemical Model of Solid Oxide Fuel Cell for Simulation at the Stack Scale II: Implementation of Degradation Processes. *Journal of The Electrochemical Society*, 158(9):B1102–B1118, September 2011.

[137] Huayang Zhu, Robert J. Kee, Vinod M. Janardhanan, Olaf Deutschmann, and David G. Goodwin. Modeling Elementary Heterogeneous Chemistry and Electrochemistry in Solid-Oxide Fuel Cells. *Journal of The Electrochemical Society*, 152(12):A2427–A2440, December 2005.

[138] E. Achenbach and E. Riensche. Methane/steam reforming kinetics for solid oxide fuel cells. *Journal of Power Sources*, 52(2):283–288, December 1994.

[139] Christoph Stiller, Bjørn Thorud, Olav Bolland, Rambabu Kandepu, and Lars Imsland. Control strategy for a solid oxide fuel cell and gas turbine hybrid system. *Journal of Power Sources*, 158(1):303–315, July 2006.

[140] Jens R. Rostrup-Nielsen, Jens Sehested, and Jens K. Nørskov. Hydrogen and synthesis gas by steam- and C02 reforming. volume 47, pages 65–139. Academic Press, 2002.

[141] D.J. Stevens. *Hot Gas Conditioning: Recent Progress with Larger-scale Biomass Gasification Systems.* 2001.

[142] T.A. Milne and R.J. Evans. *Biomass gasifier "tars": their nature, formation, and conversion.* November 1998.

[143] Devinder Singh, Eduardo Hernández-Pacheco, Phillip N. Hutton, Nikhil Patel, and Michael D. Mann. Carbon deposition in an SOFC fueled by tar-laden biomass gas: A thermodynamic analysis. *Journal of Power Sources*, 142(1-2):194–199, 2005.

[144] Ming Liu, A. van der Kleij, A. H. M. Verkooijen, and P. V. Aravind. An experimental study of the interaction between tar and SOFCs with Ni/GDC anodes. *Applied Energy*, 108:149–157, August 2013.

[145] P. V. Aravind, J. P. Ouweltjes, N. Woudstra, and G. Rietveld. Impact of Biomass-Derived Contaminants on SOFCs with Ni/Gadolinia-Doped Ceria Anodes. *Electrochemical and Solid-State Letters*, 11(2):B24, 2008.

[146] T. Kim, G. Liu, M. Boaro, S.-I. Lee, J. M. Vohs, and R. J. Gorte. A Study of Carbon Formation and Prevention in. 155(2):231–238, 2006.

[147] J. Mermelstein, M. Millan, and N. P. Brandon. The impact of carbon formation on Ni–YSZ anodes from biomass gasification model tars operating in dry conditions. *Chemical Engineering Science*, 64(3):492–500, February 2009.

[148] Ming Liu, M. G. Millan, P. V. Aravind, and N. Brandon. Influence of Operating Conditions on Carbon Deposition in SOFCs Fuelled by Tar-Containing Biosyngas. *Journal of The Electrochemical Society*, 158(11):B1310, jan 2011.

[149] Tomoaki Namioka, Taichi Naruse, and Ryosuke Yamane. Behavior and mechanisms of Ni/ScSZ cermet anode deterioration by trace tar in wood gas in a solid oxide fuel cell. *International Journal of Hydrogen Energy*, 36(9):5581–5588, May 2011.

[150] Roberto Coll, Joan Salvadó, Xavier Farriol, and Daniel Montané. Steam reforming model compounds of biomass gasification tars: conversion at different operating conditions and tendency towards coke formation. *Fuel Processing Technology*, 74(1):19–31, November 2001.

[151] R. J. Gorte, J. M. Vohs, and S. McIntosh. Recent developments on anodes for direct fuel utilization in SOFC. *Solid State Ionics*, 175(1–4):1–6, November 2004.

[152] C.h. Toh, P.r. Munroe, D.j. Young, and K Foger. High temperature carbon corrosion in solid oxide fuel cells. *Materials at High Temperatures*, 20(2):129–136, January 2003.

[153] Samuel Majerus. Fueling a SOFC with Agricultural Waste Derived Biogas, 2016.

List of Publications

Peer reviewed articles

Solid Oxide Fuel Cell Anode Degradation by the Effect of HCl in Stack and Single Cell Environments. H. Madi, A. Lanzini, D. Papurello, S. Diethelm, Ch. Ludwig, M. Santarelli and J. Van herle, *Journal of Power Sources*, 326, 349-356, 2016.

Organic-Sulfur Poisoning of Solid Oxide Fuel Cell Operated on Bio-syngas. H. Madi, S. Diethelm, Ch. Ludwig and J. Van herle. *International Journal of Hydrogen Energy*, 41, 12231-12241, 2016.

Solid Oxide Fuel Cell Anode Degradation by the Effect of Siloxanes. H. Madi, A. Lanzini, S. Diethelm, D. Papurello, J. Van herle, M. Lualdi, J. Gutzon Larsen and M. Santarelli, *Journal of Power Sources*, 279, 460–471, 2015.

Damage of Siloxanes on the Performance of Ni- YSZ Anode Supported SOFC. H. Madi, S. Diethelm, S. Poitel, Ch. Ludwig and J. Van herle, *Journal of Fuel Cells*, 15, 718–727, 2015.

The Impact of Toluene on the Performance of Anode-Supported Ni-YSZ SOFC Operated on Hydrogen and Biosyngas. H. Madi, S. Diethelm, Ch. Ludwig and J. Van herle, *ECS Transaction*, 68, 2811-2818, 2015.

Effect of Steam-to-Carbon Ratio on Degradation of Ni-YSZ Anode Supported Cells. H. Madi, S. Diethelm, J. Van herle, N. Petigny, *ECS Transaction*, 57, 1517- 1525, 2013.

Guidelines for Dealing with Fuel Contaminants in Biogas-fed Solid Oxide Fuel Cell Plants. A. Lanzini, H. Madi, D. Papurello, V. Chiodo , S. Maisano, J. Van herle and M. Santarelli. *In preparation, a review paper based on finding of SOFCOM project.*

Conference papers

SOFC Operation on Biogas: Impurity Threshold Levels, Hossein Madi, Christian Ludwig and Jan Van herle, proceedings of 12th European Fuel Cell Forum, July 2016.

Effect of Biogas Contaminants on the Performance of Anode Supported SOFC. Hossein Madi, Stefan Diethelm, Christian Ludwig and Jan Van herle, proceedings of 11th European Fuel Cell Forum, July 2014.

Oral presentation

SOFC Poisoning with Biogas Impurities. DTU Energy's annual PhD symposium, Copenhagen-Denmark, November 2015.

Effect of Biogas Contaminants on the Performance of Anode Supported SOFC. 11th European Fuel Cell Forum, Luzern- Switzerland, July 2014.

SOFC operation on Biofuels, sulfur poisoning. SOF-CH Workshop, Murten- Switzerland, May 2014.

Poster presentation

SOFC Operation on Biogas: Impurity Threshold Levels, 12th European Fuel Cell Forum, Luzern-Switzerland, July 2016.

EIS Diagnosis tool for SOFC Degradation Fueled by Biofuels, MODVAL 13, Lausanne- Switzerland, March 2016.

Sulfur Poisoning of the Reverse Water Gas Shift Reaction on Anode Supported SOFCs, ECS Conference on Electrochemical Energy Conversion & Storage with SOFC-XIV, Glasgow- Scotland, July 2015.

The Impact of Toluene on the Performance of Anode-Supported Ni-YSZ SOFC Operated on Hydrogen and Bio-syngas, ECS Conference on Electrochemical Energy Conversion & Storage with SOFC-XIV, Glasgow- Scotland, July 2015.

A Method to separate Process Contributions in Impedance Spectra- case study: Effect of sulfur on SOFC. 65th Annual Meeting of the International Society of Electrochemistry, Lausanne-Switzerland, September 2014.

Effect of Steam-to-Carbon Ratio on Degradation of Ni-YSZ Anode Supported Cells, 13th International Symposium on Solid Oxide Fuel Cells (SOFC-XIII), Okinawa- Japan, October 2013.

Hossein MADI

(Born in 1987, Iran)
Chemin de Bérée 8A
CH-1010 Lausanne, Switzerland
+41 78 882 5162 | madi.hossein@gmail.com

EDUCATION

JULY 2016	PhD, Chemical Engineering Doctoral School **Swiss Federal Institute of Technology (EPFL)**, Switzerland *Solid Oxide Fuel Cell (SOFC) Operation on Biofuels* Applied PhD. *The project funds by an European project **SOFCOM** and Swiss CCEM projects **(WOODGAS-SOFC II and SERAN)**.* Advisors: MER Dr. Jan VAN HERLE Prof. Christian LUDWIG
MARCH 2012	Master of Science in CHEMICAL and BIOCHEMICAL ENGINEERING **Swiss Federal Institute of Technology (EPFL)**, Switzerland Master thesis at **Paul Scherer Institut (PSI)**, Villigen-Switzerland Thesis: "Lagrangian Approach to Study Catalytic Fluidized Bed Reactors." Advisor: Prof. Christian LUDWIG
JULY 2009	Bachelor of Science in CHEMICAL and BIOCHEMICAL ENGINEERING **Tehran University**, Iran. Major: Process Design and Optimization Thesis: "Chemical Gas Sensor for combustible and non combustible Gases." Advisor: Prof. Yadollah MORTAZAVI

PROFESSIONAL

AUG 2015 - DEC 2015	**Technical University of Denmark (DTU)**, Department of Energy Conversion and Storage, Denmark. *Simulation and designing of methods to identify degradation processes related to SOFCs.* Advisor: Dr. Anne HAUCH
SEP 2012 - APRIL 2015	**SOFCOM**, An European project financed in the frame of Fuel Cells and Hydrogen Joint Undertaking. *Lab-scale activities e.g. cell testing and characterization, advance post mortem analysis, etc. on the effect of Biogas impurities on SOFC.*
JULY 2012 - APRIL 2016	**CCEM**, Integrated Biomass- SOFC Cogeneration, **WOODGAS-SOFC II** and Self-Regenerating Anodes **(SERAN)**. *Analyse the impact of critical biomass impurities such as sulfur on the performance of SOFC, cell characterization and testing.*
AUG 2010 - FEB 2011	**Sulzer Chemtech**, Winterthur - Switzerland *Experimental project in pilot plant scale. Admixing of additives to polymer melts and checking the performance of different static mixers.* Advisor: Dr. Philip NISING
OTHERS	Internship at **IEVB** TU Clausthal- Germany (2008), Laboratory assistant at **LLCB** EPFL (2010-11), Event organizer at **IAESTE**, Tehran University- Iran (2007).

HOBBY

Mountain ski, Half-marathon, Traveling, Whiskey tasting.